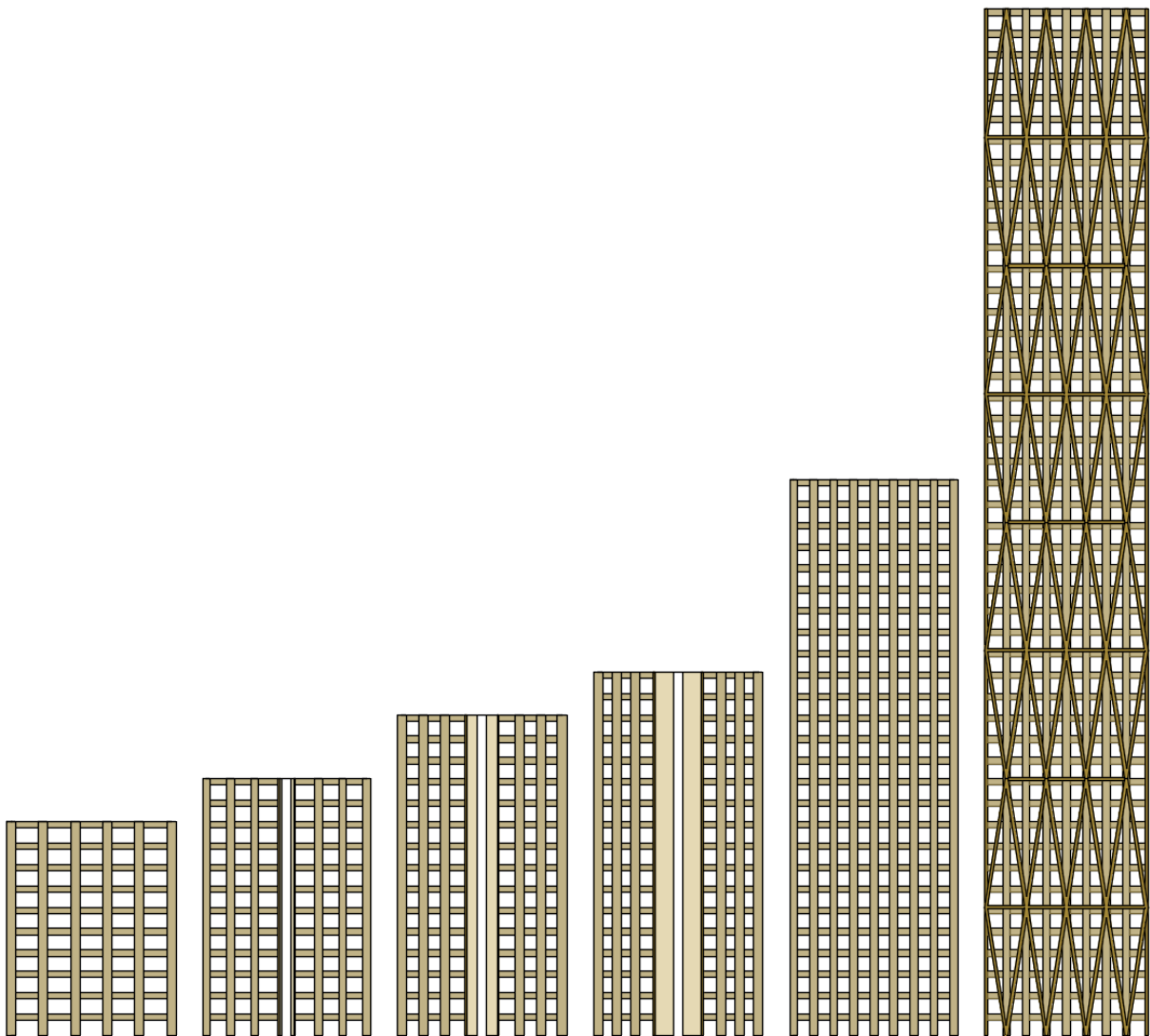


DELFT UNIVERSITY OF TECHNOLOGY

Timber High-Rise Buildings

PARAMETRIC STUDY OF THE INFLUENCE OF PRELIMINARY DESIGN PARAMETERS ON THE
WIND-INDUCED DYNAMIC RESPONSE OF TIMBER HIGH-RISE BUILDINGS



Maria Felicita - 4912896

March 20, 2021

Timber High-Rise Buildings

Parametric study of the influence of preliminary design parameters on the wind-induced dynamic response of timber high-rise buildings

by

Maria Felicita

in partial fulfillment of the requirements for the degree of

Master of Science

in Civil Engineering

at the Delft University of Technology

to be defended on Friday March 26th, 2021

Student Number:	4912896	
Project Duration	Jul. 03, 2020 – Mar. 26, 2021	
Thesis Committee:	Prof. dr. ir. J.G Rots	TU Delft, Chair
	Dr. ir. G.J.P Ravenshorst	TU Delft, Supervisor
	Ir. L.P.L van der Linden	TU Delft, Supervisor
	Ir. R Crielaard	TU Delft, Supervisor
	Ir. I Sele	Van Rossum, Supervisor

An electronic version of this thesis is available at <http://repository.tudelft.nl/>.



Abstract

The implementation of timber as a load-bearing and stabilizing material for high-rise structures has significantly increased over the last decades due to its potential of reducing the environmental footprint of a structure. Timber structures present a reduced global stiffness and self-weight compared to structures incorporating traditional construction materials, making them prone to high accelerations caused by wind load which affects the structural integrity and user comfort. The acceleration of a structure is a highly complex parameter that must be determined using modal analysis computed by a full-scale finite element model, and is significantly influenced by the magnitude of the wind and vertical loads, as well as the global stiffness of the structure.

During the preliminary design phase, it is the responsibility of structural engineers to determine the feasibility of the design and estimate the amount of material required and the distribution of the structural elements. However, this process must be done under a limited amount of time, forcing engineers to rely on rules of thumb and previous experience, which are not currently available for the design of timber high-rise structures. Therefore, the goal of this investigation is to perform a parametric study to determine the influence of various parameters on the design of timber high-rise structures and assist structural engineers in making well-argued decisions during the preliminary design phase.

The preliminary design parameters to be studied in the parametric study are: stability system design, connection stiffness and building height. The ranges for the parameters were selected based on extreme values such that clear trends regarding their influence on design could be visualized. This decision limits the design feasibility of some configurations studied in this investigation. The selected stability systems to be studied are glulam frame, CLT core and glulam diagrid. The design verification for each design alternative is done using ULS and SLS criteria provided by Eurocode, as well as a simplified method to estimate the dynamic response of the structure. Finally, the sizing of the structural elements and data collection was done by the implementation of evolutionary algorithms.

From the data collected it was determined that the most influential design parameter for the design of timber high-rise structures is the stability system selection given that it determines the global stiffness, which showed a significantly higher influence on the dynamic response of the structure than its self-weight. Moreover, the efficiency of the different stability systems was assessed based on the maximum slenderness they could achieve compared to the amount of material they required. Based on this definition, it was determined that the glulam diagrid is two times more efficient than the CLT core and three times more efficient than the glulam frame. The efficiency of the glulam diagrid is caused by its high global stiffness provided by the triangular configuration of the diagonal elements. These observations prove that the effect of timber's low density can be mitigated by the implementation of efficient stability systems.

The influence of connection stiffness was determined to be directly related to the ability of the stability system to provide lateral stability to the structure. The influence of this parameter on form stable structures such as the CLT core and the glulam diagrid, proved to be nearly negligible, while for non-form stable structures such as the glulam frame it proved to be highly influential. However, it was also determined that the addition of rotational stiffness in the connections causes an exponential increase of the costs and environmental footprint of the structure, which decreases their design feasibility. Finally, the influence of building height on the design is visualized by its effect on the dynamic response of the structure caused by the logarithmic increase of the wind speed as this parameter increases, as well as a decrease of the global stiffness proportional to the efficiency of the stability system.

Acknowledgements

I would like to acknowledge and express my gratitude to the people who have helped me over the last nine months during my thesis:

First, I would like to thank my graduation committee, Jan Rots, Geert Ravenshorst, Lennert van der Linden, Roy Crielaard and Ibrahim Selek. I am grateful for your feedback and critical questions during our meetings, that steered me in the right directions. Thanks to you I have gained valuable knowledge about the dynamic behaviour of high-rise structures, the design of timber structures, and design feasibility principles which will certainly be useful in my career.

I would like to thank my parents for always encouraging me to follow my dreams, no matter how big or small, or if those dreams take me oceans away from them. I owe this to you.

Thank you, Knut, for your infinite support during the most stressful times, your constant interest in learning about my project, your critical questions, and for reading sections of my report over and over. Last year was very difficult for everyone in the world, but having you and Tesla (our cat) by my side made it a very enjoyable ride, filled with happiness and adventures.

Thanks to my wonderful friends at TU Delft who have made this past two years and a half such an unforgettable experience.

M. Felicita
Rotterdam, March 2021

Contents

1	Introduction	1
1.1	Research Context	1
1.2	Problem Definition	3
1.3	Goals and Objectives	4
1.4	Research Questions and Outline	4
1.5	Methodology	6
1.6	Scope	6
2	Timber High Rise Buildings	7
2.1	High-Rise Structural Design	7
2.1.1	Strength	7
2.1.2	Stability	8
2.2	Dynamic Behaviour	9
2.3	Material Properties	10
2.4	Existing Structures	11
2.4.1	Treet, Norway	12
2.4.2	Brock Commons, Vancouver	12
2.4.3	Mjøstårnet, Norway	13
2.5	Fire Safety	14
2.6	Conclusions	15
3	Wind Engineering	16
3.1	Wind Load	16
3.1.1	Wind Pressure	17
3.2	Dynamic Response	18
3.2.1	Natural Frequency	18
3.2.2	Structural Damping	19
3.2.3	Along-Wind Acceleration	21
3.2.4	Cross-Wind Acceleration	22
3.3	Conclusions	22
4	Parametric Model	24
4.1	Design Parameters	24
4.1.1	Stability System Design	24
4.1.2	Connection Stiffness	29
4.1.3	Building Height	31
4.2	Design Constraints	31
4.2.1	Member Forces	31
4.2.2	Global Deflection and Interstorey Drift	32
4.2.3	Acceleration	33
4.3	System Loads	33
4.4	Design Assumptions	35
4.5	Conclusions	36
5	Parametric Study	38
5.1	Model Output	38
5.2	Optimization	39
5.2.1	Evolutionary Solver	39

5.2.2	Brute Force Method	42
5.3	Conclusions	45
6	Results and Discussion	46
6.1	Results and Observations	46
6.1.1	Glulam Frame	46
6.1.2	CLT Core	50
6.1.3	Glulam Diagrid	55
6.2	Discussion	59
6.3	Preliminary Design Tool	65
6.4	Conclusions	65
7	Conclusions and Recommendations	67
7.1	Conclusions	67
7.2	Recommendations	68
	Appendix Wind Load	73
	Appendix Connection Design	77
	Appendix Connection types	77
	Appendix Column-beam connections	79
	Appendix Semi-rigid connections	79
	Appendix Pinned connections	81
	Appendix Connection design check	83
	Appendix Member Check	88
	Appendix Verification of glulam elements	88
	Appendix Verification of CLT elements	90
	Appendix CLT Design Assumptions	92
	Appendix Results Verification	96
	Appendix Karamba Model	96
	Appendix Dynamic Behaviour	99
	Appendix EA Data	101
	Appendix Parametric Model	104

1 Introduction

1.1 Research Context

Construction Industry Challenges

The construction industry is one of the oldest disciplines in the world and throughout the years it has had to adapt to society’s changing needs. Over the last century the biggest challenge was to accommodate urbanization and overpopulation. These phenomena pushed the industry to build taller structures than ever before. High-rise buildings behave differently than low-rise buildings due to the dynamic behavior caused by the wind loads, which created a need for the implementation of stronger materials which could provide a higher stiffness, making steel and concrete the preferred construction materials.

The 21st century poses a new challenge for the construction industry and it comes from the current raise in environmental awareness. The construction industry is one of the largest polluters in the world and according to the Global Status Report 2017, the construction phase alone accounts for 11% of the global energy consumption [29]. The amount of CO₂ that comes free during the life of a structure, also known as embedded CO₂, can be divided into different stages of the life-cycle as seen in figure 1.1 and it can also be seen that the main contributing stage is the product development which is divided into raw material production, transportation and manufacturing [25]. Based on this figure it can be stated that the selection of the construction materials will have a significant impact of the embedded CO₂ of a construction project.

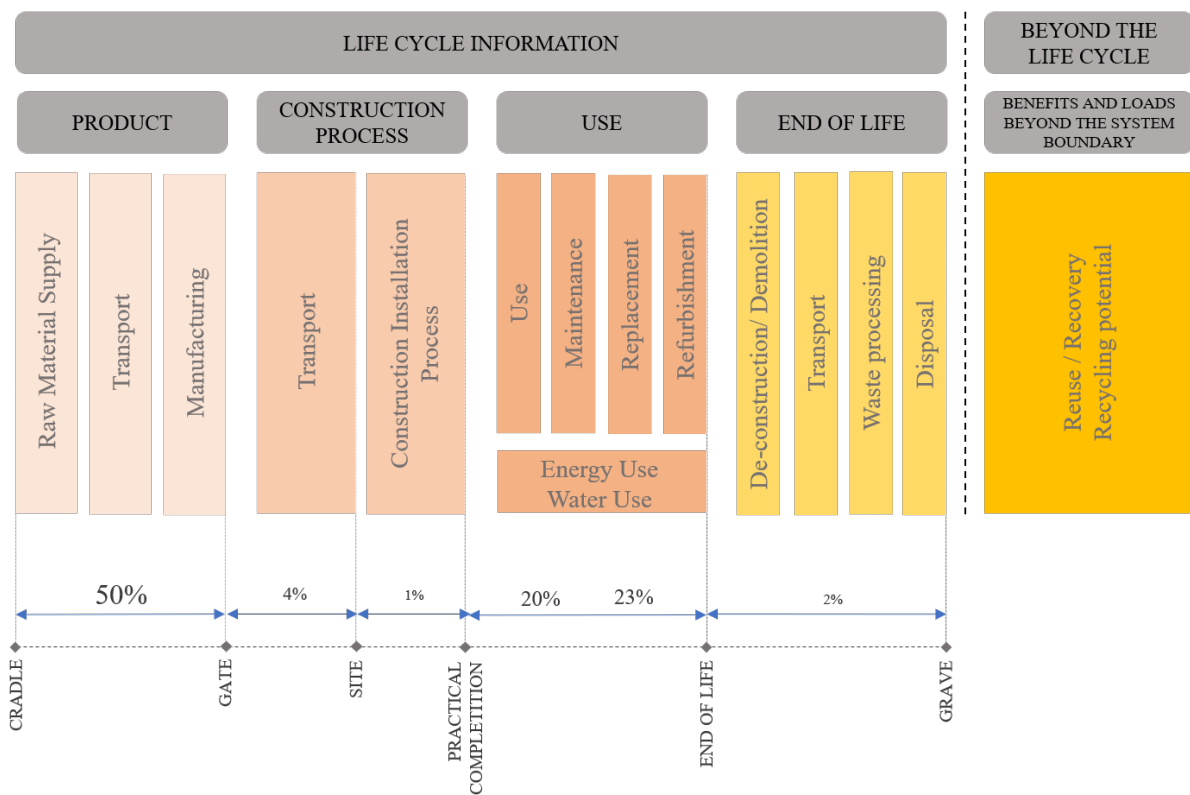


Figure 1.1: Fraction of CO₂ released at the different life-cycle stages of construction projects [25]

Currently, reinforced concrete and structural steel are the preferred construction materials; however, their production and manufacturing leave a large carbon footprint, which has increased the need to find a feasible alternative. In terms of carbon footprint reduction, timber has emerged as a potential solution due to its low embedded carbon [39]. Table 1.1 shows the kilograms of CO₂ produced by one kilogram of different construction materials, as provided by The Institution of Structural Engineers in the United Kingdom. As seen in the table, when using sustainable concrete which incorporates ground granulated blast-furnace slag (GGBS), low embedded CO₂ per kilogram can be achieved; however, when you consider the density of the material, timber products show a lower embedded of CO₂. Moreover, when you consider the impact of the reinforcement bars, the footprint of reinforced concrete significantly increases, making the embedded CO₂ of timber almost negligible compared to other construction materials.

Material specifications	$kgCO_2/kg$	Density kg/m^3	$kgCO_2/m^3$
Reinforced Concrete			
Unreinforced concrete, C30/37 (35% GGBS)	0.103	2500	258
Reinforcement bars, world average	1.99	7850	15622
Structural Steel			
Structural sections S355, world average	1.55	7850	12168
Structural Timber			
Cross laminated timber, C24	0.437	420	184
Glue laminated timber, C24	0.512	420	215
Softwood, C24	0.263	420	110

Table 1.1: *Embedded carbon of different construction materials [25]*

When considering the construction life stages, figure 1.1 shows that the environmental footprint of a construction can be decreased not only by reducing the embedded CO₂ of individual stages, but also by reusing, recovering or recycling the waste produced during the end of life stage and reintegrating it back into the system in a process known as circularity [17]. This process can be incorporated into a project through the design of the structure or by the use of circular materials [31]. Circular material usage implies selecting materials that are renewable or reusable, while circular design implies the implementation of design components which can be reused in a different project or service after its lifetime. The use of timber as a load bearing material provides potential for implementing these two approaches into the design given that timber is a naturally occurring material classified as renewable, and it predominantly uses dry connections, which makes it easy to disassemble [18]. The circularity potential of timber is mainly assessed by its efficacy to be disassembled. Therefore, the type of connections used is an important design parameter in terms of not only structural design, but also circularity.

Timber High-Rise Buildings

Urbanization and overpopulation together with reducing the environmental footprint are some of the biggest challenges that the construction industry has faced over the last century. Timber high-rise structures emerge as a feasible solution to overcome these challenges. High-rise buildings are exposed to high horizontal loads caused by the wind, and given their tendency for high slenderness, the dynamic behaviour of these structures tends to govern their design [35]. The dynamic behaviour of a structure is quantified in terms of acceleration, which is determined based on the structure's self-weight, cross-sectional stiffness, and height. Timber has a significantly lower density than other construction materials, which poses an additional challenge for the structural design of these structures.

High-rise structures must be designed to reduce the acceleration and to transfer vertical loads to the foundations. When using sawn timber as the main load-bearing material, the cross-section of the structural elements must be significantly larger than for other materials in order to increase the self-weight and provide enough capacity. After a certain building height, the cross-sections become too large and impossible to manufacture due to the tree size limitation [40]. In order to overcome this limitation, engineered timber materials such as glued laminated timber (glulam) and cross-laminated timber (CLT) were developed. Glulam consists of various layers of sawn timber glued together creating longer and bigger structural members, which can be used as beams and columns. CLT also consists of various layers of sawn timber glued together; however, in this case each layer is placed such that its grain direction is perpendicular to the one above, counteracting the material’s anisotropy and producing structural elements with consistent mechanical properties in two directions which can be used as slabs, walls and diaphragms [23]. The emergence of engineered timber products helped the development of taller structures using timber as the main load bearing material. There has been a significant increase on the height and development of such structures over the past 10 years as seen in figure 1.2. However, in order to build even higher structures, the influence of various design parameters on the dynamic response of the structure must be assessed to provide insight for designers about the possibilities and limitations of these structures.

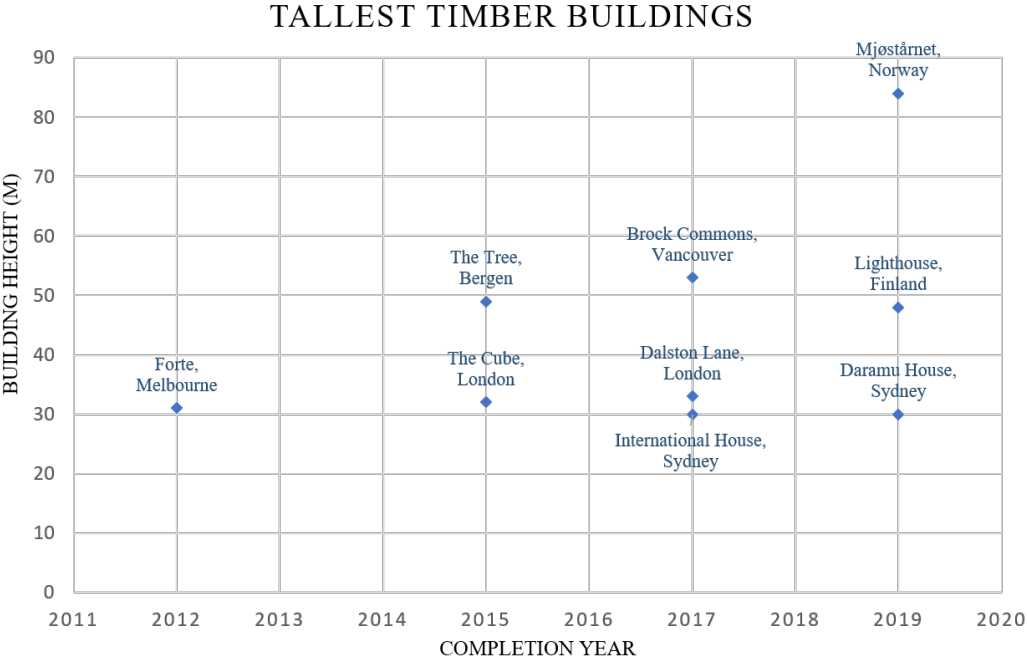


Figure 1.2: *Development of Timber High-Rise Structures*

1.2 Problem Definition

The design of a high-rise structure incorporates designs from different disciplines, and the task of the structural engineer is to determine in an early stage the feasibility of incorporating all of them into a safe and efficient structure. Due to timber’s low density it is expected that the dynamic behaviour will be the governing design criterion for all mid- and high-rise structures, resulting in a shift from the traditional static design approach to a dynamic one. The dynamic behaviour

of a structure is commonly quantified with the acceleration rate of the structure, which is highly sensitive to geometric and structural designs. The acceleration of a structure is determined based on its self-weight, global stiffness, and height, but also on dynamic parameters such as natural frequency and structural damping. During the preliminary design phase, some relevant parameters which highly influence the global stiffness and stability of the structure are selected, such as building height, stability system design and connection rigidity. The selection of these parameters determines the dynamic response of the structure; however, due to the complexity of dynamic studies, finite elements models (FEM) are required to accurately predict the effect of the parameters on the acceleration of the structure. However, FEM are time consuming and computationally expensive, for which they are usually omitted during the preliminary design phase [26]. Studying the influence of preliminary design parameter selection on the dynamic response of timber high-rise structures can provide crucial insight for the structural designers on the behaviour of these structures and early design opportunities, assessing them in making well-argued decisions during the preliminary design phase. The insight provided to structural designers may prevent significant changes at a later design phase, decreasing the risk of cost underestimation and deviations from the original architectural design.

1.3 Goals and Objectives

Goals

The main goal of this research project is to perform a parametric study to determine the influence of stability system design, connection stiffness, and building height on the design of timber high-rise buildings based on the wind-induced dynamic behaviour. The results of this study can assist structural engineers in making well-argued decisions during the preliminary design phase.

Objectives

In order to achieve the goal of the investigation, the following objectives are set:

1. Determine the acceptable ranges for the different preliminary design parameters and design constraints
2. Develop a parametric model incorporating the preliminary design parameters and design constraints
3. Develop a tool to visualize the influence of the preliminary design parameters on the design of timber high-rise buildings

1.4 Research Questions and Outline

The report is divided as shown in figure 1.3. Each chapter provides an answer to individual research questions which will provide sufficient insight to answer the following main research question.

What is the influence of stability system design, connection stiffness, and building height on the structural design of timber high-rise buildings based on the wind-induced dynamic response?

Part I - Literature Review

Part I consists of a literature study on timber high-rise buildings, and wind engineering. The goal of this section is to collect sufficient information to fulfil the first objective of the investigation, and to determine the parameters and constraints that must be incorporated into the model.

- Chapter 2: Timber High-Rise Buildings

What are the most influential design parameters for the design of timber high-rises?

- Chapter 3: Wind Engineering

How can the dynamic behaviour of a high-rise structure be quantified?

Part II - Sensitivity Study

Part II contains the core of the investigation, focusing on the development of the parametric model and the tools to visualise the influence of the parameters on the design of timber high-rises.

- Chapter 4: Parametric Model

How can a representative 2D model to collect data for the parametric study be developed?

- Chapter 5: Parametric Study

How can the data from the sensitivity study be used in the preliminary design of a timber high-rise?

Part III - Research Outcome

Part III summarizes the findings of the investigation and discusses relevant trends and observations from the data collected.

- Chapter 6: Results and Discussion

Which design parameters have the most influence on the design of timber high-rises?

- Chapter 7: Conclusions and Recommendations

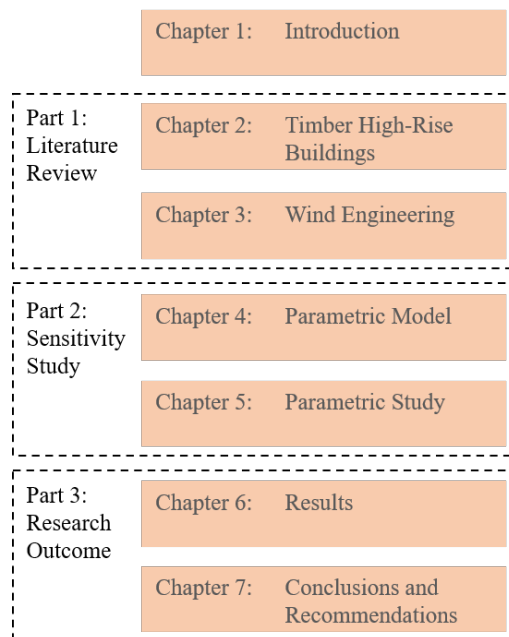


Figure 1.3: Thesis Outline

1.5 Methodology

Literature Review

The literature review is divided into two chapters which together provide sufficient insight on the behavior of timber high-rise buildings in order to build a functional parametric model which integrates all of the preliminary design parameters and is bounded by the design constraints. In order to achieve this, the literature review also focuses on researching methods to quantify the design parameters and constraints.

Parametric Model

Once all the relevant methodology and information is collected during the literature review, a parametric model incorporating all the design parameters is developed. The output of this model is the amount of material per unit height, as well as the net floor area which is obtained by the set constraints. For the purposes of this investigation, the design constraints are acceleration, interstorey drift, member resistance, and global deflection.

Parametric Study

The purpose of developing the multi-parameter parametric model is to collect sufficient data on different combinations of parameters to determine their impact on the design of the structure. The data collected is used to develop a tool that visualizes the influence of the parameters which could be used as a guide for the preliminary design of timber structures.

1.6 Scope

The stability system selection for this investigation is limited to individual systems that incorporate only timber load-bearing and stabilizing elements. However, due to current conventions in the industry, the connections between the structural members include steel elements. Different stability systems include various types of connections, but due to limited available literature, the influence of rotational stiffness on the design is only assessed for column-beam connections. The structural verification for each design alternative is done by checking for compliance with ultimate limit state and serviceability limit state criteria. Fire limit state is considered outside the scope of this investigation and assumed to comply with regulations due to design for encapsulation.

2 Timber High Rise Buildings

The implementation of timber as the main load bearing material for the design of mid- and high-rise structures can be of great influence for reducing the environmental footprint of the construction industry. However, due the behavior of high-rise structures and the material properties of timber, their design can become significantly challenging, especially during a preliminary design phase. Determining the influence that certain parameters have on their design can assist structural engineers in making well-argued decisions during a preliminary design phase, decreasing the complexity of the required calculations, and reducing the potential for budget underestimations. The most important criterion for performing a parametric study for the design of timber high-rises is determining the most influential design parameters which will provide structural engineers the most insight on the behavior of this type of structures. The main goal of this chapter is to study the structural and dynamic behavior of timber high-rise structures, as well as to gain insight on the design of existing structures to determine the parameters whose influence will be studied during this investigation. This chapter will focus on answering the following research question:

What are the most influential design parameters for the design of timber high-rises?

2.1 High-Rise Structural Design

Smith and Coull (1991) define a high-rise as a structure whose design is governed by the lateral forces caused by wind or earthquake actions due to its height. In addition to this definition, it has been proven that self-weight and global stiffness also play a big role on the acceleration of a building, for which the height at which this happens can vary for different materials. For the purpose of this investigation, buildings whose design is governed by their dynamic behaviour will be considered high-rise.

Most structures are designed using Ultimate Limit State (ULS) and Serviceability Limit State (SLS) and this is done to ensure structural capacity and user comfort. ULS ensures that that structural elements in the building have enough capacity to withstand critical loads like strong earthquakes, while SLS checks that the entire structure remains functional during frequent high loads, such as wind [3]. The design of high-rise structures will be influenced by ULS criteria; however, SLS will usually govern the design. The serviceability limit state of a high-rise structure can be divided into two main criteria which are maximum lateral displacement and acceleration, both of which are determined based on the dynamic behaviour of the structure.

2.1.1 Strength

The ultimate limit state criteria for the structure will be translated into the strength of the structural elements. The structural capacity of an element will be determined by its material and cross-sectional properties, which together will dictate the maximum allowable stress the element can withstand. In order to determine if an element has sufficient strength, this capacity needs to be compared to the forces and stresses caused by the critical load combination, which can occur at any point in the building's lifetime [35]. Determining the structural capacity of individual elements is very critical in order to prevent member failure, which could lead to a progressive collapse. The design of structural elements goes beyond its material and cross-sectional properties, given that the rigidity of the connection will determine the load distribution along the elements.

The vertical and horizontal loads applied on the building need to be taken by the structural system and transferred to the foundations. The stress distribution along the height of the structure due to the applied loads can be seen on figure figure 2.1. The maximum stress at the bottom will be used for the design of the foundations, and this will depend on both the externally applied load and the load-bearing structure. Due to the nature of the vertical loading, which only loads the structure axially, it will only cause compression loads at the bottom of the structure. However, the horizontal loads will create bending stresses which will cause both tension and compression at the bottom of the structure. The magnitude of these stresses combined with the load-bearing structure design will determine if the foundation piles carry both tension and compression forces, or only compression forces, which will play a big role in the material selection for their design in order to ensure sufficient strength to carry the transferred loads [3].

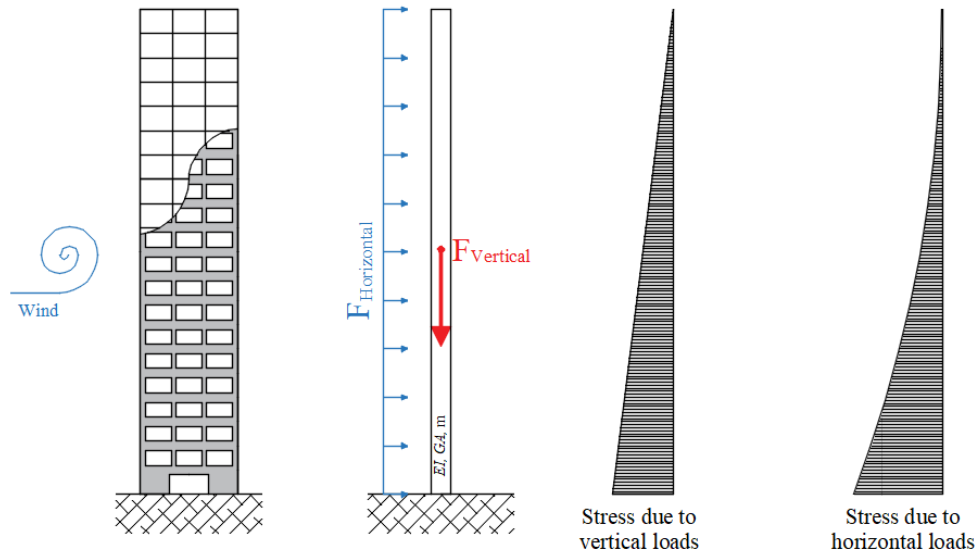


Figure 2.1: *Stress distribution along height of high-rise structures due to vertical and horizontal loads*

2.1.2 Stability

Stability is a criteria that is relevant for both ULS and SLS. In terms of ULS the design focus is on the slenderness and vertical loading of the building. The slenderness will increase the potential of the structure to tip over and in order ensure that this does not occur the moment produced by the horizontal load is compared to the moment resistance caused by the vertical loading and it needs show enough capacity to keep the structure in place [3].

$$M_{vertical} = \frac{1}{2} \cdot F_{vertical} \cdot width \quad (2.1)$$

$$M_{horizontal} = \frac{1}{2} \cdot F_{horizontal} \cdot height^2 \quad (2.2)$$

$$M_{vertical} > M_{horizontal} \quad (2.3)$$

SLS focuses on the user comfort and in terms of stability it needs to check that the deflections at the top of the structure, remain below the limit. According to Eurocode NEN-EN 1991-1-1

(EC1) and the Dutch National Annex, for high-rise structure it is recommended to keep the maximum deformation under 1/500 of the structural height. This limit mitigates the need to take into account the influence of second order effects and ensures that the building remains functional [35].

The global stiffness, which is proportional to the design of the load bearing structure, will determine the magnitude of the maximum deflection. As seen on figure figure 2.1, high-rise buildings can be modelled as a clamped beam with a given bending stiffness (EI) and shear stiffness (GA), which are determined based on the structural floor plan distribution. High rigidity systems will significantly increase the magnitude of the shear stiffness (GA), making the shear deformations almost negligible. However, for slender structure such as high-rises, both bending and shear deformations are considered, with a predicted behaviour as seen in figure figure 2.2, this type of system is also known as Timoshenko beams [35]. The behaviour of such structures is described using formula 2.4.

$$q(z) = EI \cdot \frac{d^4 u}{dz^4} + GA \cdot \frac{d^2 u}{dz^2} \quad (2.4)$$

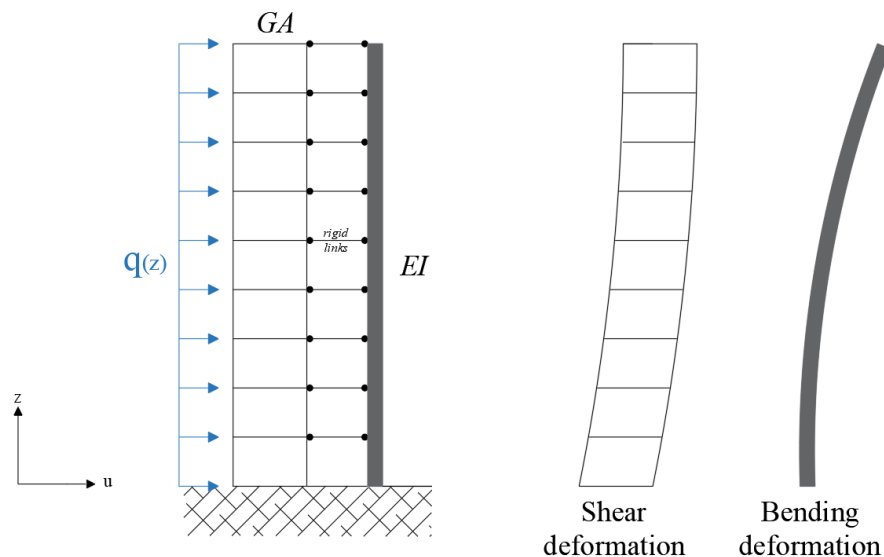


Figure 2.2: *Simplified high-rise model of shear and bending deformations*

2.2 Dynamic Behaviour

When a high-rise structure is excited by a horizontal force such as wind, it will start oscillating at a certain acceleration whose magnitude will determine the level of comfort of the users, this is known as the dynamic behaviour of high-rises. The magnitude of the acceleration is determined by various design parameters such as building height, self-weight and global stiffness, but it is also influenced by some dynamic parameters such as natural frequency and structural damping. Due to the influence of different parameters, dynamic studies are very complex, and in order to accurately predict this behaviour finite element models are needed. However, it is possible to determine the approximate behaviour by using simplified models, which will be addressed in chapter 3.

The acceleration of a building is the parameter used to quantify the dynamic behaviour of a structure. As previously mentioned, this parameter is determined by the interaction of various structural and dynamic parameters, after being excited by the wind. High accelerations are not necessarily critical for the integrity of the structure, but they can cause fear and discomfort on the users. Eurocode, as well as some other building regulations, present acceleration limits in the form of recommended ranges which have different effects on human perception levels as seen on table table 2.1.

Range	Acceleration [m/s^2]	Effect
1	< 0.05	Humans cannot perceive motion
2	0.05 - 0.10	Sensitive people can perceive motion; hanging objects may move slightly
3	0.10 - 0.25	Majority of people will perceive motion; level of motion may affect desk work; long-term exposure may produce motion sickness
4	0.25 - 0.4	Desk work becomes difficult; ambulation still possible
5	0.40 - 0.5	People strongly perceive motion
6	0.50 - 0.60	Most people cannot tolerate motion and are unable to walk naturally
7	0.60 - 0.70	People cannot walk or tolerate motion
8	> 0.85	Objects begin to fall and people may be injured

Table 2.1: *Human comfort levels based on building accelerations [35]*

2.3 Material Properties

The mechanical properties of timber depend on different parameters such as species, moisture content and loading direction [35]. Eurocode classifies the structural classes based on their bending strength and the type of material used. The mechanical properties of glulam are based on those of the structural class which was used to create the built-up element; however, the interaction of the glue and the different layers, enhance their mechanical properties. Product standard EN-14080:2005, provides tabulated values for different glulam classes with depths larger than 600 mm and lamination thickness larger than 40 mm. Table 2.2 shows the mechanical properties for some of the most commonly used homogeneous glulam classes.

Property	Symbol	GL 24h	GL 28h	GL 32h
Bending strength	$f_{m,g,k}$	24	28	32
Tensile strength	$f_{t,0,g,k}$	19,2	22,3	25,6
	$f_{t,90,g,k}$		0,5	
Compression strength	$f_{c,0,g,k}$	24	28	32
	$f_{c,90,g,k}$		2,5	
Shear strength	$f_{v,g,k}$		3,5	
Rolling shear strength	$f_{r,g,k}$		1,2	
Modulus of elasticity	$E_{0,g,mean}$	11500	12600	14200
	$E_{0,g,05}$	9600	10500	11800
	$E_{90,g,mean}$		300	
	$E_{90,g,05}$		250	
Shear modulus	$G_{g,mean}$		650	
	$G_{g,05}$		540	
Rolling shear modulus	$G_{r,g,mean}$		65	
	$G_{r,g,05}$		54	
Density	$\rho_{g,k}$	385	425	440
	$\rho_{g,mean}$	420	460	490

Table 2.2: *Product standard EN-14080:2005 Glulam mechanical properties*

The mechanical properties of CLT are also based on those of the base material, which for CLT the most used lamellae structural class is C24. The interaction of the perpendicular layers will have a significant influence on the strength and anisotropy of the material. The density of the material is usually assumed to remain constant, unless the lamination thickness is less than 10 mm, where the strength of the adhesive would start to play a big role. Table 2.3 shows the mechanical properties for CLT using C24 lamellae as provided by product standard EN-338 using $k_{mod} = 0,8$ and $\gamma_m = 1,25$.

Property	Symbol	C24	Units
Density			
Characteristic minimum bulk density	ρ_k	350	kg/m^3
Mean bulk density	ρ_{mean}	420	kg/m^3
Stiffness			
Modulus of Elasticity	$E_{0,mean}$	11000	N/mm^2
	$E_{0,05}$	7400	N/mm^2
	$E_{90,mean}$	370	N/mm^2
Shear Modulus	$G_{0,mean}$	690	N/mm^2
Strength			
Flexural strength	$f_{m,d}$	15,3	N/mm^2
Tensile strength	$f_{t,0,d}$	9,3	N/mm^2
Compressive strength	$f_{c,0,d}$	13,4	N/mm^2
	$f_{c,90,d}$	1,6	N/mm^2

Table 2.3: *Mechanical properties of C24 CLT according to EN-338*

2.4 Existing Structures

Figure 1.2 shows a list of the tallest completed buildings in the world which use timber as the main load bearing material. In order to determine the design parameters which could potentially have a bigger impact on the design of such structures, it is important to understand the architectural and structural design of these existing structures, for which a brief description of the three tallest timber buildings in the world will be presented.

2.4.1 Treet, Norway

General Description

The Tree (Treet) is a 14-storey timber building inaugurated on Spring 2015, becoming the tallest of its kind at the time [2]. It primarily serves as a residential building, incorporating 62 apartments. The structural design was done by SWECO, Norway, who calculated that the load bearing structure will bind more than 1000 tonnes of CO₂ [37] during its lifetime.



Figure 2.3: *The Tree, Norway* [2]

Stability System Design

The stability system of Treet consists of glulam frame and trusses along the facade, which provide sufficient lateral stability to the structure, to withstand the wind loads. CLT walls are used as a core to transport the vertical loads from the elevators and emergency stairs [2]. The building incorporates prefabricated modulus made out of CLT panels and they enclose four storeys per element. Between the modules, concrete slabs are added in order to provide vertical load transfer as well as reinforcement for the dynamic behaviour of the structure. The wind loads cause tensile forces on the columns and diagonal elements, which are transferred to the concrete foundations by the addition of anchoring joints [2]. The loads from the facade and balconies are taken by the external trusses.

2.4.2 Brock Commons, Vancouver

General Description

The Vancouver Brock Commons serves as a student residential building for the University of British Columbia (UBA). It was completed during Fall 2017, becoming the first and tallest mass timber, structural steel and reinforced concrete hybrid building in the world, with a height of 54 meters [6]. It was estimated that the load bearing structure will bind more than 1753 tonnes of CO₂ and that the incorporation of mass timber had a reduction of approximately 679 tonnes of CO₂ on the footprint of the construction [6].



Figure 2.4: *Brock Commons, Vancouver [6]*

Stability System Design

The stability system of Brock Commons consists of a timber frame and two concrete cores to counteract the building's slenderness in one direction. The lateral stability was provided by the concrete floor slabs enclosed by CLT panels, which transferred the loads to the concrete cores [6]. The main challenge of this hybrid structure was the difference in axial shortening, which could cause cracking over the elements, so thick shim steel plates were added at column-to-column connections, decreasing the axial shortening of the timber elements [6]. Due to the complexity of the design, a full 3D model was used in order to make decisions in terms of fabrication and construction.

2.4.3 Mjøstårnet, Norway

General Description

Mjøstårnet was completed during Spring 2019 and it is currently the tallest framed mass timber building in the world with 18 storeys and a structural height of 84 meters. Mjøstårnet incorporated sustainability into the design by local sourcing of the material and green assembly of the structure, where all elements were prefabricated and assembled on-site in order to reduce the amount of waste produced and enhance the flexibility of the design [1].



Figure 2.5: *Mjøstårnet, Norway [1]*

Stability System Design

The stability system of Mjøstårnet consists of a primary system which provides lateral stability to the structure and counteracts the wind loads and a secondary system which carries the vertical loads. The primary system consists of a glulam frame and external trusses as well as CLT floor slabs which transfer the loads and increases the global stiffness. In order to account for the dynamic behaviour of the structure, concrete floors were added on the last 6 storeys, increasing the self-weight of the structure and increasing its natural frequency. A full finite element model was built in order to evaluate the dynamic behaviour of the structure, where a structural damping of 1,8% was assumed to check that the accelerations complied with code regulations. Moreover, the secondary load bearing structure is formed by a CLT core, which does not contribute to the lateral stability of the structure but serves to transfer the vertical loads from the elevators and emergency stairs to the foundations.

2.5 Fire Safety

Timber is a combustible material, which presents a high risk in terms of the fire safety of a building, especially high-rises. Combustible materials burn, and this not only affects the integrity of the material itself, but it also contributes to the propagation of the fire and the production of smoke. In terms of the structural design of a building the focus will be the fire resistance and the degradation of the mechanical properties of the members exposed to fire. When timber is exposed to heat a process called pyrolysis initiates, where combustible gases are produced, and mass is lost. During this process a charred layer starts to form on the surfaces that are directly exposed, reducing the effective cross-section of the member. The char layer does not carry any loads, which as a result decreases the mechanical properties of the element. However, it also works as a protective layer for the remaining cross-section, which slows down the degradation process [11].

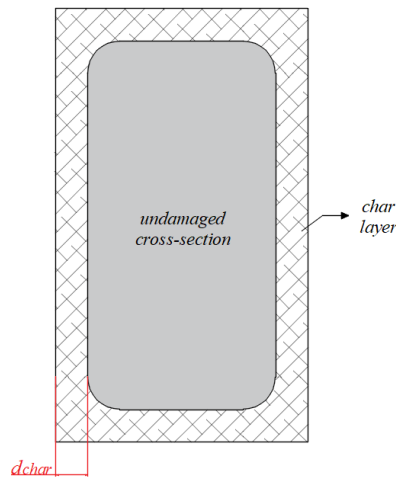


Figure 2.6: *Timber charring behaviour*

According to the Dutch Building Decree, all buildings taller than thirteen meters should be designed such that their load bearing structure can maintain its integrity during a fire of 120 minutes. In order to comply with regulations, a commonly used methodology for timber and steel buildings is to incorporate design for encapsulation. Full or partial encapsulation can be achieved by enclosing the load bearing elements using panels which will delay their contact with fire [15]. The thickness and material of the panels will determine the encapsulation time, given

that they will also char and after a certain time they will leave the load bearing elements exposed to the fire. The encapsulation time can be calculated using formula equation (2.5). Eurocode 1995-1-2 provides tabulated values for the charring rate of different unprotected timber materials, which can be seen in the table table 2.4. The tabulated values are based on standard ISO-834 exposure and assumes a linear behaviour of the material with a constant charring rate [7].

$$d_{char} = \beta \cdot t \quad (2.5)$$

β = rate of charring *mm/min*
 t = time of exposure to fire *min*

Design charring rates	β_0 <i>mm/min</i>	β_N <i>mm/min</i>
Softwood and beech		
Glued laminated timber with a characteristic density of $> 290kg/m^3$	0.65	0.70
Solid timber with a characteristic density of $> 290kg/m^3$	0.65	0.80
Hardwood		
Solid or glulam hardwood with a characteristic density of $290kg/m^3$	0.65	0.70
Solid or glulam hardwood with a characteristic density of $> 450kg/m^3$	0.50	0.55
LVL		
With a characteristic density of $> 480kg/m^3$	0.65	0.70
Panels		
Wood panelling	0.90	
Plywood	1.00	
Wood-based panels other than plywood	0.90	

Table 2.4: Charring rates according to Eurocode 1995-1-2

2.6 Conclusions

Throughout this chapter it was seen that in terms of strength, stability and dynamic behaviour, the most important parameters for the structural design of timber high-rise structures are building height and global stiffness. Building height is a design parameter on its own; however, the global stiffness of a building will be influenced by many other parameters such as stability system design, connection stiffness and member sizes. It was also seen that the current tallest timber structures in the world use similar stability system designs such as glulam rigid frame, CLT core, and glulam external trusses. Finally, it was concluded that due to timber's combustible nature, fire safety plays a big role on the design of the structure. However, previous studies have shown that the fire safety conditions can be fulfilled by incorporating design for encapsulation as well as other active fire protections such as sprinkler systems.

3 Wind Engineering

The design of timber high-rise structures will be governed by the dynamic behavior caused by the horizontal wind load acting along its height. In order to design such structures, it is critical to understand the behavior, and influencing factors of the wind load and the response of the structure. The dynamic response of the structure will be influenced by various parameters; however, it can be estimated using simplified models provided by building codes. Simplified models are commonly developed using empirical formulation taken from experimental data which is commonly collected from steel and concrete elements. In order to use these simplified methodologies for timber structures, it is important to understand the assumptions that are made and if they can be applied to timber theory. The main goal of this chapter is to study the nature of the wind load acting on the structure and determine simplified models which can be used to estimate their response. This chapter will focus on answering the following research question:

How can the dynamic behaviour of a high-rise structure be quantified?

3.1 Wind Load

The wind load can be defined as the pressure applied on objects that obstruct the flow of air. This pressure increases along the height of these obstructing objects and can be turbulent towards the bottom due to the interaction with other objects [13]. Due to their significant height, high-rise structures are exposed to high wind loads and according to Oosterhout (1996) their response can be divided into three components as shown in figure 3.1, and each component will be critical for different structure shapes [24].

- Along-wind response: Critical for buildings with a width significantly larger than its depth
- Cross-wind response: Critical for buildings with cylindrical or square shapes
- Torsional response: Critical for buildings with asymmetrical shapes in terms of mass and stiffness

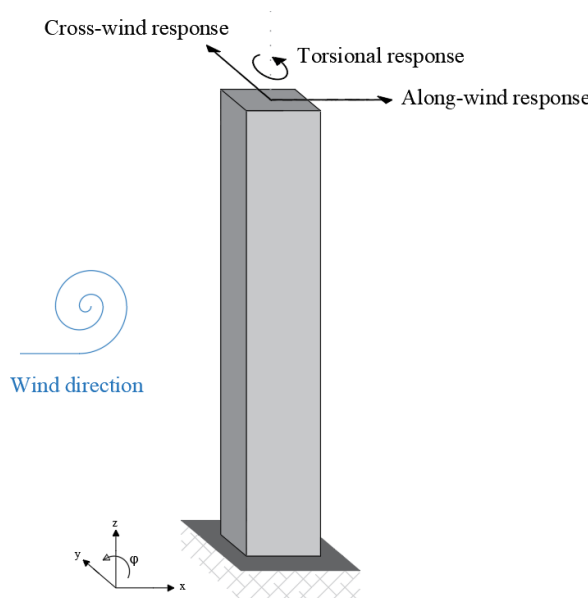


Figure 3.1: *Building dynamic response due to wind load*

In order to determine the wind pressure applied on the structure, it is critical to determine the velocity at which the air flow (wind) is travelling and impacting the building. The wind velocity will consist of two components, constant and fluctuating. The constant component of the wind will only have an effect on the direction at which the wind is applied. The fluctuating component will act along the perpendicular direction as well as the height and it will depend on the turbulence of the wind [13].

3.1.1 Wind Pressure

The wind pressure acting on the structure, can be determined using Eurocode NEN-EN 1991-1-4 (EC1-4) following the procedure shown in Appendix A. The wind pressure is highly dependent on the location of the structure, since it will have an effect on the wind velocity and the coefficients which represent the probability of wind occurrence and the turbulence of the air flow. Moreover, the wind pressure will depend on the surface area interacting with the air flow, which is determined by the width and height of the structure. For the purpose of this investigation it was assumed that the width and depth of the structure will remain constant at 30 meters, while the height will change for the different designs. Figure 3.2, shows the calculated wind pressure for different heights and their changing distribution following the methodology explained in Appendix A.

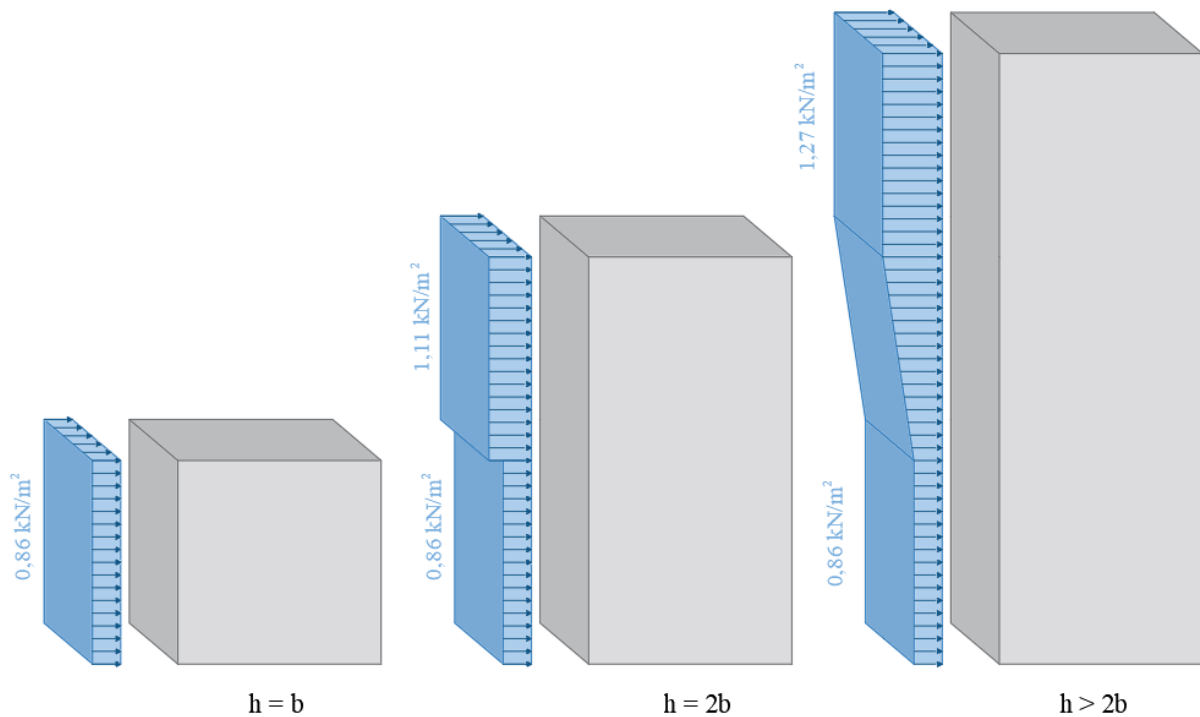


Figure 3.2: *Wind pressure distribution according to structural height*

The wind pressure causes a moment which needs to be resisted by the stability system of the structure. Each stability system has a different distribution of the moment, which will be addressed in section 4.1.1. However, regardless of the stability system, all structures will follow the behaviour shown in figure 3.3, where the wind pressure is taken by the façade, which transfers it to the floors based on the tributary width determined by the structural floor height.

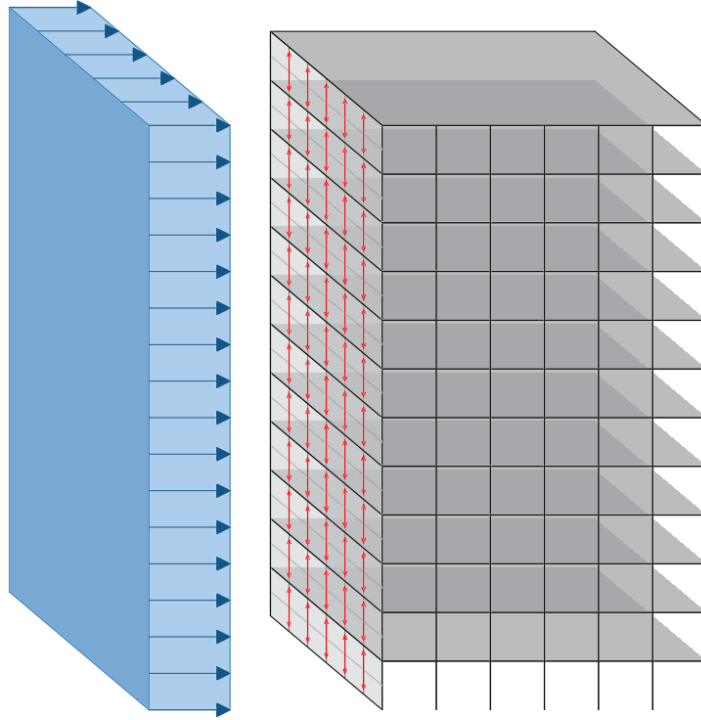


Figure 3.3: *Wind pressure distribution for different stability systems*

3.2 Dynamic Response

Section 2.2 explains that acceleration is the most commonly used parameter to quantify the dynamic behaviour of a structure, and that due to its dependency on various design, structural and dynamic parameters, determining its magnitude is commonly done using a full scale finite element model. However, some building codes have developed empirical formulae based on experimental data, to estimate its magnitude. Figure 3.1 shows that when a structure is exposed to lateral loads such as wind, it will have an along- and cross-wind response, which results in different magnitudes for the acceleration across both directions and the methodologies used to estimate them will be explained in the following sections.

3.2.1 Natural Frequency

The natural frequency of a system is defined as the frequency at which an undamped structure oscillates after being excited by an external force [24]. When an undamped structure is excited by a dynamic load such as wind, acting at the same frequency as its natural frequency, the amplitude of the response becomes infinite, significantly affecting its integrity [36]. The magnitude of the natural frequency depends on the global stiffness, geometry, and mass distribution of the structure, as well as, the damping of the system [35]. Eurocode presents an empirical formula which can be used to estimate the natural frequency ($n_{1,x}$) of a structure based on its height (h), as shown in equation 3.1.

$$n_{1,x} = \frac{46}{h} \quad (3.1)$$

However, this formula has been developed using data collected from reinforced concrete and steel buildings, which have significantly different global stiffness and damping than timber structures.

In order to study the natural frequency for different materials as well as more complex stability systems, van Oosterhout (1996) developed a method based on the maximum lateral displacement of the building, the distribution of mass, and the shear and bending stiffness, as it can be seen in equation E.6.

$$n_{1,x} = f(\alpha h) \cdot \sqrt{\frac{q_w \cdot h}{\mu \cdot \delta_{max}}} \quad (3.2)$$

$$\alpha^2 = \frac{(GA)_{tot}}{(EI)_{tot}} \quad (3.3)$$

- q_w = uniformly distributed horizontal load caused by wind
- h = height of the structure
- μ = mass distribution over height
- δ_{max} = maximum lateral horizontal displacement

The function $f(\alpha h)$ depends on the modal behaviour of the structure, which is related to the ratio of the shear and bending stiffnesses. In order to approximate the value of this function, formulae 3.4 and 3.5 can be used. However, it is presented that when the structure acts in pure shear $f(\alpha h) = 0.176$ and when the structure acts in pure bending $f(\alpha h) = 0.198$ [24]

$$0 \leq \alpha h \leq 1$$

$$f(\alpha h) = \sqrt{\left[\frac{0.3131}{(\alpha h)^2} + 0.1148 \right] \cdot \left[\frac{-1 - \alpha h \cdot \sinh(\alpha h) + \cosh(\alpha h)}{(\alpha h)^2 \cdot \cosh(\alpha h)} + \frac{1}{2} \right]} \quad (3.4)$$

$$\alpha h \geq 1$$

$$f(\alpha h) = \sqrt{\left[\frac{0.2365}{(\alpha h - 0.3)^{1.22}} + \frac{1}{16} \right] \cdot \left[\frac{-1 - \alpha h \cdot \sinh(\alpha h) + \cosh(\alpha h)}{(\alpha h)^2 \cdot \cosh(\alpha h)} + \frac{1}{2} \right]} \quad (3.5)$$

3.2.2 Structural Damping

As previously mentioned, in theory when the frequency of the exciting force equals the natural frequency of the undamped structure, the response of the system will experience infinite amplitude, also known as structural resonance. However, in reality, infinite amplitude of the response does not occur, given that the structure dissipates energy due to the work done by each structural component. The magnitude of the energy dissipated is known as structural damping, and it is defined by the summation of the energy dissipated by individual elements such as material, stability system design, and foundation design [9]. Eurocode provides approximate structural damping coefficients for reinforced concrete, steel and composite buildings as well as for timber bridges, as seen in table 3.1. However, it does not provide values for timber buildings.

Structure	ξ_s
Reinforced concrete buildings	1.59%
Steel buildings	0.80%
Composite buildings	1.28%
Timber bridges	0.96-1.91%

Table 3.1: Eurocode structural damping coefficients

In order to estimate the structural damping of timber buildings, experimental data is needed. Feldmann (2016), presented an experimental investigation, in which on-site data was collected for 10 different timber structures with a height ranging between 24-100 meters as seen in table 3.2. During this experiment, the frequency of the oscillations and the damping ratio of each structure was collected and it was found that the damping ratios ranged from 0.64-2.70%, which is higher than the values provided by Eurocode for reinforced concrete and steel buildings. The results obtained can be seen in figure 3.4.

Name of Structure	Height (m)	Number
Towers - Solid timber tube		
Himmelssturmer	38.4	6
Timber Tower	100	9
Towers - Timber frame		
Baumturm	44.5	3
Blumenthal	45.0	4
Haidelturm	35.2	5
Ochsenstiegl	25	8
Towers - Timber frame with cladding		
Altenbergturm	42.5	1
Augstbergturm	28.0	2
Kadernbern	30	7
Buildings - Solid timber, concrete core		
H8	23.9	10
Buildings - Solid timber, timber core		
Kampa	26.4	11
Buildings - Timber frame, concrete core		
Life Cycle Tower One	26.6	12

Table 3.2: Building data used during the Feldmanns's damping experiment

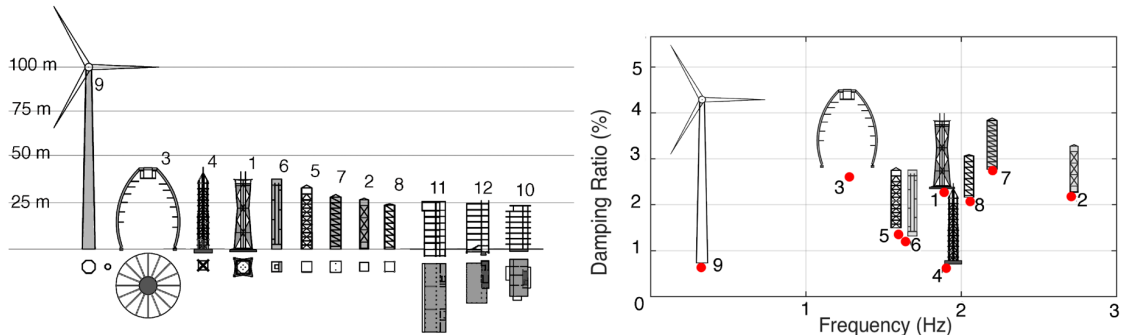


Figure 3.4: Experimental natural frequency and damping ratio of timber structures [9]

According to Petersen (2000), in order to estimate the magnitude of the structural damping of a

timber structure, the material damping of timber should be taken within the range of 0.4-0.8%, dowel type connections will provide an additional 0.6-0.9%, while glued or moment resistant connections provide an additional 0.2-0.5% [28] and foundations will provide an additional 0.1-0.3%, which will give a total structural damping which ranges from 0.7-2.1%.

3.2.3 Along-Wind Acceleration

EC1-4 states that the along-wind peak acceleration in m/s^2 of a structure can be estimated using formula 3.6:

$$a_{max}(y, z) = \sigma_{a,x}(y, z) \cdot k_p \quad (3.6)$$

$$\begin{aligned} \sigma_{a,x}(y, z) &= \text{standard deviation of the characteristic along-wind acceleration} \\ k_p &= \text{gust peak factor (see equation A.9)} \end{aligned}$$

According to EC1-4 Appendix C, the standard deviation of the characteristic along-wind acceleration ($\sigma_{a,x}(y, z)$) can be approximated using formula 3.7. The formulae used to calculate all the different parameters used in this formula can be found in Appendix A.

$$\sigma_{a,x}(y, z) = c_f \cdot \rho \cdot I_v(z) \cdot v_m^2 \cdot R \cdot \frac{K_y \cdot K_z \cdot \phi(y, z)}{\mu_{ref} \cdot \phi_{max}} \quad (3.7)$$

$$\begin{aligned} c_f &= \text{force coefficient (see equation A.18)} \\ \rho &= \text{air density} \\ I_v(z) &= \text{turbulence intensity at a specific height above the ground (see equation A.6)} \\ v_m &= \text{characteristic mean wind velocity at a specific height above the ground (see equation A.1)} \\ R &= \text{square root of the resonant response (see equation A.13)} \\ \mu_{ref} &= \text{reference mass per unit area} \\ \phi(y, z) &= \text{mode shape} \\ \phi_{max} &= \text{mode shape value at the point with maximum amplitude} \\ K_y, K_z &= \text{size reduction coefficients} \end{aligned}$$

Eurocode states that for all buildings which have a uniform horizontal mode shape and a linear vertical mode shape, the following parameters can be used:

$$\phi(y, z) = \frac{z}{h} \quad (3.8)$$

$$K_y = 1 \quad (3.9)$$

$$K_z = 3/2 \quad (3.10)$$

3.2.4 Cross-Wind Acceleration

In this direction, the turbulence of the wind can cause a phenomena called vortex shedding, which can significantly increase the effect on the structure, making it the governing design criterion [13]. Eurocode does not provide any simplified methods for estimating the cross-wind acceleration, but it provides a criterion to determine when the vortex shedding effect will take place and needs to be included in the design.

The criterion proposed by Eurocode EC1-4 in order to investigate the vortex shedding effect on the structure can be seen in formula 3.11.

$$v_{crit} \geq 1.25 \cdot v_m(z) \quad (3.11)$$

$$v_{crit} = \frac{b \cdot n_{1,x}}{S_T} \quad (3.12)$$

$$S_T = \text{strouhal number} = 0.18 - 0.06 \cdot \frac{\text{depth}}{\text{width}}$$

Given that Eurocode does not provide a method for quantifying the cross-wind response acceleration, the National Building Code of Canada (NBCC) can be use to estimate this behaviour by using formula 3.13.

$$a_w = n_{1,x}^2 \cdot k_p \cdot \sqrt{b \cdot d} \cdot \left(\frac{a_r}{\rho_B \cdot k_p \cdot \sqrt{\xi}} \right) \quad (3.13)$$

$$\begin{aligned} \rho_B &= \text{density of the building} \\ \xi &= \text{structural damping} \end{aligned}$$

$$a_r = 78.5 \cdot 10^{-3} \cdot \left[\frac{v_m(h)}{n_{1,x} \cdot \sqrt{b \cdot d}} \right]^{3.3} \quad (3.14)$$

$$v_m(h) = \text{mean wind velocity at the top of the structure}$$

3.3 Conclusions

Wind is a dynamic flow which changes over time, height and terrain type. The wind load is defined as the pressure applied on objects that obstruct this flow. EC1-4 has developed a methodology to calculate the wind speed based on a specific location, by using coefficients which take into account the return period and the roughness of the terrain. This velocity is then translated into an applied pressure considering the characteristics of the impacted surface and the response of the structure. Finally, this pressure is taken by the façade of the structure which will be in charge of distributing the load across the stability system.

The dynamic response of the structure can be quantified using the acceleration at which the structure oscillates, which is directly proportional to the applied wind load. As shown in figure

3.1 the geometry of the structure will also have an effect on the type of response. Accurately predicting the acceleration of a structure is only possible by developing full-scale finite element models. However, the magnitude of the acceleration can be estimated using simplified models such as the ones provided by EC1-4 for along-wind acceleration, and the National Building Code of Canada for the cross-wind acceleration. Simplified models are developed by incorporating design assumptions that must be considered when analyzing the data collected. The method presented by EC1-4 idealizes the building as a clamped cantilever beam, which means that the acceleration is determined by analyzing only one vibration mode. However, high-rise structures can exhibit more than one vibration mode, which can lead to underestimations of the acceleration provided by EC1-4.

The natural frequency and structural damping of the structure are determined using methods and experimental data applicable for timber high-rise structures. Oosterhout (1996) presents a method to estimate the natural frequency of the structure based on its global stiffness and mass distribution. This method estimates the natural frequency for structures acting in pure shear and structures acting in pure bending, which is determined by the stability system selected. The magnitude of the structural damping is determined based on the experimental data provided by Feldmann (2016), which concluded that the damping ratio for timber structures ranges between 0.64-2.70%. As presented in section 2.4 the damping ratio used for the structural design of Mjøstårnet was 1.8%, which is within the ranges provided by Feldmann. Due to the structural similarities between the selected stability systems and Mjøstårnet, the damping ratio for this investigation is assumed to be 1.8%, which is a conservative value based on the studied experimental data.

4 Parametric Model

The data required for performing a parametric study consist of the design output for various combinations of the relevant preliminary design parameters. The most efficient methodology for the collection of such data, is the implementation of a parametric model which can easily be adjusted. For the purpose of this investigation, the model used to collect the data for the parametric study was developed using Grasshopper, which is a visual programming language. The Grasshopper model was built based on the relevant parameters found in chapter 2, and a simple floor plan of thirty by thirty meters. The design output is found by bounding the system with the implementation of design constraints which guarantee compliance of the design with ULS and SLS regulations. Evaluating a full scale structural model for thousands of different parameter combinations is computationally expensive. Therefore, various design assumptions were made in order to reduce the complexity of the model and obtain significant data regarding the parameters influence of the design. The main goal of this chapter is to explain the design parameters, constraints, and loads which were implemented to develop the model used to collect the required data for the parametric study. Furthermore, additional design assumptions are outlined, which were made to reduce the computational cost of the study. This chapter will focus on answering the following research question:

How can a representative 2D model to collect data for the parametric study be developed?

4.1 Design Parameters

4.1.1 Stability System Design

Smith and Coull (1991) define the stability system of a structure as the combination of different structural elements which interact and provide resistance to the design loads. The structural design of high-rise structures tends to be governed by their dynamic behaviour, which means that the stability system must be designed to provide not only sufficient resistance to the design loads, but also to provide sufficient global stiffness to ensure structural integrity and user comfort. Over the last century, the height of the tallest buildings in the world has significantly increased, which has led to the development of different stability systems that enhance the global stiffness of the structure. Figure 4.1 shows the most commonly used stability systems in existing high-rise buildings, which use concrete and steel and the main load bearing and stabilizing material. The figure also shows the maximum height, in terms of number of storeys, that has been achieved using each individual system.

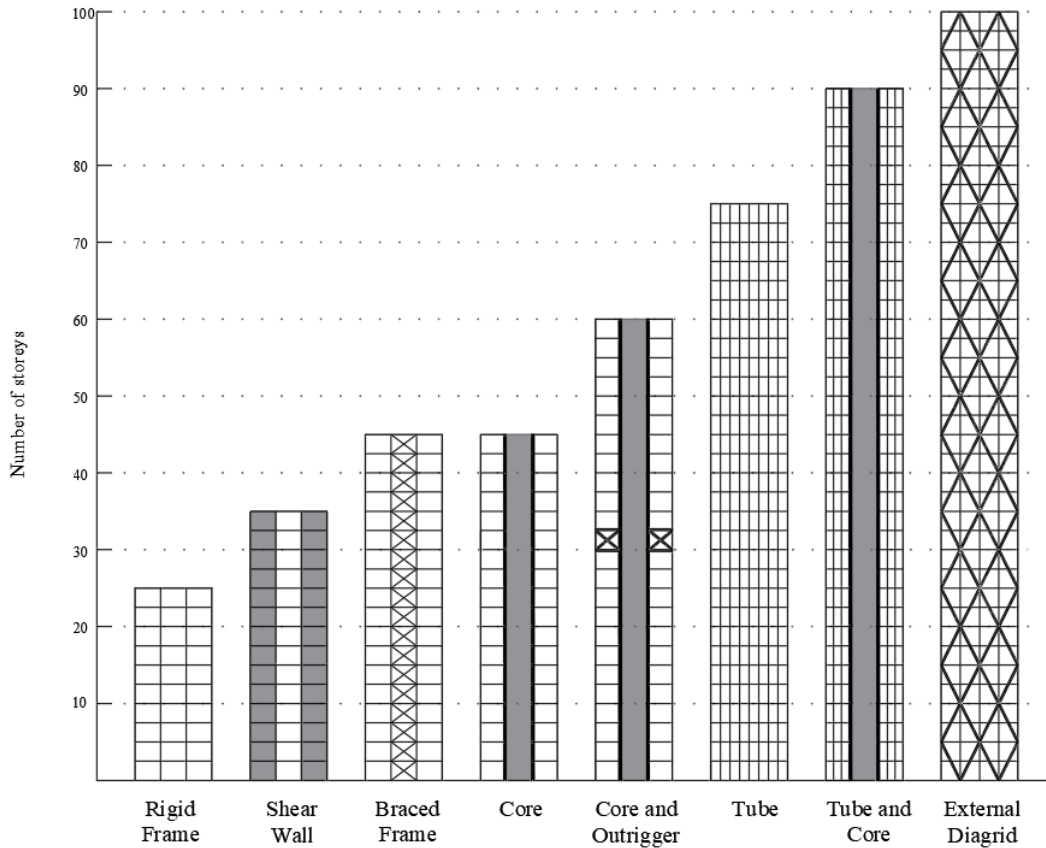


Figure 4.1: *Stability system types*

Timber stability systems for structures taller than five storeys tend to be designed strictly using timber engineered products such as glulam, CLT and other laminated products. Due to the mechanical properties and physical characteristics of these materials, not all of the stability systems seen in figure 4.1 are suitable. Mjøstårnet and Treet are the tallest buildings in the world which use timber as the main load-bearing and stabilizing material. Their stability systems incorporate elements such as glulam frame, CLT core and glulam tube bracing. The scope of this investigation focuses on studying the behaviour of three stability systems which are: glulam frame, CLT core and glulam diagrid. These systems were chosen based on the design of existing timber structures, the potential seen from figure 4.1, and the limited understanding of their individual behaviour. Most existing timber high-rise structures incorporate other stabilizing materials such as concrete cores to increase the self-weight and global stiffness of the structure. However, the goal of this investigation is to broaden the understanding of individual timber stability systems, such that sufficient stability can be achieved without incorporating concrete and steel stabilizing elements.

Glulam Frame

Frame structures rely on the interaction between beams and columns to transfer the moment caused by horizontal loads as seen in figure 4.2. The moment transfer between the structural elements is determined by the rotational stiffness of the connections, which are also responsible for the lateral stability of the building. The global stiffness of this type of structures is determined by the cross-section of the structural elements, the stiffness of the connections, and the unsupported distance between the columns, also known as effective span. The cross-section of the structural elements is limited by the capacity of manufacturers to produce and transport

larger elements, while the rotational stiffness of the connections is limited by the mechanical properties of the material and the capacity of the connectors. Finally, the effective span has an effect not only on the global stiffness of the structure, but also on the load transfer capacity of the floors, which significantly limits this parameter.

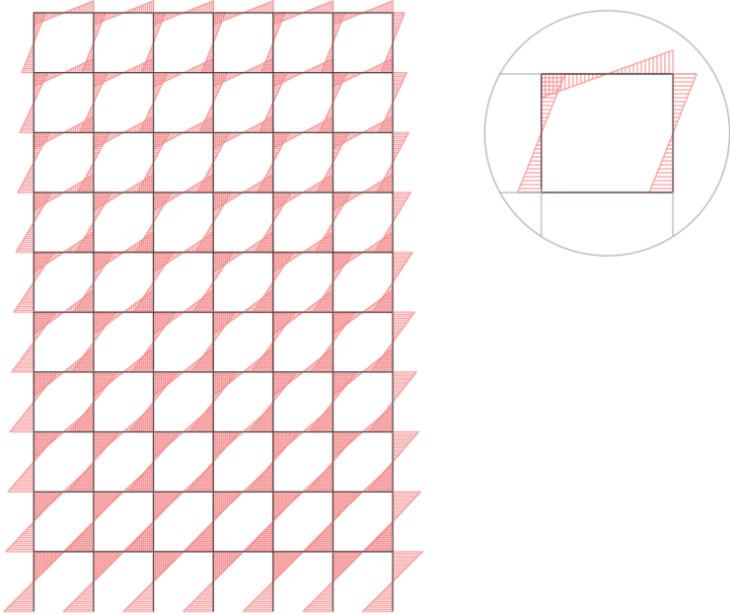


Figure 4.2: *Moment distribution in frame structures*

Two different effective spans are evaluated to determine the influence of this parameter on the dynamic response and design of the structure. Based on existing structures and the capacity of CLT floors, the selected effective span to be studied were four and six meters. Figure 4.3 shows both design configurations, together with their corresponding structural floor plan, which only shows stabilizing elements.

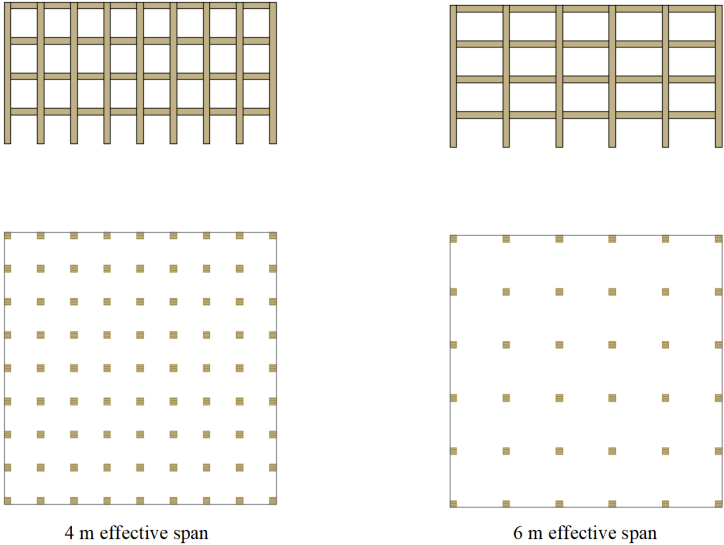


Figure 4.3: *Frame configurations*

CLT Core

Core stability systems are formed by two or more shear walls that act in orthogonal planes and interact to create a shear-resistant element which carries the moment developed by the wind load as seen in figure 4.4 [35]. This stability system is commonly used in combination with a frame which carries the vertical loads to the foundations. The global stiffness of this system is determined by the size of the core walls, as well as their cooperation with one another, also known as gamma factor. Moreover, additional global stiffness can be added by incorporating rotational stiffness in the frame connections and creating a hybrid moment transfer mechanism.

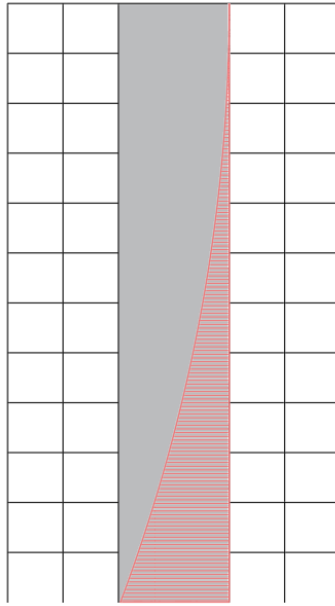


Figure 4.4: *Moment distribution in core structures*

Core stability systems are usually built using reinforced concrete; however, due to the cross-lamination of CLT, this material has the potential to be used as a substitute. The axial load transfer and interaction between the perpendicular walls (gamma factor) will differ when using CLT, and due to limited resources in the subject, several assumptions need to be made when modelling CLT cores. For the purpose of this investigation the following assumptions were made, and further elaboration can be found in Appendix D.

1. Displacements due to sliding and rocking are neglected.
2. There is no cooperation between the C-shaped cores.
3. The core is modelled using Bernoulli's beam theory.
4. Effective core width is determined to counteract shear lag effect.
5. Global stiffness is determined using Steiner's theorem.
6. Self-tapping screws (STS) will connect the core web and flanges.

Three different core widths are evaluated to determine the influence of this parameters on the dynamic response and design of the structure. Based on existing structures and the required net floor area, the selected core widths to be studied were ten, twenty and thirty percent of the building width. Figure 4.3 shows all design configurations, together with their corresponding structural floor plan. The effective span between the frame columns is taken as four meters.

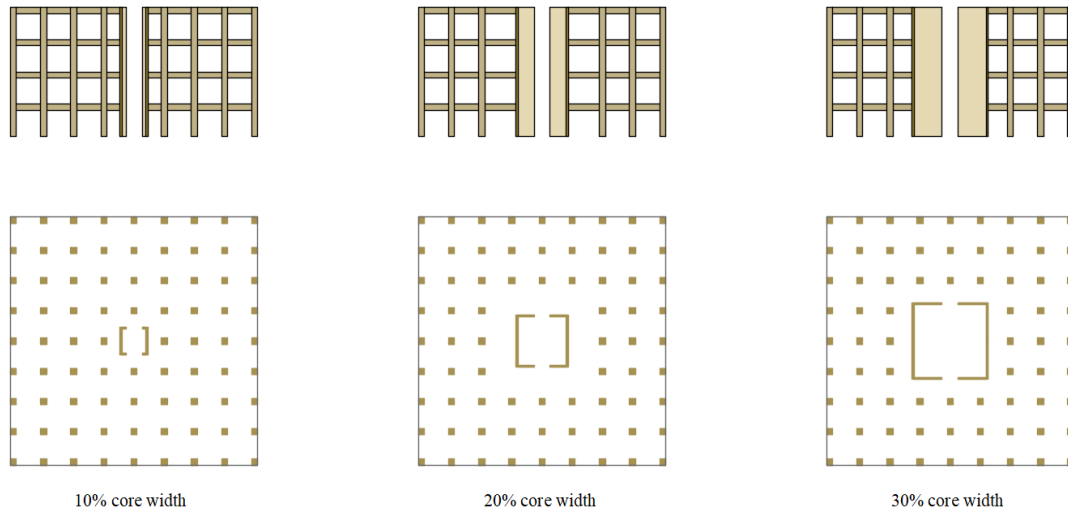


Figure 4.5: *Core configurations*

Glulam Diagrid

Diagrid structures consist of diagonal and horizontal members placed along the exterior perimeter of the building, and these members interact with each other to transfer the moment caused by the wind load as seen in figure 4.6. The figure shows that the moment is transferred by the interaction of the tension and compression developed in the diagonal members, which are stabilized by the horizontal members connecting them. This stability system is commonly used in combination with a frame which carries the vertical loads to the foundations. The global stiffness of this system relies on the triangular configuration of the exterior elements, and the efficiency of this configuration is determined by the angle of the diagonal elements.

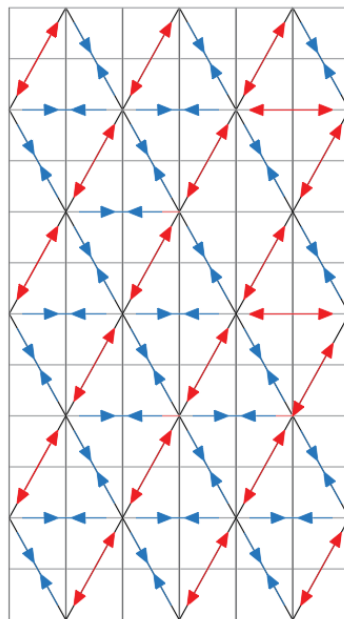


Figure 4.6: *Moment transfer in diagrid structures*

Three different diagonal angles are evaluated to determine the influence of this parameter on the dynamic response and design of the structure. The angle of the diagonals has an x and a y component, the x component corresponds with the effective span of the frame columns and the y component corresponds to the number of storeys covered by one diagonal element. During this investigation different configurations are defined by the y component of the angle. The selected diagonal angles to be studied were two, four and six storeys. Figure 4.7 shows all the design configurations, as well as the structural floor plan, which is the same for all of them. The effective span between the frame columns is taken as four meters.

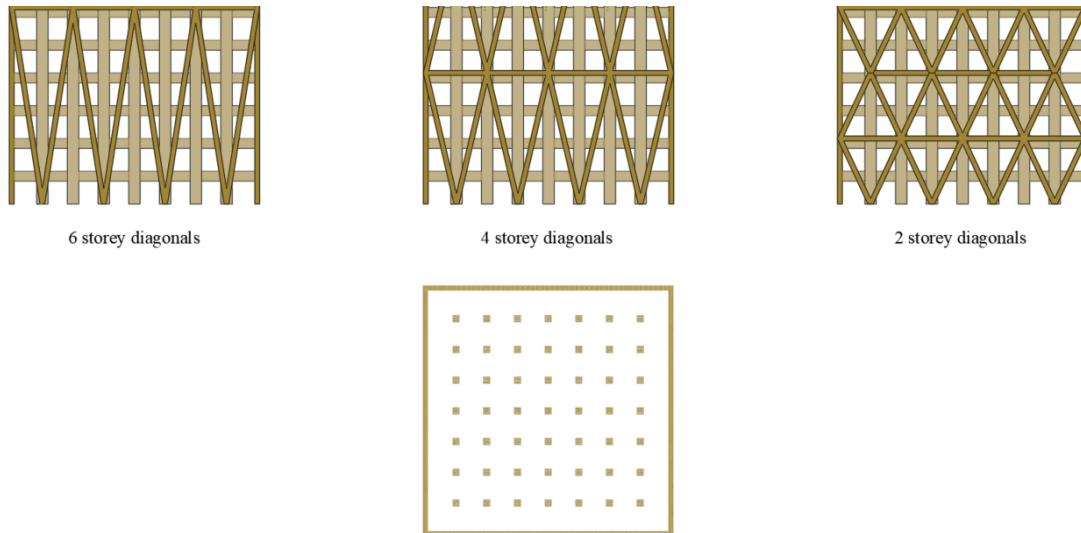


Figure 4.7: *Diagrid configurations*

4.1.2 Connection Stiffness

Some stability systems, such as frames, rely on the rigidity of the connections to provide lateral stability, which makes them highly sensitive to changes in the rotational stiffness of the joints. Traditionally when modelling timber structures, joints were assumed to be either hinged or rigid due to the lack of design methods to determine their semi-rigid behaviour [19]. However, most modern timber joints incorporating mechanical fasteners such as slotted-in steel plates and glued-in rods, provide a semi-rigid behaviour which has an effect on the moment distribution along the members, the global stiffness of the structure, and the potential of certain stability systems [14]. Currently extensive research is being done on the capacity of such connections, which is slowly being incorporated into building codes. NEN-EN 1995-1-1 (EC5) provides methodologies to determine the rotational stiffness of doweled connections with up to one slotted-in steel plate.

As previously mentioned, based on the selection of stability systems, there will be various types of connections; however, due to limited available literature, the influence of the connection stiffness on the design of timber high-rises is assessed only for column-beam connections. Appendix B.1 shows detailed drawings of the assumed configurations for the most relevant connection types. Column-beam connections will be designed using slotted-in steel plates and dowels. For the glulam frame four different rotational stiffnesses are evaluated to determine the influence of this parameter on the dynamic response and design of the structure. Based on literature and preliminary calculations which can be seen in Appendix B.3, the selected stiffnesses to be studied were 100000, 200000, 300000 and 400000 kNm/rad . For the CLT core, only two different rotational stiffnesses are evaluated, which are 100000 and 200000 kNm/rad , given that hybrid moment transfer mechanism are not commonly designed due to a significant cost increase.

Figure 4.8 shows preliminary sizes of the slotted-in steel plates and dowels that are required to achieve the different rotational stiffnesses. The procedure followed to size these elements can be found in Appendix B.2.

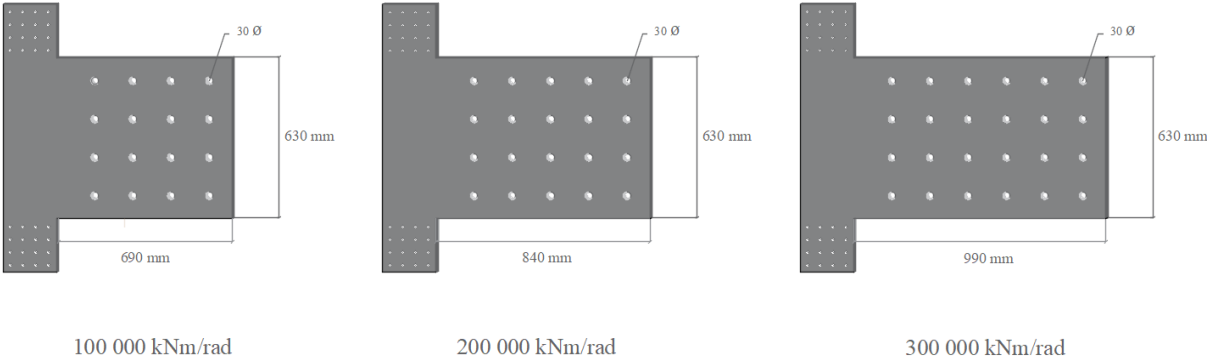


Figure 4.8: *Rotational stiffness configurations*

Incorporating rigidity to beams in two directions can significantly increase the cost of the structure and the complexity of the assembling procedure. In order to reduce the number of moment resistant connections and evaluate only feasible designs, all alternatives incorporating rotational stiffness in the column-beam connections, will have moment resistant joints only in one direction. Figure 4.9 shows an example of the configuration in one direction. This configuration will alternate for all consecutive connections, providing lateral stability to the structure. This design decision was incorporated into the 2D model, by providing only half the rotational stiffness to the connections, but calculating the moment resisted by the joint with the full stiffness.

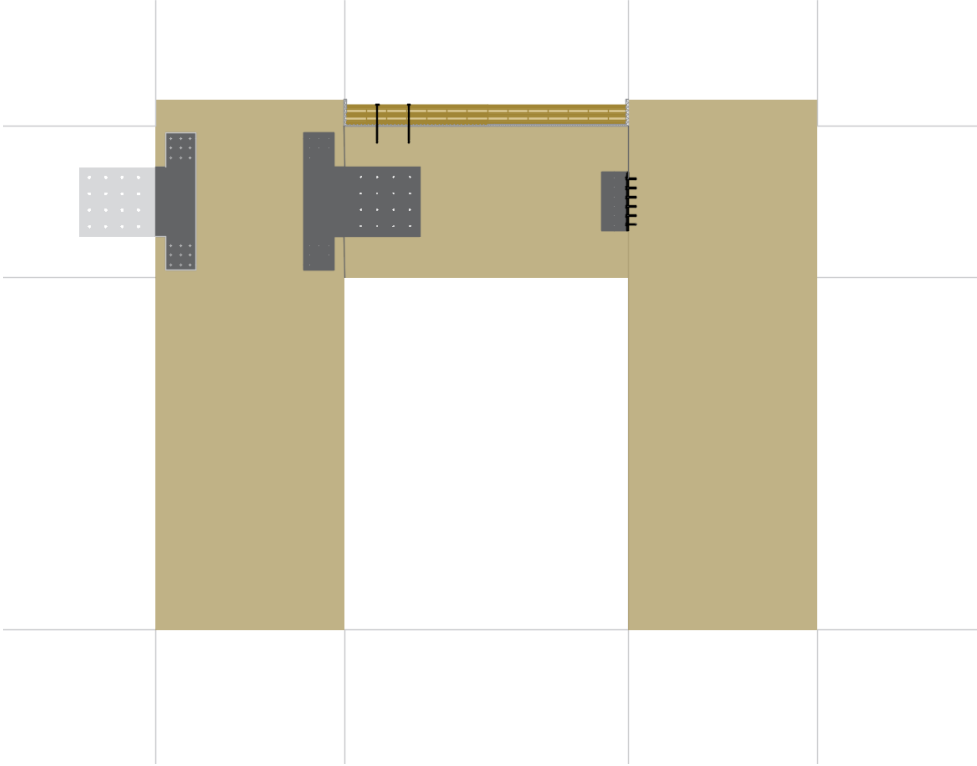


Figure 4.9: *Rotational stiffness configurations*

4.1.3 Building Height

The building height plays a significant role in the governing failure mechanism of the structure and the design of the load-bearing structure, given that taller buildings are exposed to higher vertical and horizontal loads. As previously defined, for the purpose of this investigation a high-rise building will be one whose structural design is governed by its dynamic behaviour. For timber high-rise structures it has been seen that this criterion is met for buildings as low as 30 m and a slenderness of one [2]. For the purpose of the parametric study, the building height will be taken in intervals of 10 meters starting at 30 meters until the structure reaches a height where the design constraints can not be met.

4.2 Design Constraints

4.2.1 Member Forces

Verification of Glulam Elements

The design verification of structural glulam elements is done using EC5 and EN 14080. Table 2.2 shows the characteristic strength (R_k) of glulam elements based on their structural class. In order to obtain their design strength (R_d), formula 4.1 can be used, which takes into account the load duration, service class and design safety factor. EC5 and EN 14080 state that for glulam timber elements the safety factor should be taken as $\gamma_M = 1.25$ and the selection of a modification factor, k_{mod} , should be done using table 4.1.

$$R_d = \frac{k_{mod} \cdot R_k}{\gamma_M} \quad (4.1)$$

Service class	Permanent	Long term	Medium term	Short term	Instantaneous
1	0.60	0.70	0.80	0.90	1.10
2	0.60	0.70	0.80	0.90	1.10
3	0.50	0.55	0.65	0.70	0.90

Table 4.1: Modification factor based on service and load-duration class according to EC5 and EN 14080

For ultimate limit state design, the design stress on the elements caused by the different load cases must be verified against their respective design strength, which was determined based on the mechanical properties of GL 32h. Axial, shear and bending stresses must be checked individually, as well as combined. These verifications following the validation methodology proposed by EC5 are found in Appendix C.

Verification of CLT Panels

Currently Eurocode does not provide verification methods for the design of CLT panels loaded in-plane; however, the CLT manufacturer proHolz [30] has presented a design guide based on Eurocode, which will be used for the verification of the CLT panels. In order to obtain the design strength of the elements, formula 4.1 may be used with a partial safety factor of $\gamma_M = 1.25$. The panels should be verified for ultimate limit state design of the axial and bending stresses, as well as their combined action. The verification method is shown in Appendix C.

For the verification of CLT panels that are predominantly loaded in-plane, it is assumed that the normal stresses develop in the layers parallel to the in-plane loading [30], which is known as the net area A_{net} . The net area is illustrated in figure 4.10 and obtained using formula 4.2.

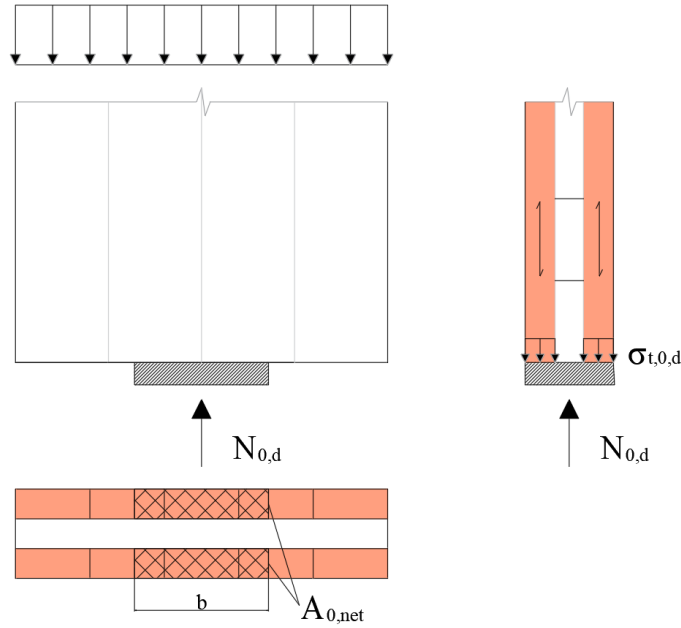


Figure 4.10: *In-plane loading CLT panel net area*

$$A_{0,net} = b \cdot d_{0,net} \quad (4.2)$$

4.2.2 Global Deflection and Interstorey Drift

Global deflection and interstorey drift are serviceability limit state criteria used to validate the design of structures loaded by lateral loads such as wind. As the name implies, global deflection (δ_{max}) studies the behaviour of the entire structure and its behaviour is determined by idealizing the building as a cantilever beam with a certain cross-sectional bending and shear stiffness as shown in figure 2.2 and the use of formula 2.4. On the other hand, interstorey drift ($\delta_{s,i}$) is referred to as the relative displacement between two consecutive storeys, and it is usually determined with the assistance of a full scale model [34]. Different building codes provide slightly different limitations for these constraints, given that they are based on collected data for existing structures. Eurocode does not provide a limiting criteria for these variables; however, the Dutch National Annex for NEN-EN 1990+A1+A1/C2 provides a limiting criteria for the global deflection of the structure as seen in formula 4.3. Smith and Coull (1991) present a criteria for limiting the interstorey drift of a structure, which is presented in formula 4.4.

$$\delta_{max} \leq \frac{h}{500} \quad (4.3)$$

$$\delta_{s,i} \leq \frac{h_s}{400} \quad (4.4)$$

- h = total height of the building
- h_s = structural storey height

4.2.3 Acceleration

Subsections 3.2.3 and 3.2.4 provide a thorough description of how to quantify the along- and cross-wind acceleration response of the structure using Eurocode EC1-4 and NBCC respectively. The serviceability limit state design of acceleration often governs the design of high-rise structures due to limitations given by human perception levels. Table 2.1 shows recommended values based on human perception and it shows that accelerations above 0.25 m/s^2 makes desk work difficult. Furthermore, acceleration should also be assessed in terms of ultimate limit state to validate the structural integrity of the design. Eurocode NEN-EN 1998-1 (EC8), which focuses on the design of earthquake resistant construction, states that the acceleration of a structure should stay below 0.39 m/s^2 to guarantee structural integrity.

4.3 System Loads

For this investigation, it was assumed that the structure is loaded both vertically and horizontally. The horizontal loads consist of the pressure created by the wind (3.1), and the vertical loads are explained in this section and determined under the assumption that the structure will be used as a residential building.

Horizontal Loads

When modelling a structure in a 2D environment, only a representative cut of the structure is analysed, which means that the pressure caused by the wind acting on the structure, must be translated into a uniformly distributed load acting on that representative cut. The width of the cut depends on the selected stability system of the structure and their moment transfer mechanism. Figure 4.11 shows the assumed representative cuts for the frame, core and diagrid stability systems, in a), b) and c) respectively. In the figure it can be seen that for the frame, the width of the cut is determined by the effective span between the columns, which is the tributary width of each bay. For the core, the width of the representative cut is taken as the entire width of the structure and this is because the core transfers the full moment caused by the wind pressure. Finally, the width of the representative cut in the diagrid equals half of the width of the structure, given that the diagrid facing the wind direction transfers the load to the two diagrids in the perpendicular direction.

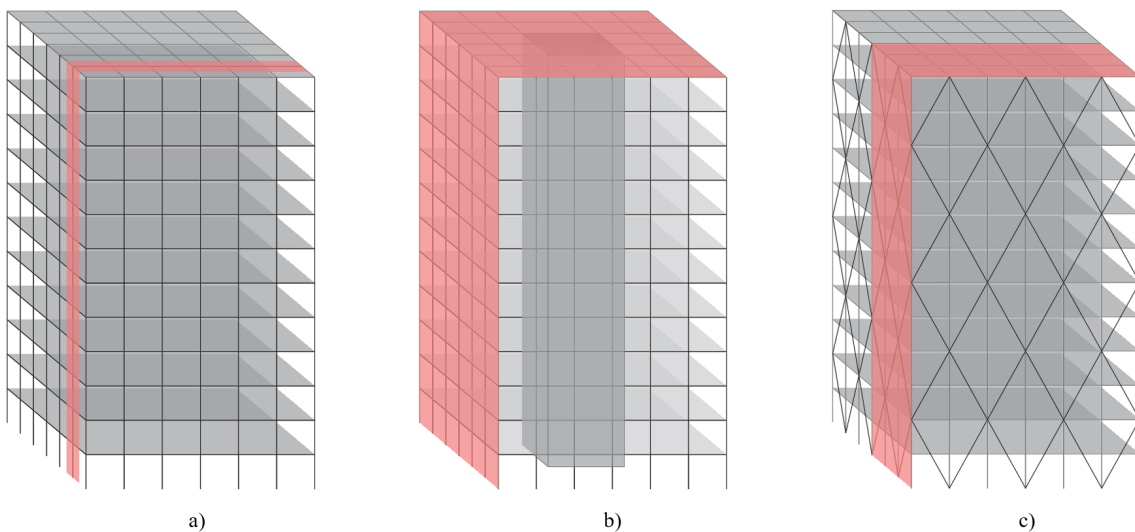


Figure 4.11: *Representative cut for 2D modelling of the structure*

Vertical Loads

The vertical load of the structure is divided into permanent and variable load. The permanent load consists of the self-weight of the structure including architectural features that will not be moved, such as interior walls and ceilings. The variable load incorporates the action of the users, which depends on the use type of the structure, as well as non-permanent loads such as snow. EC1 provides tabulated values for some of the permanent and variable loads, which is shown in table 4.3. The structural floor system plays a significant role in the self-weight of the structure, and for this investigation the pre-assembled floor system shown in figure 4.12 was used, together with the material weights shown in table 4.2.

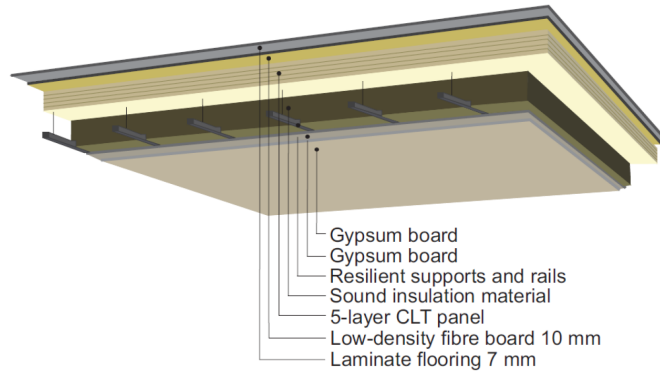


Figure 4.12: *Pre-assembled CLT floor system [22]*

Material	Self-Weight (kN/m^2)
CLT 250 mm thickness	1.500
Gypsum board	0.065
Laminate flooring	0.608
Fibre board	0.055
Total	2.23

Table 4.2: *Floor system weight*

Load type	Load pressure (kN/m^2)
Permanent load	
Floor load	2.23
Interior walls	0.50
Ceiling	0.30
Variable load	
Residential	1.75
Snow	0.56

Table 4.3: *Floor system weight*

The three stability systems studied in this investigation, include a frame structure which is responsible for transferring the vertical loads to the foundations. As seen in figure 4.13, the vertical load is applied to the floors, which transfer it to the beams, and then beams transfer it to the columns, which take it all the way to the foundations. The figure also shows that each of the panels spans in one direction, following a grid determined by the effective span between the columns. Each grid cell has a floor panel, and the panels are placed perpendicular to each other in order to provide an even distribution over the beams.

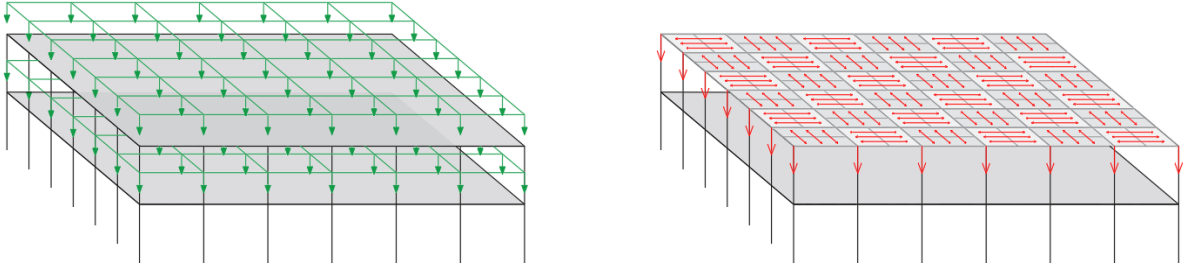


Figure 4.13: *Vertical load distribution*

Load Combinations

Eurocode NEN-EN 1990 provides load combinations based on the consequence class of the structure. Consequence class refers to risk presented by the collapse of a structure in terms of human life and economic and environmental loss. All high-rise structures are considered to be consequence class 3 (CC3), which is the highest possible. For CC3 structures, the following load combinations are presented.

$$1.1(1.35G'' + \sum_{i \geq 1} 1.5\psi_{0,1}Q_{k,i}) = 1.49G'' + \sum_{i \geq 1} 1.65\psi_{0,1}Q_{k,i} \quad (4.5)$$

$$1.1(1.2G'' + 1.5Q_{k,1}'' + \sum_{i \geq 1} 1.5\psi_{0,1}Q_{k,i}) = 1.32G'' + 1.65Q_{k,1}'' + \sum_{i \geq 1} 1.65\psi_{0,1}Q_{k,i} \quad (4.6)$$

4.4 Design Assumptions

The development of a tool which can assist the preliminary design of timber high-rise structures, is only possible with the implementation of a parametric model that incorporates relevant design parameters. In order to develop an efficient parametric model which incorporated the design parameters and constraints, and could collect all the required data under the time constraint, certain design assumptions needed to be made. Some of these assumptions have already been mentioned throughout the report; however, other critical assumptions which have an effect on the results are listed below:

- **Reference location**

The location of the project determines the wind load to which the structure is exposed, which has a significant effect on the design. For the purpose of this investigation the location of the project Cooltoeren in Rotterdam, Netherlands was chosen. The computed horizontal loads were compared to the loads used by the structural engineering firm that designed the 150 meters tower currently under development at this location.

- **Design for encapsulation**

As explained in section 2.5, all high-rise buildings must comply with strict fire safety regulations, which guarantees a safe evacuation of the structure. Due to timber's combustible nature, special attention must be given to the fire safety design. There are many active and passive methods that can be used to meet the requirements. In order to simplify the scope of this investigation, it is assumed that the fire safety regulations are met for design for encapsulation, and section 2.5 provides an explanation to how this method works.

- **Rotational stiffness of the foundations**

Foundations are designed to take the load from the structure and transfer it to the ground, but more importantly they are designed to prevent the building from overturning. The load bearing capacity of individual foundations is determined by the material, size and the soil properties [38]. The rotational stiffness provided by the foundations is determined by the number of piles, their capacity, and distance to the rotational center. The influence of the rotational stiffness of the foundations on the design of high-rise structures is a complex subject which can be highly project specific. For the purpose of simplifying the scope of this investigation, it is assumed that the rotational stiffness provided by the foundations is infinite, resembling a fully clamped cantilever beam.

- **Floor vibrations**

As previously mentioned, it is assumed that the load-bearing floor system is made out of CLT panels. The floor system not only carries the loads to other structural elements, but it is also subjected to constant excitations from user activities which can cause vibrations leading to user discomfort. Due to its low density and stiffness, CLT panels are more susceptible to human induced vibrations, and the magnitude of these vibrations are determined by the span of the panel and the stiffness of the supporting beams [16]. The magnitude of these vibrations is a complex dynamic problem, which must be assessed with the development of a finite element model. In order to simplify the scope of this investigation it was assumed that based on the floor thickness, the maximum effective span, and the cross-section of the supporting beams, vibrations are kept under the acceptable range provided by EC5 of 8 Hz [16].

4.5 Conclusions

Collecting data for a parametric study can become computationally expensive, given that in order to capture the influence of a parameter, various models must be developed implementing different values for the parameter and their outcome must be analysed. For the purpose of this investigation, it was decided that the most efficient and representative way to collect such data was to develop a 2D parametric model. A parametric model can be built based on the design parameters, such that their magnitudes can be easily changed, and the model automatically adjusts. For the purpose of this investigation, three design parameters were studied, which are: stability system design, connection stiffness, and building height. Different ranges for the building height and connection stiffness can easily be incorporated into the model; however, the stability system design will significantly change the geometry and structural model, so separate models were built for each proposed stability system.

The assembled structural model computes the forces developed in the elements and the global behaviour of the structure based on provided element cross-sections, geometry and loads. As explained in section 4.2, the validation of each design variable was done by the implementation of five design constraints which are member forces, global deflection, interstorey drift and along- and cross-wind acceleration. These are computed based on the output from the structural model, which is verified in Appendix E. Finally, in order to develop a representative and efficient model, several design assumptions were made as seen in section 4.4, which together with the design decisions made in sections 4.3 will influence the data collected and are acceptable for a preliminary design study. However, in order to perform a final structural design, the data from the parametric study must be used together with a full scale structural model. Figure 4.14 shows an overview of all the parameters and constraints that were incorporated in the model.

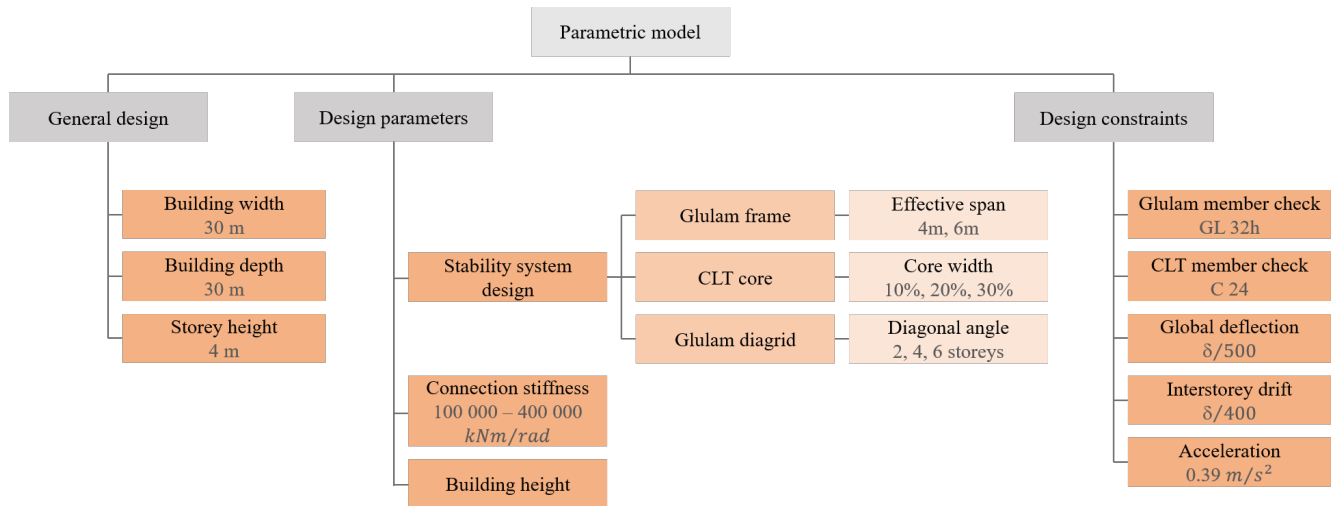


Figure 4.14: *Parametric model overview*

5 Parametric Study

The structural design of each design alternative consists of determining the required member cross-sections to comply with the design constraints mentioned in section 4.2. The size of the structural elements highly influences the output of the design, so in order to directly compare between different design alternatives, the sizing needs to be done using consistent methods. For this investigation two different optimization tools were implemented for sizing the cross-sections and collecting the data. The first tool uses evolutionary algorithms, while the second tool uses brute-force algorithms. The main goal of this chapter is to provide insight to the methods used to collect the data for the parametric study, and explain how the output can be used for the preliminary design of timber high-rise structures. This chapter focuses on answering the following research question:

How can the data from the parametric study be used in the preliminary design of a timber high-rise?

5.1 Model Output

The parametric model developed using Grasshopper integrates all the concepts discussed in chapter 4 and was used to collect the data. A design alternative consists of the combination of different design parameters and is evaluated based on the design constraints. Each data point consists of the selection of design parameters that describe that specific alternative, as well as the output of the design in the form of unity checks, amount of material required, and net floor area for a given combination of element cross-sections. Figure 5.1 is a visual representation of one data point, showing the design parameters selected and the output of the design. The applied element cross-sections are illustrated on the structure itself, together with its utilization, which is determined based on the member capacity checks.

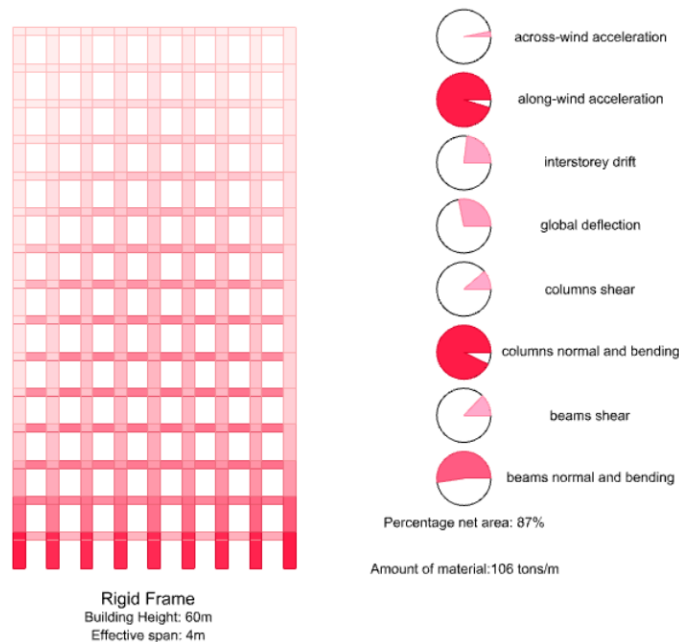


Figure 5.1: *Distribution of the vertical loads*

5.2 Optimization

The main goal of this investigation is to perform a parametric study to determine the influence of different design parameters on the design of timber high-rise structures. Determining the influence of a parameter requires the analysis of full structural designs for different ranges and combinations of the parameters, including sizing of the cross-sections. The sizing of the cross-sections has a great influence on the behavior of the structure, thus it must be done in a consistent manner such that it does not have an effect on the results obtained on the influence of individual parameters. For this investigation two different methods were studied for sizing the cross-sections and collecting the data. The first method is the implementation of an evolutionary algorithm optimization, which focuses on finding the optimal member cross-sections that maximizes the net floor area while complying the design constraints. The data collected using this method is ideal for recognizing trends and determining the influence of a parameter. However, it has a limited potential for the development of a preliminary design tool given that the data is biased based on the definition of “optimal” solution, which can change for different projects. The second method is the implementation of a brute-force optimization, which instead of searching for an optimal solution, it simply collects the data of all possible cross-sections for each design alternative. The data collected using this method is ideal for creating a preliminary design tool, allowing the user to define the optimal design criteria. However, it presents a challenge to recognize trends of the influence of individual parameters.

5.2.1 Evolutionary Solver

Evolutionary algorithms (EA) are used to obtain optimal solutions in a large population of potential solutions by using biological evolution principles such as mutation, crossover, natural selection and survival of the fittest. EA evaluate all the individuals of a population by their fitness, which in evolutionary computations is a user defined function that rates the quality of an individual. Each individual has certain characteristics which is also known as its genome. In each iteration, the EA evaluates the fitness for a certain number of individuals and based on the qualities of the best individuals, it creates a new population which is evaluated in the same way until an optima has been found [32]. Evolutionary solvers are tools which incorporate EA theory. Grasshopper has an integrated evolutionary solver called Galapagos, which is used for single objective optimization and takes as input a genome and fitness, as seen in figure 5.2. Figure 5.3 shows the design workflow which was used to collect the data using this method.



Figure 5.2: *Galapagos component*

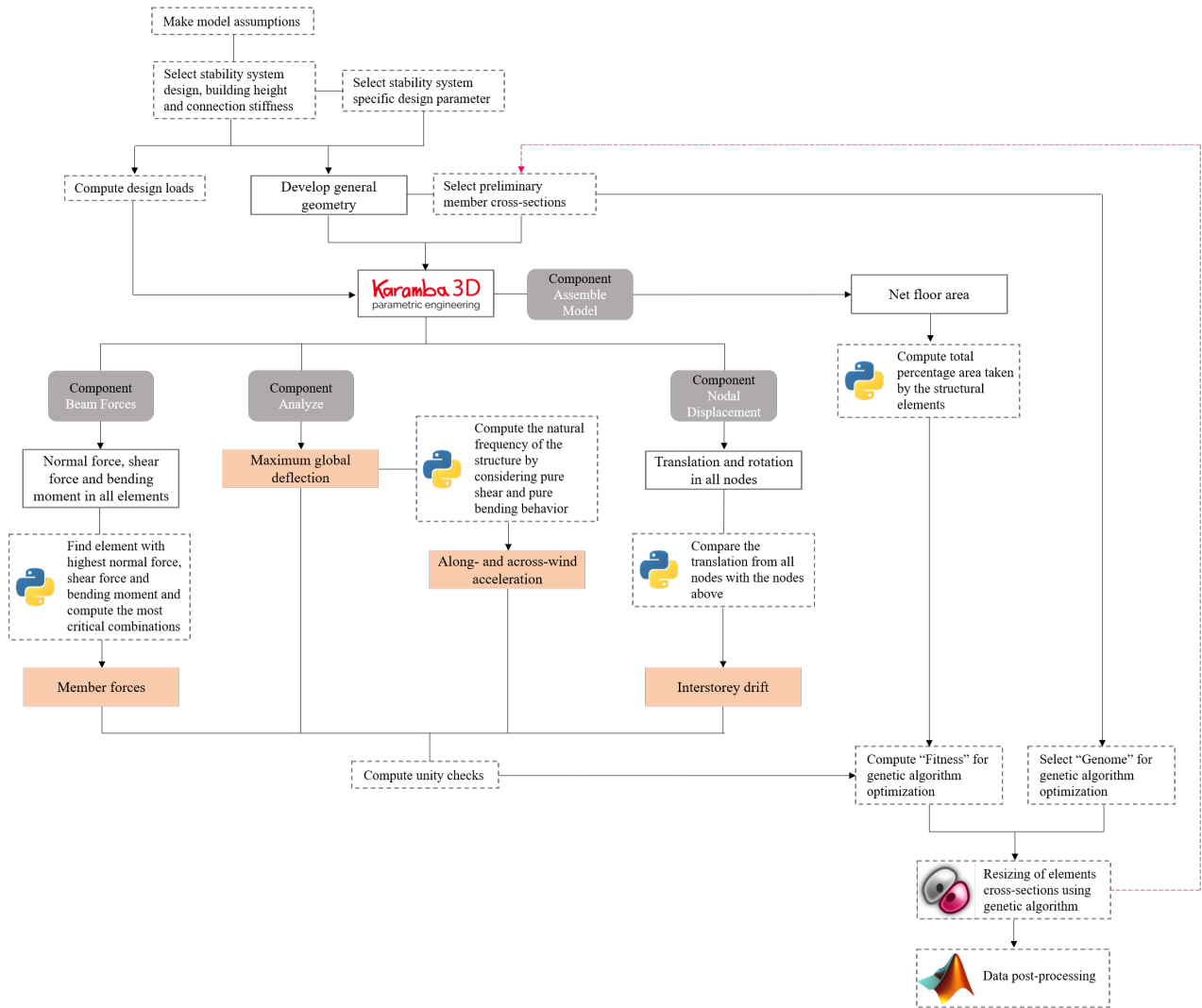


Figure 5.3: *Evolutionary algorithm workflow*

Genome

As seen in figure 5.3, for this method the genome was taken as the cross-section of the structural elements, which was inputted in the form of lists of standard glulam cross-sections. The cross-section of the columns is highly influenced by the horizontal wind load. The model used for this investigation was developed in a 2D environment, which means that the structure is only horizontally loaded in one direction. In reality, the wind direction can change, so the columns must provide the same resistance in both directions. In order to consider this phenomenon in the data, the genome of the columns consisted of cross-sections with equal height and width. Table 5.1 shows the ranges for the different elements which were selected based on literature and existing projects. The addition of diagonals cross-section to the genome is only applicable for the glulam diagrid system.

Structural element	Width (cm)	Height (cm)
Columns	20-180	20-180
Beams	20-80	20-130
Diagonals	10-50	10-50

Table 5.1: *Evolutionary algorithm genome range*

Fitness

The fitness for the EA is defined as a function which aims to maximize the net floor area, while assuring compliance with the design constraints. In order to achieve this goal, the fitness function was determined using the area taken by the structural elements and a python script that checked for unity check compliance. If a combination of cross-sections yielded to an exceedance of any unity check, the script will apply a penalty on that alternative, which will make the EA discard the option as a possible optimum. Figure 5.4, shows a visual representation of the fitness function for this methodology.

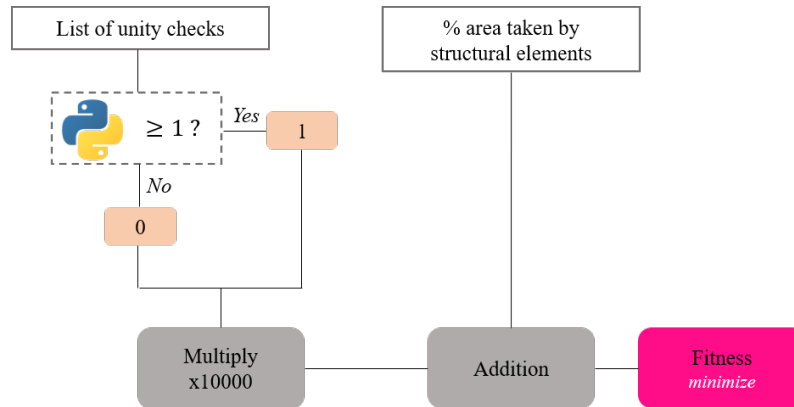


Figure 5.4: *Galapagos fitness function*

Population and Convergence

An evolutionary algorithm is an efficient method for collecting data, because in each iteration it selects the best alternatives and uses them as a starting point for the next iteration, which reduces the size of the search space. However, this creates a potential challenge in large search spaces for determining whether the solver converges after finding a local optima or if it finds the global optima of the system. Table 5.1 shows the ranges for the different parameters that define the genome for this method. The frame and core uses steps of 5 for the columns and steps of 10 for the beams, which results in a total of 4608 possible combinations. The diagrid uses steps of 10 for both the columns and beams and steps of 5 for the diagonals, which results in a total of 5760 possible combinations. Figure 5.5 shows the settings which were used to run each optimization together with the interface showing the behaviour of the fitness throughout each iteration, and table 5.2 explains some of the used terms.

Max. Stagnant	Number of consecutive generations without finding a local optima for termination of the solver
Population	Number of possible solutions which are evaluated every iteration
Initial Boost	Multiplication factor for population of first iteration
Maintain	Percentage of the population which is kept for the next iteration

Table 5.2: *Galapagos settings definitions*

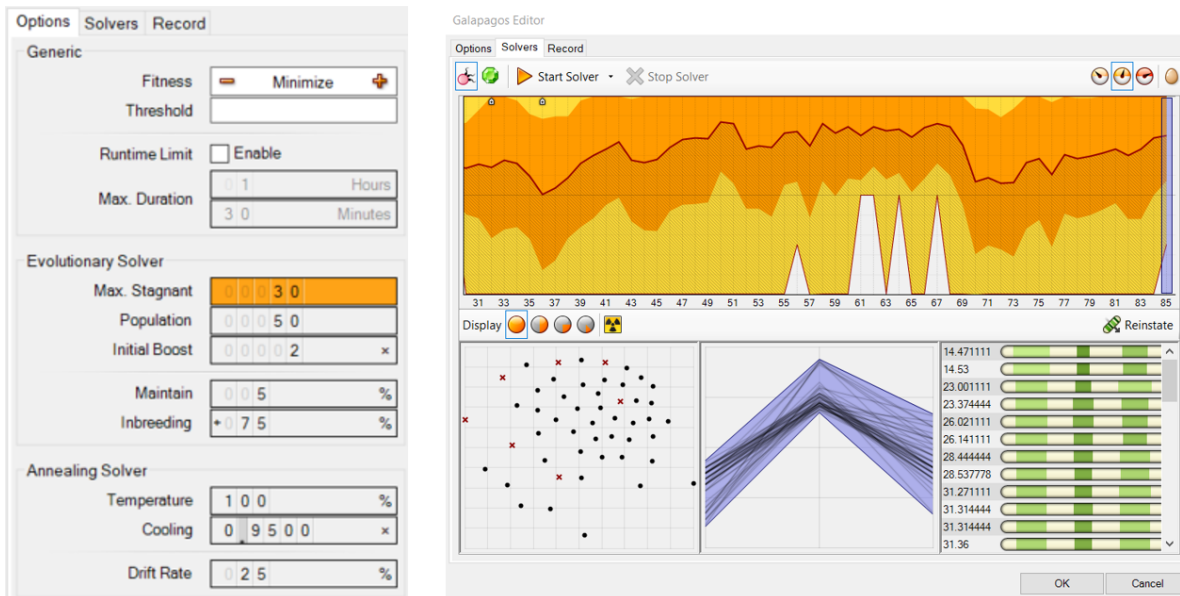


Figure 5.5: *Galapagos optimization settings*

As shown in figure 5.5, each iteration evaluates the fitness of 50 individuals, meaning that for the stability system with the largest search space, 115 iterations are required in order to study all possible combinations. However, due to the biological evolutionary principles incorporated in the algorithm, it is not necessary to study the entire search space. The convergence criteria was set to 30 consecutive iterations without any local optima. This criteria is considered to be conservative given the size of the search space and the population of each iteration. Nevertheless, preliminary tests were done in order to verify this decision, where three consecutive optimizations were performed in order to check that no optimal solutions occurred after the convergence of the first one.

5.2.2 Brute Force Method

Brute-force algorithms (BFA) are implemented to collect the data for all possible combinations within a constrained search space. BFA do not evaluate the fitness of each individual, but it rather records all the attributes that define an individual (genome) and all the characteristics of that specific combination of attributes (phenome). BFA iterators are tools which apply the described theory. Colibri is a Grasshopper iterator that can be used together with other plugins to gather data, which can be postprocessed and developed into a design tool. Figure 5.6 shows the design workflow used to collect the data using this method.

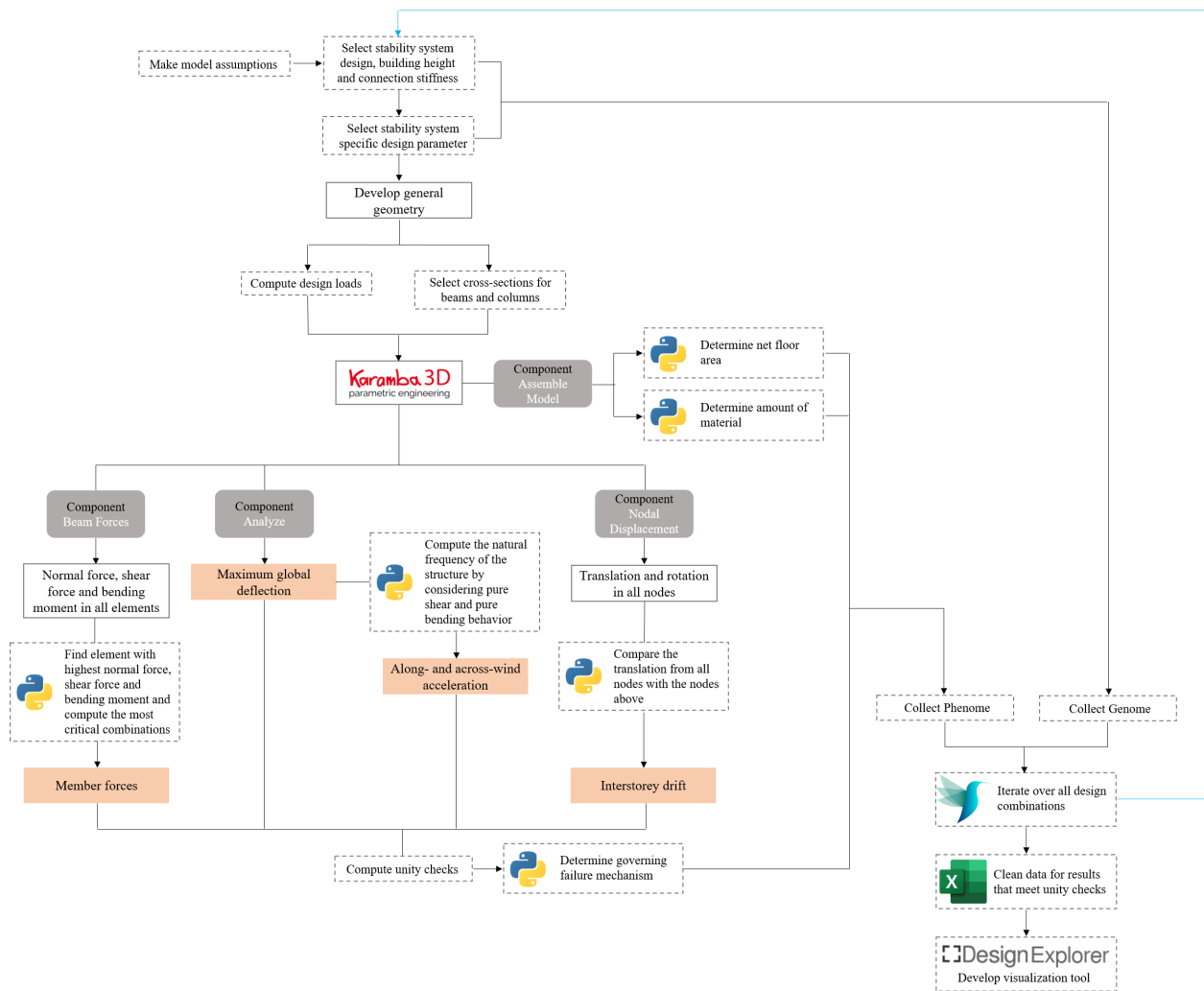


Figure 5.6: *Brute force method workflow*

Genome

The genome implemented for this methodology incorporates the same ranges presented in table 5.1 for the member cross-sections. However, it also includes other attributes that describe the individual such as building height, connection stiffness, and other stability system specific parameters. The ranges for the additional parameters follow the information provided in section 4.1. Figure 5.7 shows the Colibri component used to collect the BFA data for the glulam frame. In the figure it can be seen that there are 15600 different combinations of the attributes, and with approximately 30 seconds per iteration, this process was completed in two hours and a half.

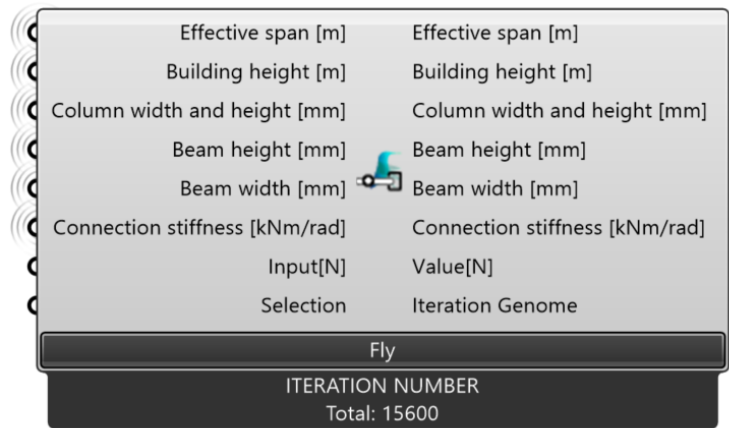


Figure 5.7: *Brute force method genome*

Phenome

The phenome in a BFA analysis is a user defined set of outputs or characteristics used to describe the quality of each individual. As shown in figure 5.8, the selected phenome for this method consisted of the percentage net floor area, governing failure mechanism, amount of material, acceleration, and moment resistance in the connections. The phenome was chosen based on what was defined as the most relevant information for both a structural engineer and a client. As previously mentioned, Colibri does not rate or evaluate the individuals before collecting the data, so many of the individuals collected do not comply with the design constraints. In order to exclude the individuals that do not meet the required constraints during the post-processing, a simple python script was written in Grasshopper that checks for compliance, and whenever a unity check failed, all the elements of the phenome were multiplied by zero.

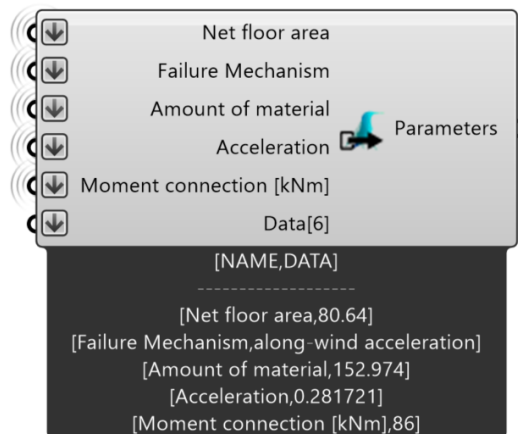


Figure 5.8: *Brute force method phenome*

Design Explorer

Design explorer (DE) is a visualization interface developed by CORE studio, that allows the users to search through all the individuals of an optimization, and filter specific ranges of the genome or phenome to obtain a list of individuals that meet the requirements. The interface developed in DE can be used as a preliminary design tool, which allows engineers to efficiently investigate different options. DE takes data files and gives the possibility of linking images to

each individual, creating a visual tool. The data collected by the Colibri iterator, is stored in an Excel file, where it can be sorted and cleaned before inputting it into DE. For this investigation, individual interfaces were created for each stability system. Figure 5.9 shows the interface created for the glulam frame.

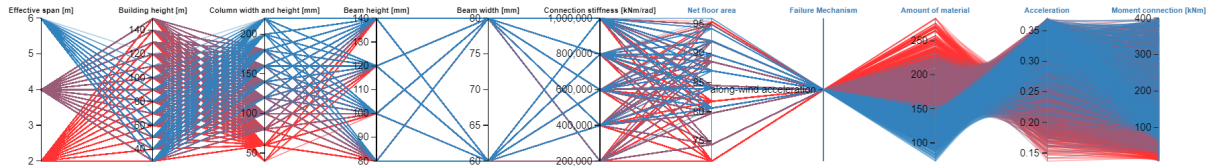


Figure 5.9: *Design explorer interface for glulam frame*

5.3 Conclusions

The preliminary design of a structure is done for the purpose of determining the feasibility of the architectural design and creating a cost estimate for the project. Ideally, it can be done without a full-scale finite element model and detailed designs such as connections. Due to the complex behaviour of timber high-rise structures, it has been seen that the preliminary design very often underestimates the dynamic behaviour of the structure, leading to significant structural design changes in order to increase the self-weight and cross-sectional stiffness of the structure, which results in budget increases and deviations from the architectural design. Parametric studies are performed in order to provide structural engineers with insight on the effects certain parameters can have, assisting them in making well-argued decisions during the preliminary design phase, which may prevent major changes at a later stage. Parametric studies can also serve as design tools, decreasing the need for complex modelling and calculation during the preliminary design phase.

This chapter addressed the two methods used to collect data for the parametric study, and the characteristics of this data. The first method was the implementation of EA, which search for an optimal solution for each design alternative based on a user defined fitness criterion. For this investigation, the optimal solution was defined as the combination of member cross-section which yielded the maximum net floor area and complied with the defined design constraints. Optimal solutions for all combinations of stability system design, building height and connection stiffness were found and recorded. The data created using this method is ideal for developing graphs which show the influence of individual parameters and can assist the structural engineers in preliminary design decisions. The second method was the implementation of BFA, which studies all the possible solutions in a constrained search space instead of finding an optimal solution. Individual analyses were made for the three stability system designs, which were used to create interfaces such as the one seen in figure 5.9. The interfaces developed using this method are can be used as preliminary design tools, which can assist the structural engineers in creating more accurate estimates and predictions of the behaviour of the structure.

6 Results and Discussion

As explained in Chapter 5, two methods are used for sizing the structural elements and collecting the data for the parametric study. The goal of implementing two methods is to validate the data and mitigate the limitations of each individual method. The first method uses evolutionary algorithms, which results in ideal data for identifying trends on the influence of various parameters. The second method uses brute-force algorithms which result in ideal data for the development of a preliminary design tool. The main goal of this chapter is to show the results obtained from both methods and provide some relevant observations and discussion. This chapter will focus on answering the following research question:

Which design parameters present the most influence on the design of timber high-rises?

6.1 Results and Observations

This section focuses on presenting the data collected using the EA method. As previously mentioned, three parametric models were developed, corresponding to each selected stability system, and incorporating all design parameters and constraints, so the data in this section is presented for each stability system individually.

6.1.1 Glulam Frame

For the glulam frame stability system, the parameters effective span, connection stiffness and building height were evaluated. As presented in figure 4.14 this study focuses on assessing the behaviour of the structure with two different effective spans (four and six meters), and four different rotational stiffnesses in the column-beam connections (100 000 - 400 000 kNm/rad). The behaviour of the structure for different combinations of parameters is studied based on the influence on the structural design (net floor area, amount of material and moment resistance), and the influence on the structural behaviour (unity checks).

Influence on Structural Design

Data collected for four meters effective span is presented in figures 6.1, 6.2, and 6.3, respectively showing the behaviour of the net floor area, amount of material per unit height and moment resistance in the connections with increasing building height for different rotational stiffnesses. The design alternatives incorporating six meters effective span proved to have a height limitation of 40 meters, significantly reducing the number of data points collected using this parameter. Given that trends can not be visualized with two data points, the data collected for six meters effective span is presented in table 6.1.

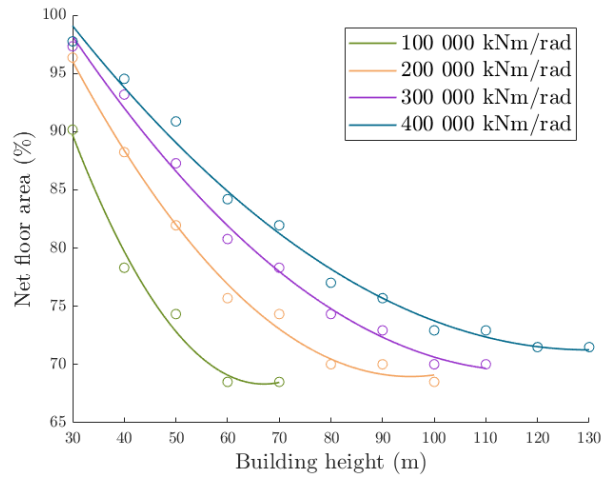


Figure 6.1: *Glulam frame - 4 meters span: Net floor area*

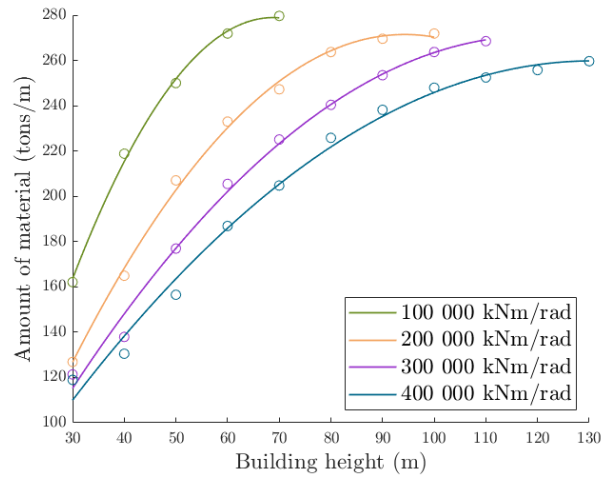


Figure 6.2: *Glulam frame - 4 meters span: Amount of material per unit height*

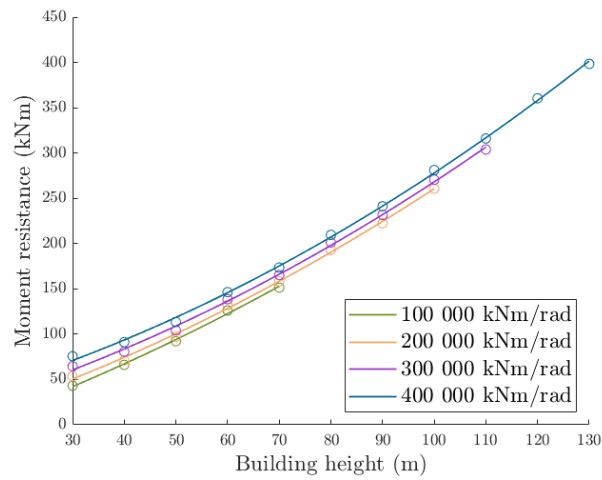


Figure 6.3: *Glulam frame - 4 meters span: Moment resistance*

Building height (<i>m</i>)	Rotational stiffness (<i>kNm/rad</i>)	Net floor area (%)	Amount of material (<i>tons/m</i>)	Moment resistance (<i>kNm</i>)
30	200 000	87.4	139.7	101
30	300 000	93	107.7	107.1
30	400 000	96	90.9	118.4
40	400 000	85.8	141.8	168

Table 6.1: *Glulam frame - 6 meter span*

The following observations can be made from the presented graphs and table:

1. The maximum height the four-meter span design can achieve is 130 meters, while the six-meter span design can only reach a height of 40 meters. However, the maximum height is significantly influenced by the rotational stiffness of the column-beam connections. For the four-meter span the maximum height goes from 130 meters to 70 meters when the rotational stiffness of the connections is reduced from $400000kNm/rad$ to $100000kNm/rad$. On the other hand, in order to reach a height of 30 meters for the six-meter span a rotational stiffness of at least $300000kNm/rad$ is required and to reach a height of 40 meters a rotational stiffness of at least $400000kNm/rad$ is required.
2. From figures 6.1 and 6.2 it can be seen that the net floor area decreases at the same rate that the amount of material increases as the structure becomes taller. This trend suggests, that the cross-section of the beams is maximized early in the optimization, so as the building height increases and the structure needs more self-weight and global stiffness to meet the constraints, the cross-section of the column is increased accordingly.
3. From figures 6.1 and 6.2 it can also be seen that the influence of increasing the rotational stiffness of the column-beam connections decreases as the stiffness increases. When increasing the rotational stiffness from $100\ 000\ kNm/rad$ to $200\ 000\ kNm/rad$, the net floor area increases approximately 10% and the amount of material decreases approximately $40\ tons/m$. While when increasing the stiffness from $300\ 000\ kNm/rad$ to $400\ 000\ kNm/rad$, the net floor area increases approximately 3% and the amount of material decreases approximately $10\ tons/m$.
4. Figure 6.3 provides a visualization on the effect that increasing building height has on the moment that the connections need to resist. From the figure it can be seen that the moment resistance increases nearly exponentially with increasing height, following the same trend for all the different rotational stiffnesses.

Influence on Structural Behaviour

The behaviour of the structure will follow similar trends with different rotational stiffness in the column-beam connections; however, the sensitivity of some constraints to building height will change for different stiffnesses. To understand the behaviour of the structure the trends followed by the unity checks are assessed for both the lowest and highest rotational stiffnesses. Figure 6.4 shows the behaviour of the structure with $100\ 000\ kNm/rad$ rotational stiffness, and figure 6.5 shows the behaviour of the structure with $400\ 000\ kNm/rad$ rotational stiffness. The red dotted line in both figures shows the limit for the unity check that was set in the parametric model.

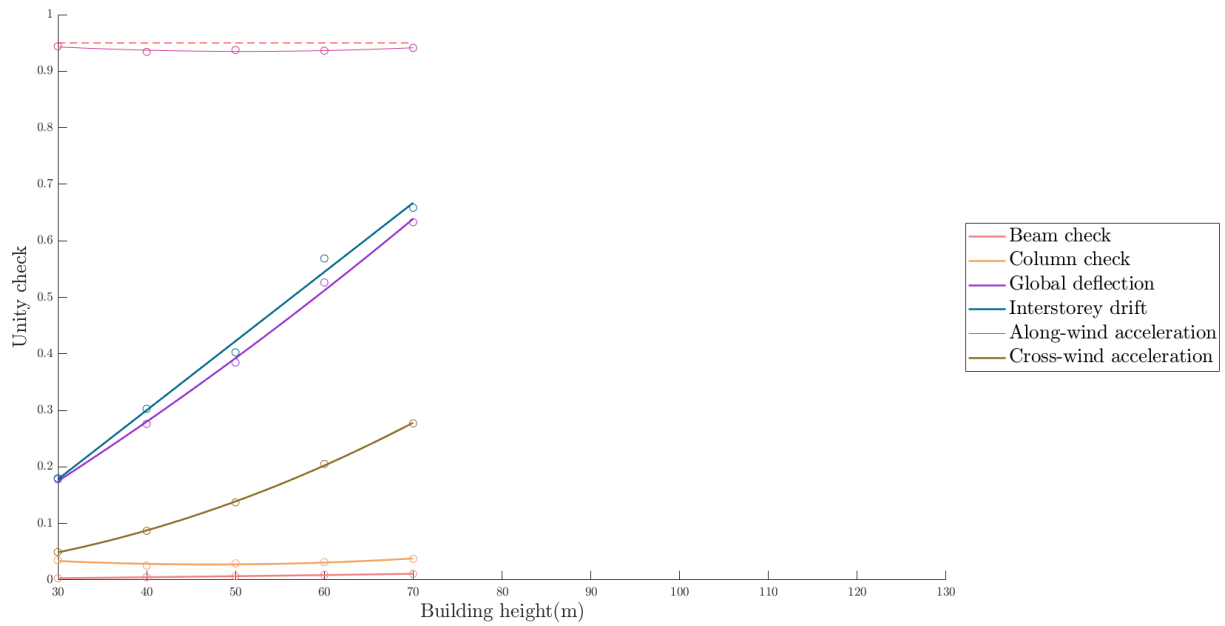


Figure 6.4: *Glulam frame - 4 meters span: 100 000 kNm/rad*

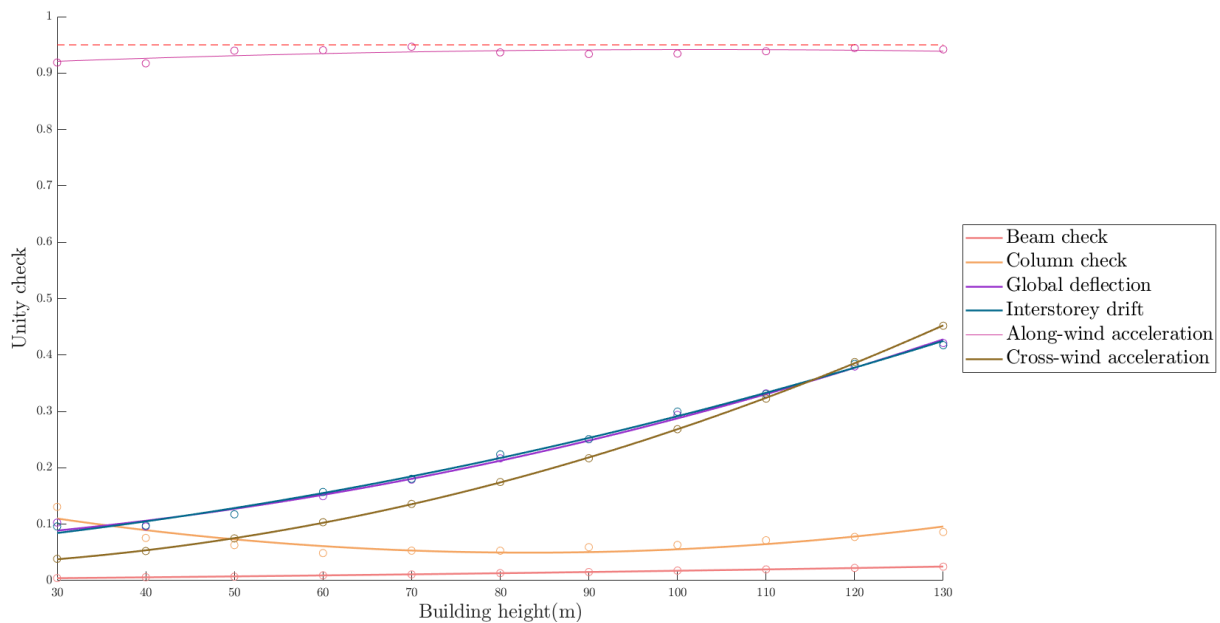


Figure 6.5: *Glulam frame - 4 meters span: 400 000 kNm/rad*

The following observations can be made from the presented graphs:

1. The governing failure mechanism throughout all building heights for both alternatives is the along-wind acceleration. However, this constraint is always pushed to the limit, showing the effect of the optimization criteria on the data. Maximizing the net floor area causes a reduction in the self-weight, which has a direct effect on the dynamic behaviour of the structure.
2. All unity checks follow a similar behaviour for both alternatives; however, the designs using 100 000 kNm/rad rotational stiffness are more sensitive to changes in building

height, increasing at a significantly higher rate. This trend is caused by a significant global stiffness reduction.

3. Global deflection and interstorey drift follow the exact same trend for the 400 000 kNm/rad rotational stiffness alternative, while for the 100 000 kNm/rad alternative they start to slightly deviate as the building height increases. Lower rotational stiffness causes larger deflection in the columns which has an effect on the interstorey drift of the structure.
4. The cross-wind acceleration follows a similar trend for both alternatives, significantly increasing for taller buildings. The trend shows that this constraint could potentially become the governing failure mechanism. The difference between the two alternatives shows the dependency of this constraint on the global stiffness of the structure.
5. The member checks follow the same trend for both alternatives. Beam check is nearly negligible, showing that the beams are significantly oversized due to the optimization criteria. While the column check shows a slightly decreasing trend, caused by the abrupt increase in the amount of material seen in figure 6.2.

6.1.2 CLT Core

For the CLT core stability system, the parameters core width, connection stiffness and building height were evaluated. As presented in figure 4.14 this study focuses on assessing the behaviour of the structure with three different core widths (ten, twenty and thirty percent of the building width). However, for this system only two different rotational stiffnesses in the column-beam connections are studied (100 000 and 200 000 kNm/rad). The reason for decreasing the number of rotational stiffnesses studied is that hybrid moment transfer mechanism with core and rigid frame are not common in practice due to a significant cost increase; however, for the purpose of this study it is relevant to understand the influence that this parameter would have on the design. The behaviour of the structure for different combinations of parameters is studied based on the influence on the structural design (net floor area, amount of material and moment resistance), and the influence on the structural behaviour (unity checks). Finally, to get a better understanding about the behaviour of the core structure, the influence of the parameters on the cooperation between the panels (gamma factor) is studied.

Influence on Structural Design

Figure 6.6 shows the behaviour of the net floor area, amount of material per unit height and moment resistance in the connections with increasing building height for the different core widths. Each individual graph shows different rotational stiffness in the connection, including pinned connections (0 kNm/rad) and the other two stiffnesses previously mentioned.

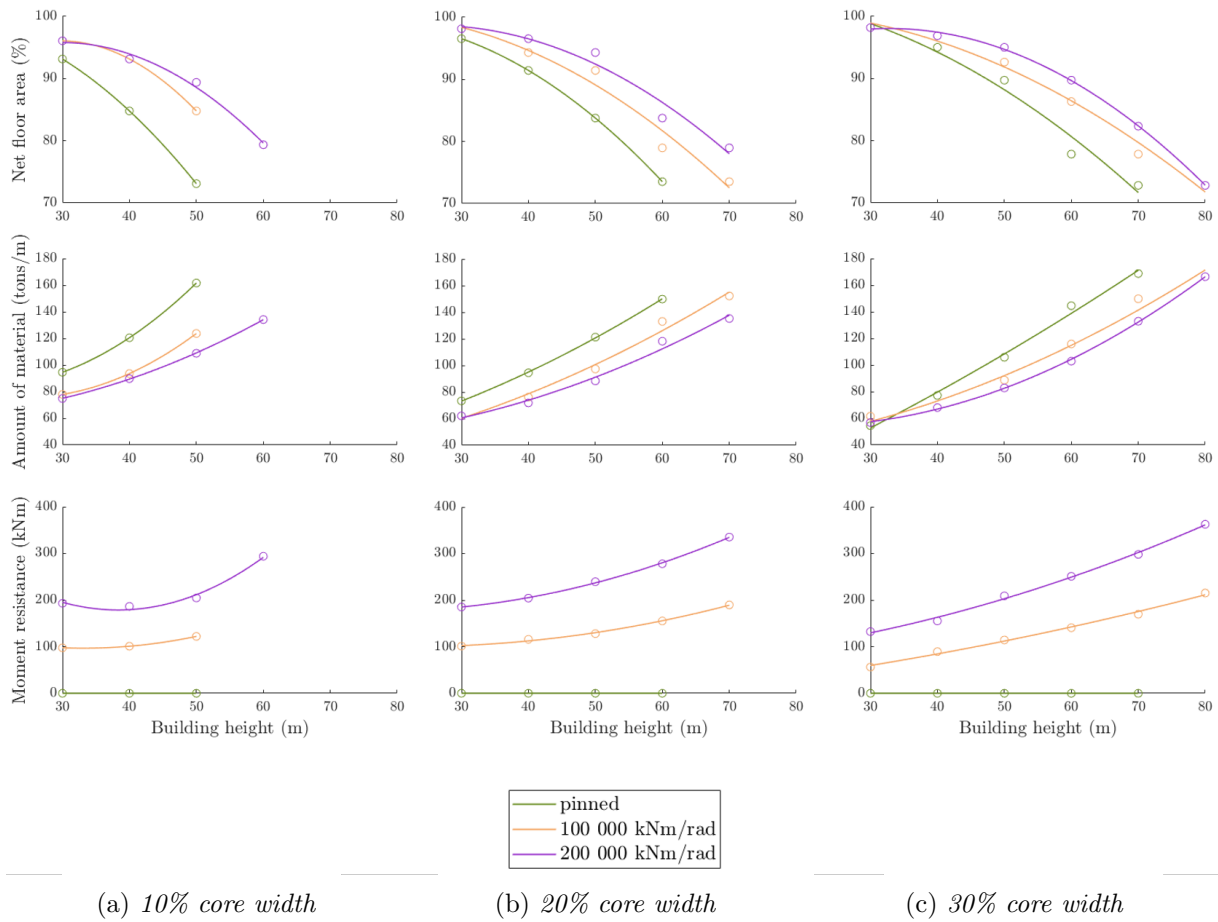


Figure 6.6: *CLT core*

The following observations can be made from the presented graphs:

1. The maximum height when using pinned connections is 50 meters for ten percent core width, 60 meters for twenty percent core width, and 70 meters for thirty percent core widths. When rotational stiffness is added in the column-beam connections the maximum height can increase up to 10 meters for all the different core widths.
2. Looking at the trends followed by the net floor area and the amount of material per unit height, the net floor area decreases at a similar rate than the amount of material increases. However, small deviations are noticed, specially for lower building heights. This trend suggests that the cross-section of the beams is maximized early in the optimization, but not for buildings lower than 40 meters. Once the beams have been maximized the same trend can be seen in both design outputs given that the structure relies on increasing the column cross-sections to increase its self-weight and global stiffness.
3. Looking at the trends followed by the net floor area and the amount of material per unit height, it can also be seen that the influence of adding rotational stiffness to the column-frame connections reduces as the core width increases. For the ten percent core width alternative going from pinned connections to 100 000 kNm/rad rotational stiffness causes the net floor area to increase approximately 10% and the amount of material to decrease approximately 20 $tons/m$. While for the thirty percent core width alternative going from

pinned connections to 100 000 kNm/rad rotational stiffness causes the net floor area to increase approximately 5% and the amount of material to decrease approximately 10 $tons/m$.

- The graphs showing the moment resisted by the column-beam connections for the different core widths show an exponential increase with additional rotational stiffness. This exponential increase translates into higher costs and complexity of assembling.

Influence on Structural Behaviour

The behaviour of the structure in terms of unity checks is analysed for all the different core widths. However, this study focuses on structures with pinned column-beam connections. As previously mentioned, hybrid moment transfer mechanism between core and frame are not common in practice due to increased costs and from figure 6.6 it was seen that the additional cost does not provide a significant improvement on the design of the structure. Figures 6.7, 6.8 and 6.9 show the trends followed by the unity checks for ten, twenty and thirty percent core width respectively.

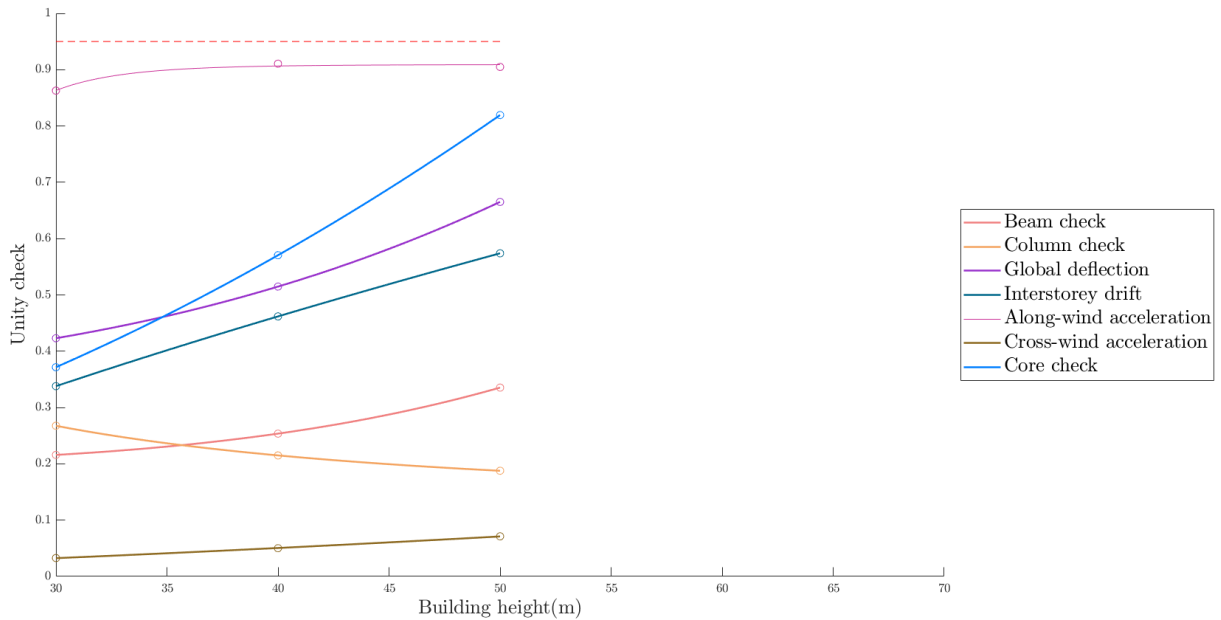


Figure 6.7: *CLT core - 10 % core width*

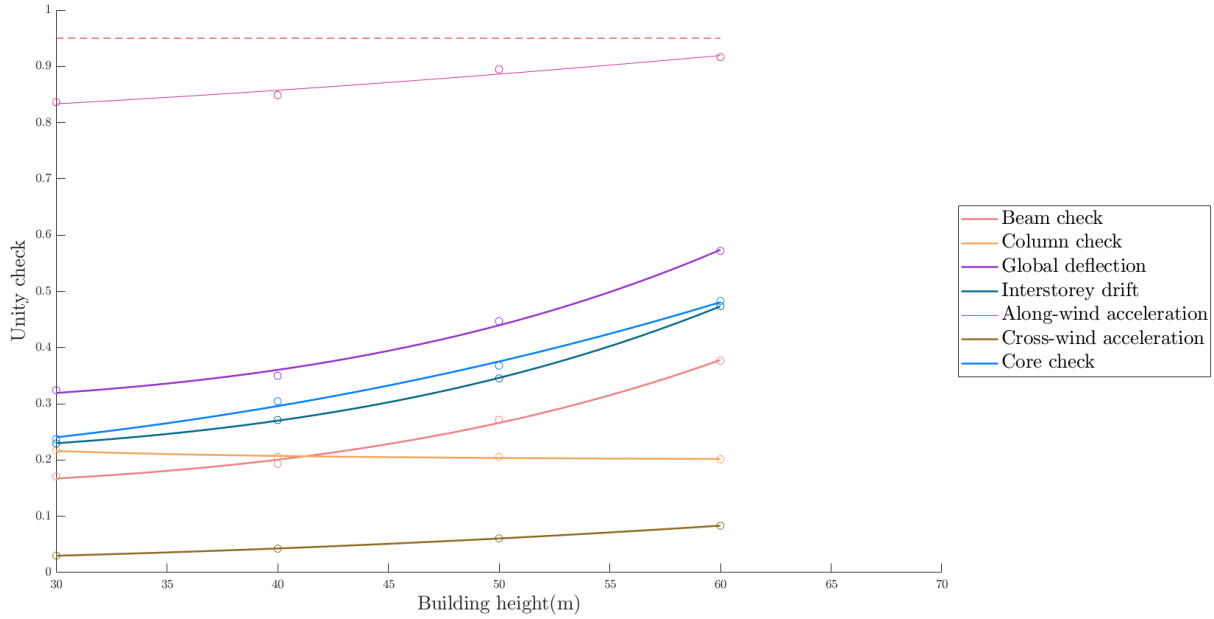


Figure 6.8: *CLT core - 20 % core width*

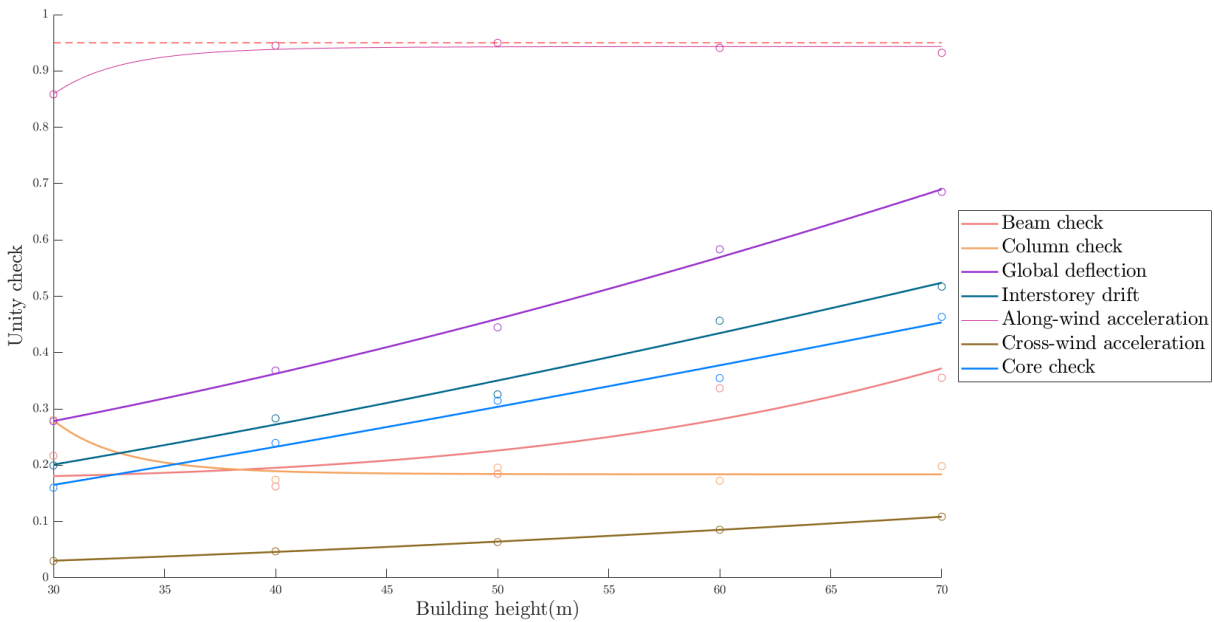


Figure 6.9: *CLT core - 30 % core width*

The following observations can be made from the presented graphs:

1. The governing failure mechanism throughout all building heights for the three core width alternatives is the along-wind acceleration. As seen for the behaviour of the glulam frame, this constraint is always pushed to the limit, showing the effect of the optimization criteria.
2. Most unity checks follow a similar behaviour for the three core width alternatives; however, the designs incorporating ten percent core width are more sensitive to changes in building height. The core structure increases the global stiffness of the system, and this increase is proportional to the size of the core.

3. The capacity of the CLT panels loaded in plane, is evaluated with the core unity check. The different figures show that both the core width and the building height have a significant influence on the behaviour of this constraint. The trends show a linear increase with building height, and the slope of the line decreases as the core width increases. The width of the core walls is constant for all building heights and core widths, which explains the mentioned trends.
4. For all core widths, the global deflection and interstorey drift follow an almost identical behaviour to one another. However, the global deflection shows a more critical behaviour. The difference between the two constraints is given by the behaviour of the structure as a pure bending beam, which is caused by the moment transfer mechanism.
5. The cross-wind acceleration follows a slightly increasing trend with building height. The difference in the behaviour of this constraint for the different core widths is almost negligible.
6. The member checks follow a similar trend for the different alternatives. Beam check increases at the building height increases. This trend shows that as opposed to the glulam frame, the beam cross-sections are not oversized based on the optimization criteria, and that this stability system relies on the beams to transfer the horizontal loads.
7. The column check shows a slightly decreasing trend for all the different core widths. This trend is caused by the significant decrease in net floor area with increasing height seen in figure 6.6, which suggests that the column cross-sections rapidly increase to provide self-weight and global stiffness to the structure.

Influence on Gamma Factor

As explained in section 4.1.1 the gamma factor is the parameter that quantifies the interaction between the perpendicular walls that form the core structure. This parameter will influence the global stiffness of the core, so the influence of the preliminary design parameters on its magnitude is studied. The method used to calculating the gamma factor in the parametric model is presented in Appendix D.

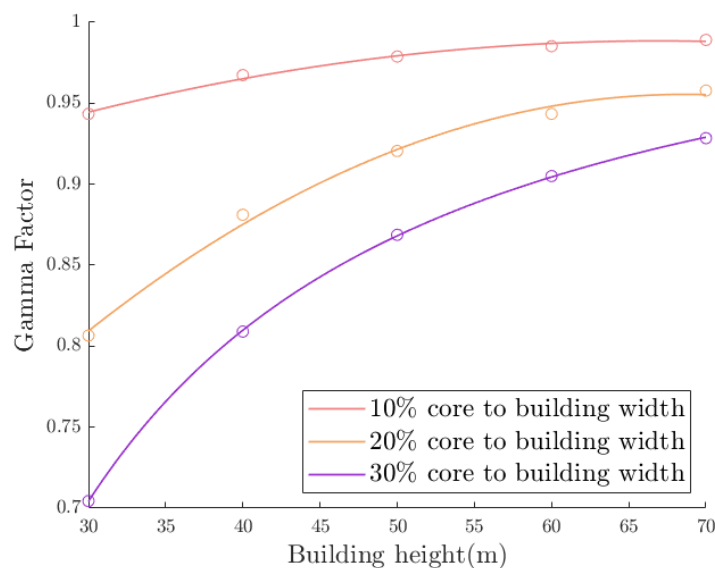


Figure 6.10: *CLT core gamma factor*

The following observations can be made from the presented graph:

1. The core width shows a significant influence on the gamma factor for lower building heights. However, this influence decreases as the building height increases.
2. The parameter building height shows a higher influence on wider cores, showing an almost negligible effect for the ten percent core width alternative. This phenomena is caused by the method used to calculate the gamma factor, which indicates that its magnitude is inversely proportional to the area and directly proportional to the height squared.

6.1.3 Glulam Diagrid

For the glulam diagrid stability system, the parameters diagonal angles and building height are evaluated. As presented in figure 4.14 this study focuses on assessing the behaviour of the structure with three different diagonal angles (two, four and six storeys). The parameter rotational stiffness in the column-beam connections is not included in this study given that the hybrid moment transfer mechanism has a negligible effect for this stability system, so all connections are assumed to be pinned. The behaviour of the structure for different combinations of parameters is studied based on the influence on the structural design (net floor area and amount of material), and the influence on the structural behaviour (unity checks).

Influence on Structural Design

Figures 6.11 and 6.12 respectively show the behaviour of the net floor area and amount of material per unit height with increasing building height for the different diagonal angles.

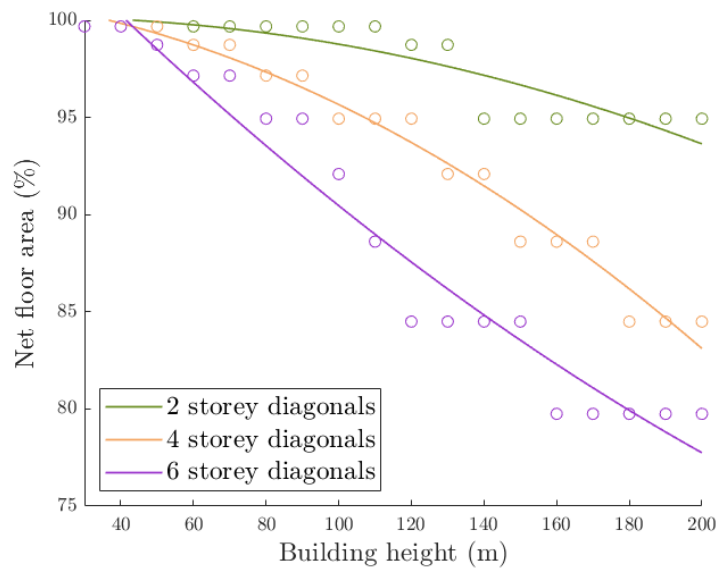


Figure 6.11: *Glulam diagrid net floor area*

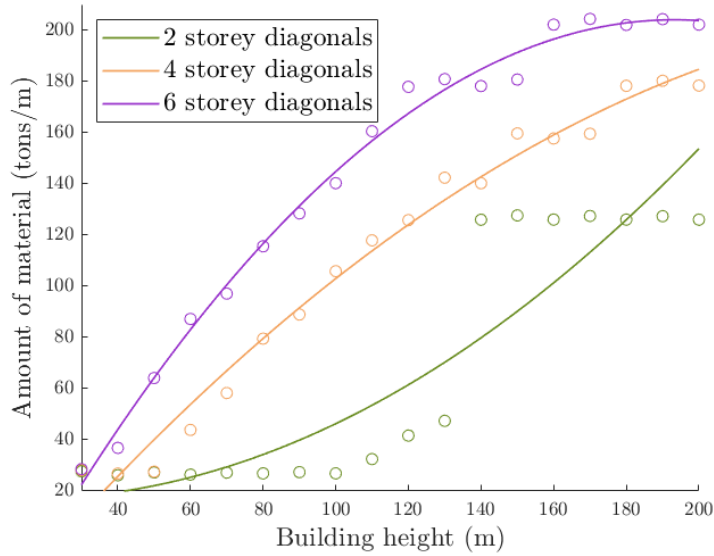


Figure 6.12: *Glulam diagrid amount of material per unit height*

The following observations can be made from the presented graphs:

1. The data collected for the net floor area and amount of material respectively decrease and increase in steps as the building height increases. The number of steps increases as the angle of the diagonal increases, having a more even distribution. These steps are caused by the genome of the optimization and the moment transfer mechanism of this system. The main influencing factor in the output is the cross-section of the frame columns, which is defined by the list provided in the optimization genome. The cross-sections in this list increase in steps of 20 cm, which causes the steps in these graphs. The global stiffness and dynamic behaviour of this system are determined by the configuration of the diagrid elements, which has a higher efficiency for lower diagonal angles. Due to the efficiency of the system, the column cross-sections increase at a lower pace than in other stability systems causing the steps and step sizes.
2. All the different diagonal angle alternatives allow the structure to reach a height of 200 meters. However, this limitation is given by the six storeys alternative, the other configurations can potentially yield significantly taller structure, but the number of diagonal connections required must be considered due to their complexity and required assembly precision. The influence of the diagonal angle is nearly negligible for lower rise buildings, but it significantly increases as the building height increases due to the dependency of this system on the efficiency of the diagrid configuration to increase the global stiffness.
3. The amount of material per unit height shows a more rapidly increasing trend than the decreasing of the net floor area, especially for lower rise buildings, which corresponds with the number of steps seen in each graph. These phenomena are caused by the cross-section of the diagonals. In the parametric model it was assumed that as the diagonals increase in size, they grow both inwards and outwards, which means that 50% of their cross-section is not considered in the net floor area. The moment transfer mechanism of this system relies on the efficiency of the diagrid configuration, so the size of the diagonals increases at an accelerated rate as the structure requires additional global stiffness, and once their cross-section is maximized, the cross-section of the other structural elements is increased.

Influence on Structural Behaviour

The behaviour of the structure in terms of unity checks is studied for the four and six storey diagonal alternatives. The two storey design alternative is not evaluated due to the high number of complex connections and the architectural limitations it provides, which makes it not a common solution in practice. Figures 6.13 and 6.14 show the trends followed by the unity checks for four and six storey diagonals respectively.

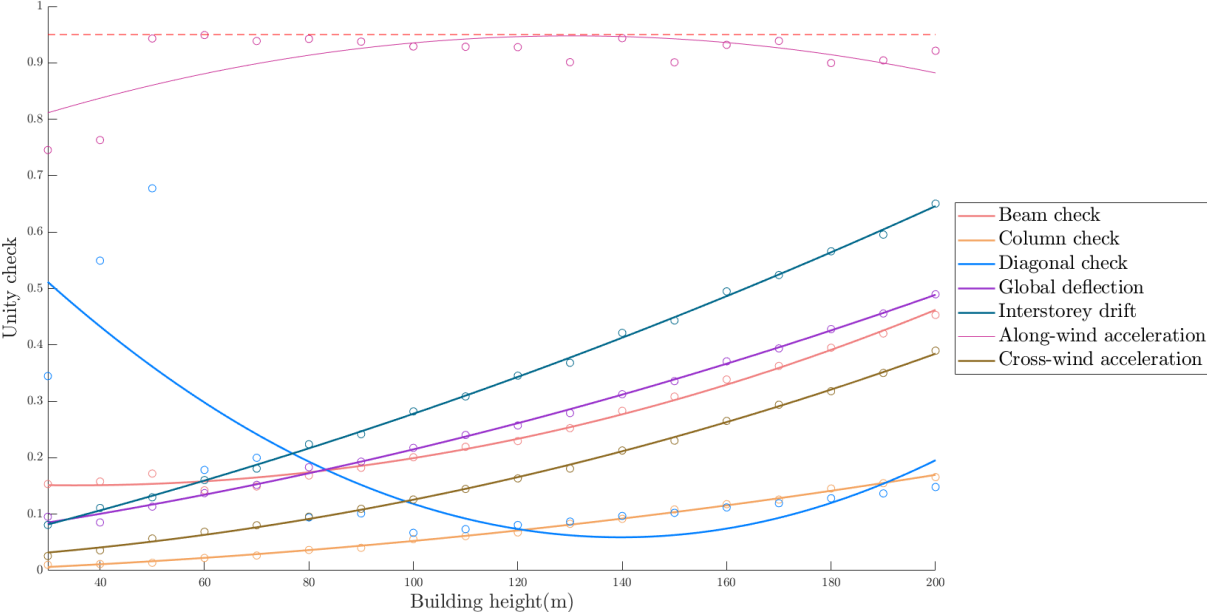


Figure 6.13: *Glulam diagrid - 4 storey diagonals*

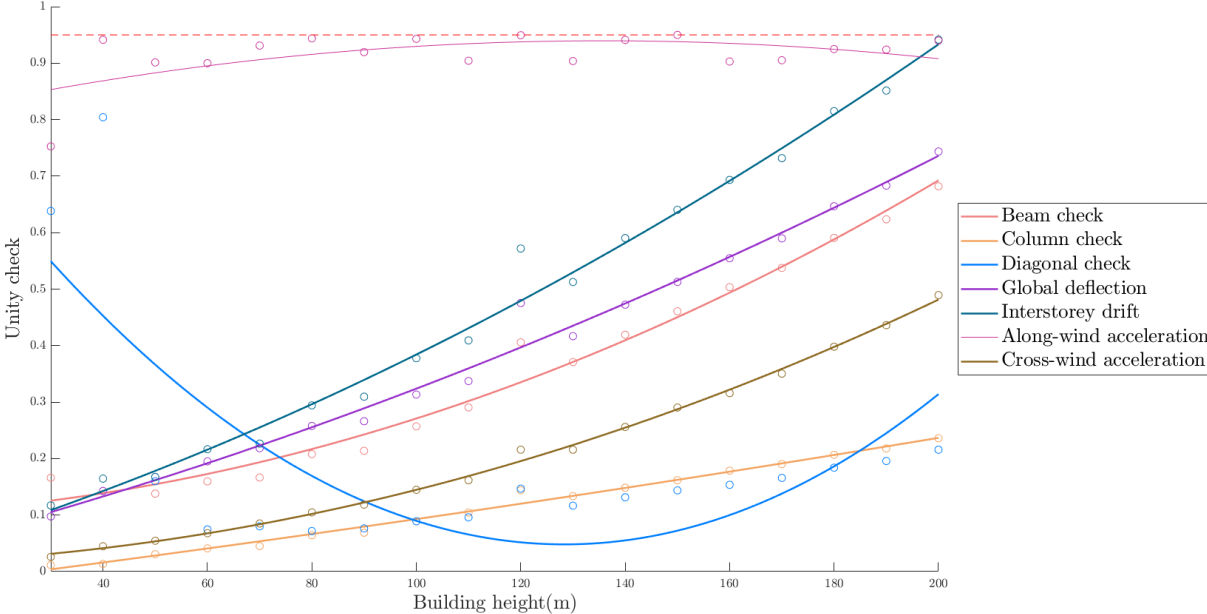


Figure 6.14: *Glulam diagrid - 6 storey diagonals*

The following observations can be made from the presented graphs:

1. The governing failure mechanism for all building heights for the two studied alternatives is the along-wind acceleration. As seen for the behaviour of the other two stability systems, this constraint is always pushed to the limit, showing the effect of the optimization criteria.
2. The capacity of the diagrid elements is studied with the constraint called diagonal check. The trend follow by this unity check shows a more abrupt decrease for the six storey alternative, especially when the building height goes from 30 to 80 meters. Once the decreasing trend stabilizes for both alternatives, it starts to show an increasing trend. The behaviour of these trends is caused by the dependency of the system on the efficiency of the diagrid configuration, which causes a rapid increase in the diagonals cross-section. However, once the diagonals have been maximized, and the building height keeps increasing, the unity check starts to increase.
3. The cross-wind acceleration increases with increasing building height at a slower rate than for the other stability systems. This trend is caused by the dependency of this constraint of the global stiffness of the structure, which is significantly higher for this stability system.
4. The beam and column unity checks follow a gradually increasing trend for both design alternatives. This trend is caused by the moment transfer mechanism and dynamic behaviour of this system, which does not rely on the cross-sections of these structural elements to stabilize the building. The increasing trend corresponds to the gradual increase of the vertical loads as the building height increases.
5. The global deflection and interstorey drift follow a rapidly increasing trend as the building height increases. The trends followed by these unity checks are very similar for lower rise building; however, as the building height increases their trends deviate, with the interstorey drift increasing at a much critical rate. This deviation is caused by the bending behaviour of the diagrid system and the shear behaviour of the frame. Figure 6.15 shows the deflected shape of the diagrid model, where it can be seen that the openings in the diagrid leave the frame columns exposed to shear deformation, which increases the interstorey drift.

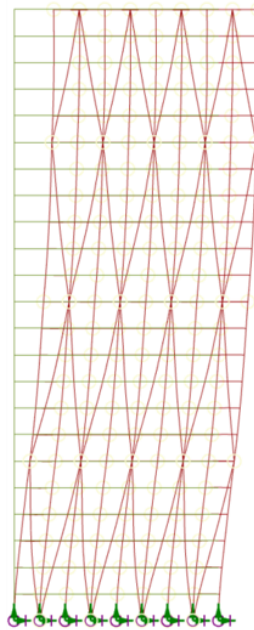


Figure 6.15: *Deflected glulam diagrid system*

6.2 Discussion

This section focuses on discussing the results and observations presented in section 6.1. Previously the results were presented individually for each stability system, so this section provides a comparison between the systems in terms of performance and behaviour. Moreover, the data used to visualize the influence of the preliminary parameters on the design was collected using EA optimization, which rates design alternatives based on a user defined criterion. Both the data collection method and the optimization criteria have an influence on the results which is discussed in this section. Finally, there is a reflection on the design feasibility of the presented design alternatives in terms of costs, architectural design and assembly methods.

Stability System Comparison

This investigation focused on studying three different timber stability systems; however; as presented in section 6.1, different configurations for each stability system are studied based on the defined ranges for the preliminary design parameters. Figure 6.16 shows the maximum building slenderness that can be achieved by the most relevant and representative design configurations. The presented glulam frame configurations have a rotational stiffness of 300 000 kNm/rad in the column-beam connections, while the CLT core configurations have pinned column-beam connections. For the glulam diagrid only the 6 storey diagonal angle configuration is presented, given that the height limitation for this system was determined based on it.

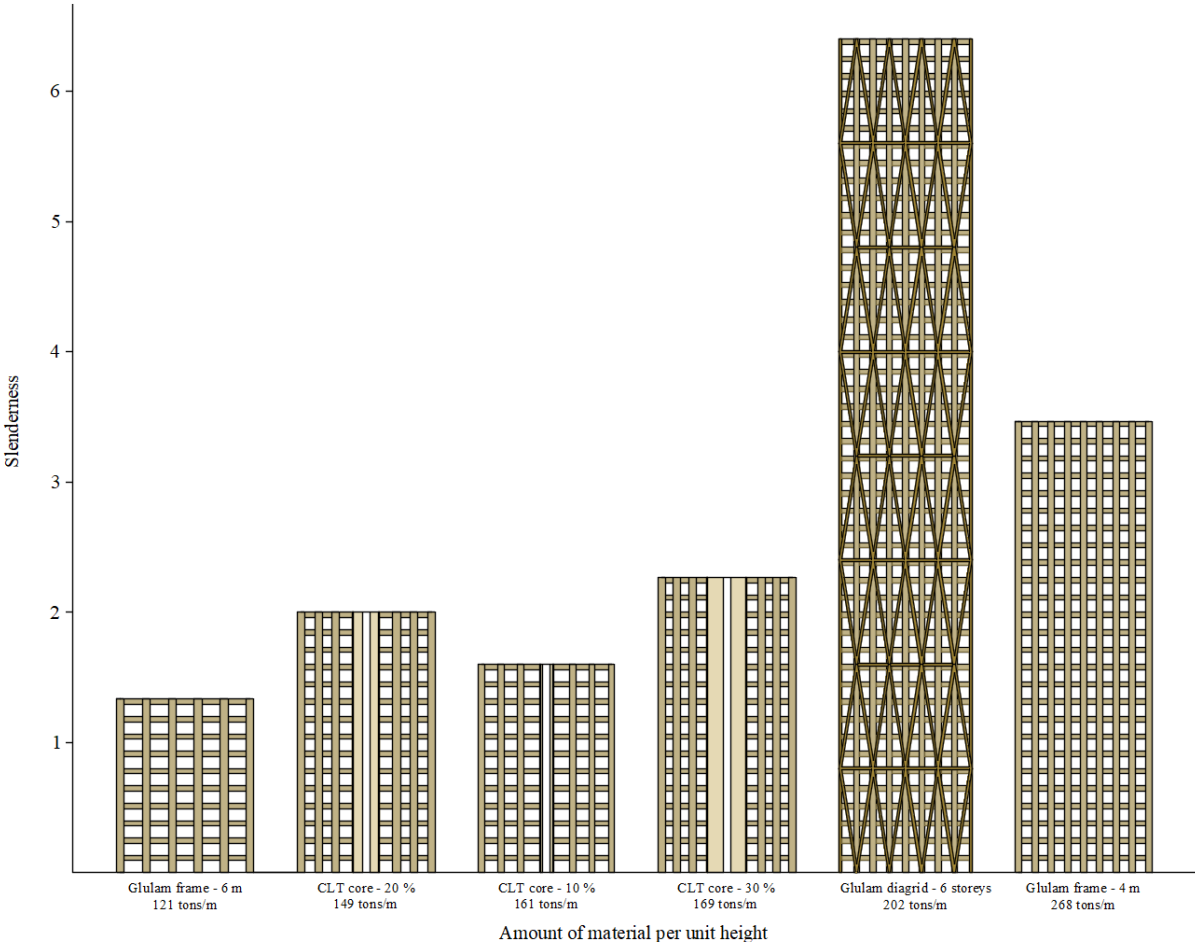


Figure 6.16: Amount of material to reach maximum height

Figure 6.16 shows the amount of material per unit height required to achieve the presented building slenderness. The efficiency of each design configuration can be defined by the ratio of required amount of material and building slenderness, showing that the glulam diagrid is significantly more efficient than the other systems. Provided that the governing failure mechanism for all design configurations is the along-wind acceleration, the efficiency of the system relies on their moment transfer mechanism and global stiffness. From the results presented in section 6.1 it is seen that the global stiffness and dynamic response of the glulam frame and CLT core rely on the cross-section of the frame elements, while the glulam diagrid relies on the efficiency of the diagrid configuration, making this system significantly more efficient. Special attention must be given to comparing the efficiency of the glulam frame and the CLT core. Figure 6.16 shows that some configurations of the CLT core are slightly more efficient than the glulam frame configurations; however, the CLT core incorporates pinned column-beam connections while the glulam frame has an additional $300\,000\text{ kNm/rad}$ rotational stiffness, which translates into an exponential increase of the cost, and the complexity of the design and assembly. When the mentioned effects are taken into account, the CLT core shows a significantly higher efficiency than the glulam frame.

The maximum building slenderness presented in figure 6.16 can be compared with the slenderness of existing structures. As mentioned in section 2.4 currently the tallest timber building in the world is Mjøstårnet with a total height of 84 meters, and a slenderness of 2.3 in the along-wind direction and 4.9 in the cross-wind direction. The stability system of Mjøstårnet consists of a moment resistant glulam frame and glulam bracing, with approximately seven meters effective span. The slenderness of this building is significantly larger than what was found to be the maximum slenderness for the six meter span glulam frame configuration; however, this is explained by the addition of bracings, which as the glulam diagrid it efficiently increases the global stiffness of the structure. Moreover, it is important to note that based on the assumed location for this investigation, the basic wind speed in the model was 22% higher than the basic wind speed used to design Mjøstårnet [1].

Available Net Floor Area

When performing a parametric study on the structural design of a building where hundreds of different design configurations are evaluated, it is important to consider the feasibility of implementing the designs in practice. One of the most important parameters for office and residential buildings is the amount of area available to be rented (net floor area). During this investigation the minimum net floor area required for a design alternative to be considered was 70%. For some design configurations this limitation determined the maximum building slenderness that could be achieved. Figure 6.17 shows the net floor area and structural floor plan distribution required to achieve the maximum building slenderness of each of the design configurations presented in figure 6.16. From the figure it can be seen that the height limitation for the different CLT cores and the four-meter span glulam frame was determined by the net floor area, causing a significant reduction of the floor plan flexibility of these configurations. Moreover, it is important to mention that the net floor area in this investigation was determined based on the structural elements required to provide lateral stability to the building; however, additional structural elements might be required to carry the loads from elevators and emergency stairs, which will reduce the net floor area for all configurations.

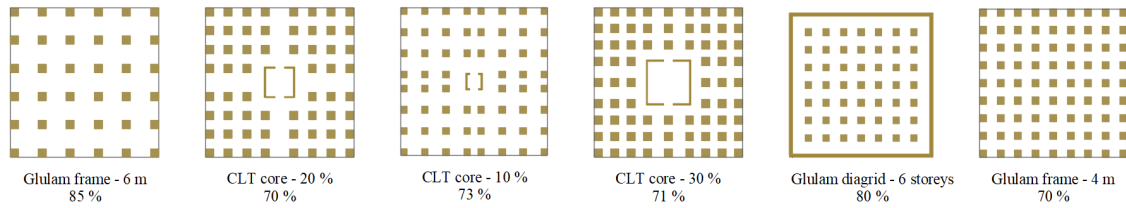


Figure 6.17: *Net floor area to reach maximum slenderness*

Architectural Limitations

The design feasibility of the different design configurations can also be defined by the architectural limitations that they provide, which can be divided into floor plan flexibility and façade design. As previously mentioned, in terms of floor plan flexibility, the CLT core configurations as well as the four-meter span glulam frame present a significant reduction caused by the required column cross-section and the clear spacing between the structural elements. This limitation is given by the dynamic behaviour of these configurations which relies on the self-weight of the structural elements to reduce the along-wind acceleration. The center-to-center distance between the columns in the glulam diagrid configurations is the same as the other systems; however, the efficiency of this system in terms of global stiffness results in significantly smaller column cross-section, increasing the clear spacing between the structural elements.

On the other hand, in terms of façade design, the glulam diagrid presents a significant limitation compared to the other stability systems. The diagrid elements are placed across the entire perimeter of the structure, causing a disruption in the daylight intake and the view from the rentable area. As seen in the results presented in section 6.1 the angle of the diagonal elements determines the efficiency of the of the system, which significantly influences its structural design. However, it can also be noted that the angle of the diagonals will also determine the level of the disruption on the façade design, decreasing the feasibility of configurations incorporating small diagonal angles. As seen in figure 6.17 the only structural elements across the perimeter of the structure for the glulam frame and CLT core configurations are the columns, which have a significantly lower effect on the façade design.

Element Cross-Sections

Appendix F provides the data collected using the EA method for each stability system, including the size of the cross-sections required to stabilize individual configurations. The column cross-sections range from 20-20 to 180-180 *cm*. These cross-section sizes correspond to the genome of the optimization determined based on the capability of glulam manufacturers to produce them. However, the feasibility of implementing the larger cross-section in practice can be assessed based on the maximum cross-sections used in existing structures. Mjostarnet incorporates corner column cross-sections of 160 x 65 *cm*, which based on their area suggest that cross-sections larger than 120-120 *cm* might have a limited potential to be implemented in practice. This practical limitation could decrease the maximum slenderness each stability system can achieve. As previously mentioned, less efficient stability systems such as the glulam frame rely on their self-weight for decreasing the dynamic response, which means that this additional limitation has a higher influence on the maximum slenderness they can achieve. Figure 6.18 shows an updated version of figure 6.16 when this practical limitation is taken into consideration. From the figure it can be seen that the maximum slenderness of each stability system significantly decreased, especially for the glulam frame configurations. The maximum slenderness of the glulam frame with four-meter effective span decreased by 60%, while for the glulam diagrid it decreased 25%. The glulam frame configuration with six-meter effective span became not feasible. On the other

hand, this decrease of the maximum building slenderness is accompanied by a significant increase of the clear spacing between the structural elements and the net floor area available. Figure 6.19 shows an updated version of figure 6.17 when the element cross-section feasibility is taken into consideration.

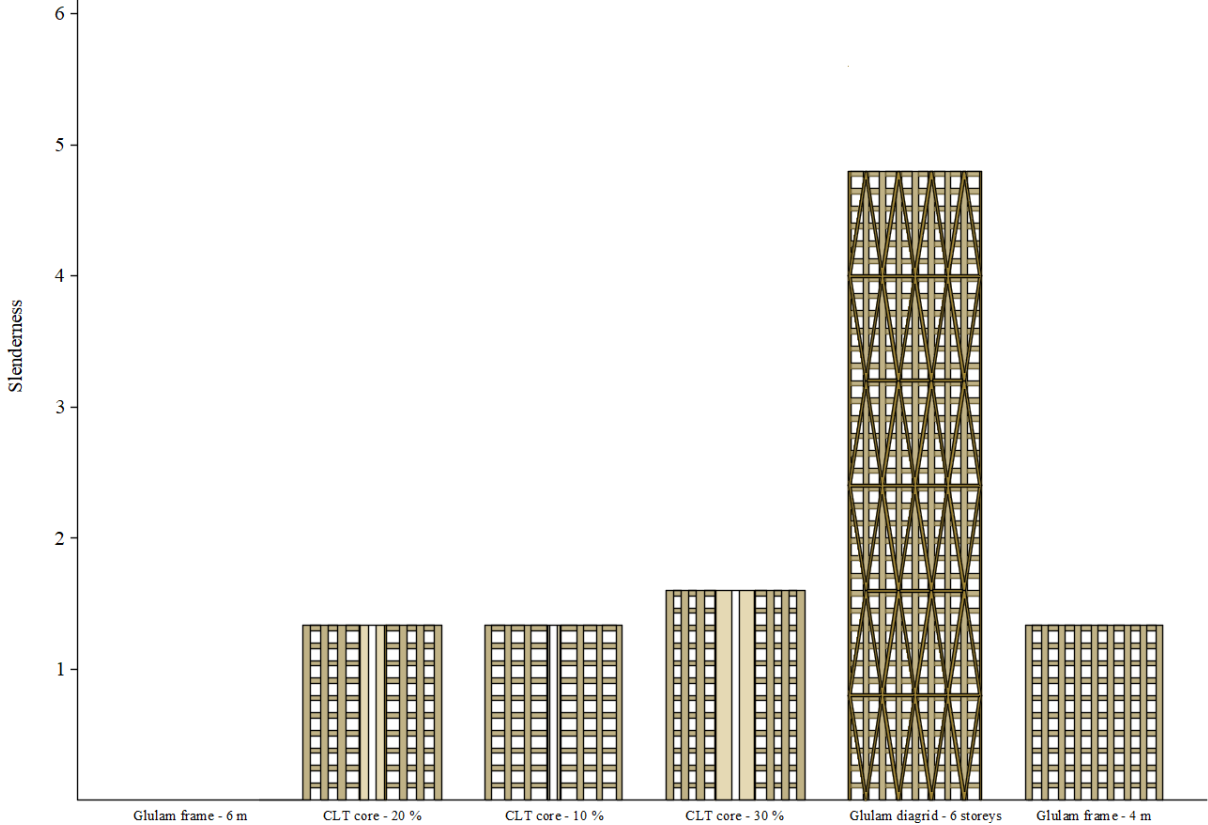


Figure 6.18: *Maximum slenderness reduced column cross-sections*

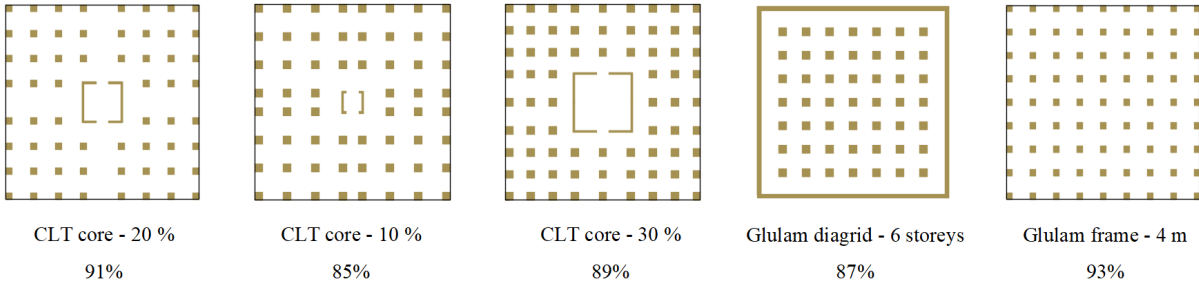


Figure 6.19: *Net floor area reduced column cross-sections*

Moreover, the feasibility of incorporating large column cross-sections across the entire structure must be assessed. Commonly column cross-sections decrease towards the top of the structure, proportionally to the design loads. However, this investigation assumed that all columns have the same cross-section to decrease the computational cost of the optimization. This assumption might not be feasible in practice due to a significant increase of the material costs, which could also decrease the maximum slenderness less efficient stability systems can achieve.

Connection Design

The stiffness of the connections between the structural elements was one of the studied parameters in the parametric study; however, this parameter should also be assessed in terms of design feasibility. Appendix B.3 provides examples of connection design for a given design configuration when the rotational stiffness ranges from 100 000 – 400 000 kNm/rad . From the presented calculations it can be seen that the design of these connections is governed by the required rotational stiffness, which significantly increases the required amount of steel elements. The configuration of these connections includes two steel plates that penetrate both the beam and column, which are set in place by large a number of steel dowels. The presented connection designs present an exponential increase on the cost of the structure driven by the required amount of material and the complexity of the assembly method. The installation of the steel plates and dowels requires high on-site precision, which translates into a significant increase on labor costs. Moreover, Appendix B.1 provides the design configuration of pinned connections. This connection type incorporates one steel plate that penetrates only the beam and requires significantly less dowels than the semi-rigid designs. The difference in amount of material between the different connections has an effect not only on the costs, but also on the environmental footprint of the structure caused by the large amount of CO₂ released during the production of steel.

The complexity of the connection design and their required amount of steel connectors determines the feasibility of a design configuration to be used in practice. As previously mentioned, for column-beam joints, the difference between implementing pinned or semi-rigid connections is exponential in terms of assembly method and required volume of steel, which significantly limits the potential of including rotational stiffness in the design of timber high-rise structures. During this study the influence of rotational stiffness on design was investigated for both the glulam frame and CLT core stability systems. While frame alternatives rely on the connection stiffness for lateral stability and moment transfer, the CLT core design is form stable and has the capacity to transfer the full moment caused by the wind through the core structure. From the results presented in section 6.1 it can be seen that adding rotational stiffness in the column-beam connections for the CLT core, has a positive influence on the required amount of material and net floor area, increasing the maximum slenderness the building can achieve. However, this slightly enhanced behaviour comes with an exponential increase in the costs and environmental footprint of the structure, which makes these configurations not a feasible solution in practice. On the other hand, for the glulam frame, the rotational stiffness in the column-beam connections is required for lateral stability, which significantly limits the potential of this stability system to be implemented in practice as the main load-bearing and stabilizing system.

The design feasibility of a design configuration based on the connection design is not only determined by their moment transfer capacity. As previously mentioned, the connection between the diagrid elements are designed as pinned, since the triangular configuration of the elements is form stable and provides sufficient stiffness. However, the complexity of this connection is given by the high number of intersecting members. Appendix B.3 shows an example connection design, for the critical intersection of a given design configuration. The connection design includes one steel plate that penetrates each diagonal member, as well as various steel dowels. The assembling of these connections requires high on-site precision, significantly increasing the labor costs. The angle of the diagonal elements determines the number of connections required. Decreasing the diagonal angles from four to two storeys increases the number of connections by 100%, which means that design configurations incorporating smaller angles have significantly lower potential to be implemented in practice.

Optimization criteria

The data used during this part of the parametric study was collected using EA optimization. During this process the optimal solution was defined as the combination of cross-sections that yielded the maximum net floor area while complying with all design constraints. The data collection method and the defined optimization criteria have an effect on the results presented in section 6.1. The implementation of EA pushes each design alternative to the limit of the governing design constraint, as seen for the structural behaviour of all the stability systems. This effect limits the possibility to visualize the influence of the design parameters on the governing failure mechanism. The genome of the EA optimization (member cross-sections) was defined based on the selection provided by glulam manufacturers; however, this has an effect on the maximum slenderness presented in figure 6.16. Increasing the global stability of a given design configuration is done by increasing the cross-section of the structural elements, which means that once they have been maximized, the structure can not increase in height.

As previously mentioned, both the glulam frame and the CLT core rely on the addition of material to reduce the dynamic response of the structure. Provided that the optimization criteria aimed to maximize the net floor area, the cross-section of the beams increased rapidly to add weight to the structure without reducing the net floor area. Appendix F shows the data collected using the EA method for each stability system, and there it can be seen that for the glulam frame this phenomenon caused the cross-section of the beams to be maximized for all design alternatives, with a cross-section of 80-130 *cm*. This beam cross-section is significantly large for a residential building; however, as seen in figure 6.20 when considering the floor thickness and beam height, the architectural storey height is 2.4 meters, which is still considered to be within the acceptable range in the Dutch Building Decree.



Figure 6.20: Available floor to ceiling height

6.3 Preliminary Design Tool

This section presents the data collected using the BFA method. As previously mentioned, BFA focus on gathering the design output for all possible combinations within a constrained search space. For this investigation the search space was formed by all design configurations as well as all possible element cross-sections. The data was collected based on the parametric model, which means individually for each stability system. As previously mentioned in section 5.2.2 the visualization interface Design Explorer is used to transform the post-processed BFA data into a preliminary design tool. This tool allows users to define ranges for the preliminary design parameters and the desired output, and find an estimation of the required amount of material and element cross-sections required. The output presented in the tools consists of the net floor area, governing failure mechanism, amount of material per unit height, and maximum acceleration. Figure 6.21, shows a QR code that directs to each individual preliminary design tool, as well as a permanent link that can be used to access them.



Figure 6.21: *Preliminary Design Tools*

6.4 Conclusions

The structural design of timber high-rise structures is governed by the dynamic response of the structure when exposed to dynamic horizontal loads such as wind. The dynamic response of a structure is quantified in terms of the acceleration at which it oscillates. This acceleration is determined by the self-weight and global stiffness of the structure, which are highly influenced by the selection of preliminary design parameters. Sections 6.1 showed the influence of individual parameters on the structural design of the building based on the net floor area, amount of material per unit height, and moment resistance of the connections required to meet the design constraints. The data was presents individually for each stability system followed by a discussion about the comparison of the different systems provided in section 6.2. When the data from the different systems was compared, it was concluded that the most influential preliminary design parameter in the design of timber high-rise structures is the stability system given that it determines the global stiffness of the structure, which showed a significantly higher influence on the dynamic response than the self-weight.

Section 6.2 defined the efficiency of a stability system as the ratio of maximum building slenderness versus the amount of material per unit height required to achieve it. In this comparison it was noted that the diagrid stability system is significantly more efficient than the other studied stability systems, caused by the high global stiffness provided by the triangular configuration of

the diagrid elements. When comparing the efficiency of the glulam frame and CLT core alternatives, two criteria were considered, the ratio of slenderness versus amount of material, and the complexity of their connections. The glulam frame is not a form stable structure, which makes this system rely on the stiffness of the connections for lateral stability. Semi-rigid connections showed an exponential increase on the cost and environmental footprint of the structure, which significantly reduces the efficiency and design feasibility of the glulam frame. On the other hand, the CLT core is a form stable structure without including rotational stiffness in the column-beam connections, which makes this system significantly more efficient than the glulam frame.

7 Conclusions and Recommendations

7.1 Conclusions

Research Question

The results and observations found during this investigation can be used to answer the main reach question, which is as follows:

What is the influence of stability system design, connection stiffness, and building height on the structural design of timber high-rise buildings based on the wind-induced dynamic response?

• Stability System Design

1. The selection of stability system is the most influential parameter for the design of timber high-rise structures, due to its high influence on the global stiffness.
2. The global stiffness has a higher influence on the design of timber high-rise structures than the self-weight, proving that the effect of timber's low density can be mitigated by the implementation of efficient stability systems.
3. Based on the studied stability systems, the glulam diagrid was determined to be the most efficient system for the design of timber high-rises due to its high global stiffness provided by the triangular configuration of the diagonal members.

• Connection Stiffness

1. The influence of connection stiffness in the design of timber high-rise structures is related to the ability of the stability system to provide lateral stability. Non-form stable structures such as glulam frames are very sensitive to changes in connection stiffness, while the effect in form stable structures such as CLT cores and glulam diagrids is nearly negligible.
2. Current methods provided by Eurocode and other building codes for incorporating rotational stiffness in timber connections, rely on the addition of steel elements. Therefore, the implementation of moment resistant connections in the different stability systems translated into an exponential increase in the costs and environmental footprint of the structure, reducing their feasibility of being implemented in practice.

• Building Height

1. The influence of building height on the design of timber high-rise structures is visualised by the influence of this parameter on the wind speed and lateral stability. As the building height increases, the wind speed increases logarithmically, while the global stiffness decreases proportionally to the efficiency of the stability system. These trends significantly affect the dynamic response of the structure, showing the high influence of this parameter on the design of these structures.

Research Methodology

Regarding the methods used to estimate the dynamic behaviour of the structure, the following is concluded:

1. The gust factor approach provided by EC1-4 provides an estimation of the acceleration of a structure that can be used for the preliminary design. However, its idealization of the structure as a clamped cantilever beam with one vibration mode causes an underestimation of the dynamic response, which must be considered by decreasing the acceptable limit for the acceleration unity check.
2. The method provided by Oosterhout (1996) to estimate the natural frequency of a structure is ideal for the preliminary design of timber high-rise structures, given that the magnitude is estimated based on the global stiffness and mass distribution, rather than empirical data. However, this method requires an assumption regarding the shear and bending stiffness of the structure, which must be assessed during the design phase.
3. The experimental data provided by Feldmann (2016) can be used to estimate the magnitude of the structural damping of a timber structure. However, this parameter depends on the moment transfer mechanism of the structure, which limits its applicability to the type of structures assessed in the study.

Regarding the optimization criteria and design assumptions used to collect the data for the parametric study, the following is concluded:

1. The optimization criteria used to collect the EA data aimed to maximize the net floor area of each design configuration, which resulted in a reduction of the self-weight of the structure that affected its dynamic response. The implementation of multi-objective optimizations that maximize the net floor area and minimize the dynamic response of the structure could yield a more accurate representation of timber high-rise design.
2. The element cross-sections used for the genome of the optimizations was determined based on the capacity of glulam manufacturers. However, the implementation of column cross-sections larger than 120-120 *cm* was determined to be not feasible in practice. This additional limitation proved to have an effect on the maximum slenderness each stability system could achieve, with a greater influence in less efficient systems.

7.2 Recommendations

This section presents recommendations for future work in the field of timber high-rise design based on the observations and conclusions found during this investigation.

1. Moment resistant connections

The results collected during the parametric study for connection stiffness suggest that this is a very influential parameter on the design of not form stable structures like glulam frames, and that it can potentially enhance the efficiency of form stable structures like CLT cores. However, it was concluded that the addition of rotational stiffness in the column-beam connections translates into an exponential increase on the costs and environmental footprint of the structure. In order to feasibly incorporate this parameter in the design of timber high-rise structures, methodologies to increase the rotational stiffness of timber connection while decreasing the required volume of steel connectors must be studied. The implementation of carpentry joints shows a significant potential to achieve

this goal; however, further research on their rotational stiffness capacity and large-scale assembly is required.

2. Structural damping

The structural damping ratio of a structure is a very complex parameter that incorporates the energy dissipated by different elements of a system. This parameter has a significant influence of the dynamic response of a structure, yet currently there is limited literature on methods to accurately determine its magnitude. However, it is known that the selection of load-bearing and stabilizing materials significantly influences the energy dissipation of the system, and that timber presents a potential to increase the structural damping of a structure [24]. Developing methods to accurately predict the structural damping based on the selection of preliminary design parameters, can significantly increase the understanding of the dynamic response of timber high-rise structures and assist on determining the potential and limitations that these structures present.

3. Braced stability systems

The output of this investigation concluded that the selection of stability system design is the most influential preliminary design parameter for the design of timber high-rise structures. The selection of stability system determines the efficiency of the global stiffness, which can mitigate the effect of timber's low density on the dynamic response of the structure. From the studied stability systems, it was concluded that the glulam diagrid was the most efficiency system, due to its high global stiffness provided by the triangular configuration of the elements. This observation suggests that other stability systems incorporating braced triangular elements must be studied to determine their efficiency and potential to mitigate the architectural limitations provided by the diagrid system which were discussed in section 6.2. Some stability systems that present a high potential to be implemented for the design of timber high-rise structures are outrigger systems and braced tubes. Finally, the potential of incorporating different braced systems into the design can also be assessed given that it could result in a highly efficiency system with increased architectural flexibility. This concept can be visualized in figure 7.1 which shows a design concept for a timber high-rise structure in Chicago, presented by Perkins Will incorporating glulam diagrid in the along-wind direction and bracing in the cross-wind direction [41].

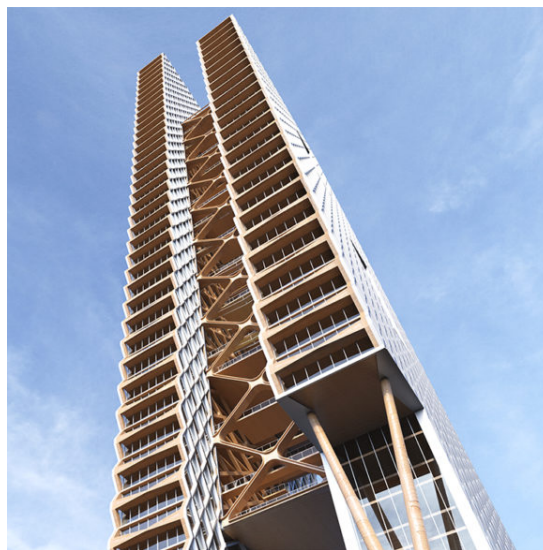


Figure 7.1: *River Beach Tower design concept by Perkins & Will [41]*

4. Design tools

The preliminary design of a structure is usually done using simplified models and rules of thumb due to time constraints. However, this is not possible for the design of timber high-rise structures due to the complexity of their dynamic behaviour. The goal of this investigation was to determine the influence of preliminary parameters on the design of timber high-rise structures to assist engineers in making well-argued decisions during this phase. However, the output of this investigation might still require a significant amount of engineering judgement and calculations during the preliminary design phase. Developing rules of thumb would significantly increase the efficiency of the preliminary design of timber high-rise structures. However, accurately predicting the dynamic response of a timber structure can be computationally expensive, making the data collection process for the development of such a design tool computationally infeasible with the implementation of commonly used methods. Machine learning probabilistic algorithms can be implemented to significantly decrease the computational cost of large-scale finite element models.

5. Tuned mass dampers

Tuned Mass Dampers (TMD) are devices which can be installed at a given location in a structure to absorb the kinetic energy produced by lateral excitations, significantly reducing the amplitude of the induced vibrations [12]. Given that the design of timber high-rise structures is governed by the dynamic behaviour, TMD show significant potential to improve the behaviour of these structures by allowing them to increase their maximum slenderness and reduce the required amount of material. Studying the effect of the different types of TMD on the acceleration of timber high-rise structures could significantly simplify the study of their behaviour and incentivize their development. The effect of installing a TMD should be considered during the preliminary design phase, given that it would significantly influence the design of the structure.

References

- [1] Rune A. “Mjøstårnet – Construction of an 81 m Tall Timber Building”. In: *Internationales Holzbau-Forum IHF* (2017).
- [2] Arne K Abrahamsen R. “Structural Design and Assembly of “Treet” a 14-storey Timber Residential Building in Norway”. In: *World Conference of Timber* (2014).
- [3] R van den Berg. *Investigation of damping in high-rise buildings*. 2012.
- [4] C BlaßH.Sandhaas. *Timber Engineering Principles for Design*. KIT Scientific Publishing, 2017.
- [5] R Brandner R. Tomasi. “Properties, testing and design of cross-laminated timber”. In: *COST European Cooperation in Science and Technology* (2018).
- [6] Canadian Wood Council. *Brock Commons Tallwood House - The advent of tall wood structures in Canada*. 2018.
- [7] R Crielaard. *Self-extinguishment of cross laminated timber*. 2015.
- [8] CEG Faculty TU Delft. *Concrete building structures*. 2016.
- [9] H Feldmann A. Huang. “Dynamic properties of tall timber structures under wind-induced vibrations”. In: *Wood Conference of Timber Engineering* (2016).
- [10] K Flatscher K. Bratulic. “Screwed joints in cross-laminated timber structures”. In: *World conference of timber engineering* (2014).
- [11] M Frangi A. Fontana. “Fire Safety of Multistorey Timber Buildings”. In: *Institution of Civil Engineers* (2009).
- [12] M Gaspar. *The mechanism and application of Tuned Mass Damper (TMD)*. 2017.
- [13] C Geurts. *Wind-induced pressure fluctuations of on building facades*. 1997.
- [14] S Guo J. Zhan. *Theoretical evaluation of moment resistance for bolted timber connections*. 2019.
- [15] C Hasburgh L. Dagenais. *Fire performance of mass timber encapsulation methods and the effect of encapsulation on char rate of cross-laminates timber*. 2016.
- [16] Y Huang H. Gao. “Human-induced vibrations of cross-laminated timber (CLT) floor under different boundary conditions”. In: *Elsevier* (2020).
- [17] Amory J. *A Guidance Tool for Circular Building Design*. 2018.
- [18] M. Jelec, V. Rajcic, and Varevac D. “Cross-Laminated Timber (CLT) - A State of the Art Report”. In: *Gradevinar* (2018).
- [19] S Kanerva P. Peltola. *Design method for utilization of rotational stiffness of mechanical joints on the design of timber structures*. 2014.
- [20] J Katunsky D. Huang. *Responsive architecture*. MDPI, 2019.
- [21] A Kwan. “Shear lag in shear/core walls”. In: *Journal of Structural Engineering* (1996).
- [22] M. Espinoza O Laguarda. *Outlook for cross-laminated timber in the United States*. 2014.
- [23] N. Mohd Yusof et al. “Mechanical and Physical Properties of Cross-Laminated Timber Made from Acacia Mangium Wood as Function of Adhesive Types”. In: *Journal of Wood Science* (2019).
- [24] G van Oosterhout. *Wind-induced dynamic behaviour of tall buildings*. 1996.

- [25] O Orr J. Gibbons. “A brief guide to calculating embodied carbon”. In: *The Institution of Structural Engineers* (2020).
- [26] Y Paauwe. *Obtaining insight into the influence of the main design parameters in the preliminary structural design on the wind-induced dynamic response including soil-structure interaction effects of high-rise buildings in the Netherlands*. 2019.
- [27] M. Pedersen. *Dowel type connections, strength modelling*. 2002.
- [28] C Petersen. *Dynamics of building construction*. Springer, 2000.
- [29] United Nations Environmental Programme. “Global Status Report 2017”. In: *World Green Building Council* (2017).
- [30] proHolz. *Cross-laminated timber structural design, basic design and engineering principles according to Eurocode*. 2014.
- [31] Geldermans R.J. “Design for Change and Circularity - Accommodating Circular Materials Product Flows in Construction”. In: *Energy Procedia* (2016).
- [32] V Samanta S. Balas. “Quantum-inspired evolutionary algorithms for scaling factor optimization during manifold medical information embedding”. In: *Quantum Inspired Computational Intelligence* (2017).
- [33] A Simone. *An introduction to the analysis of slender structures*. 2011.
- [34] J Skolnik D. Wallace. “Critical assessment of interstorey drift measurements”. In: *Journal of Structural Engineering* (2010).
- [35] A Smith B. Coull. *Tall Building Structures: Analysis and Design*. John Wiley Sons. Inc, 1991.
- [36] A Spijkers J. Vrouwenvelder. *Lecture Notes on Structural Dynamics CT 4140 - Structural vibrations*. 2005.
- [37] SWECO. *The world’s tallest timber-framed building: an innovative and sustainable building*. 2014.
- [38] R Tinjum J. Christensen. “Site investigation, characterization and assessment for wind turbine design and construction”. In: *Wind Energy Systems* (2011).
- [39] M van Vliet. *Disassembling the steps towards building circularity redeveloping the building disassembly assessment method in the building circularity indicator*. 2018.
- [40] Chan W. *Global Stability of High-Rise Timber Buildings*. 2016.
- [41] Perkins & Will. *River Beech Tower, Chicago Illinois*. 2018.
- [42] T Znabei. *A post-tensioned cross-laminated timber core*. 2020.

Appendix A Wind Load

Wind Velocity

According to Eurocode NEN-EN 1991-1-4, the mean wind velocity function over the height of a high-rise structure, can be described using formula A.1.

$$v_m(z) = c_r(z) \cdot c_o(z) \cdot v_b \quad (\text{A.1})$$

- c_r = roughness factor
- c_o = orography factor : Dutch National Annex states $c_o = 1.0$
- v_b = standard wind velocity at reference height of 10m

$$v_b = c_{dir} \cdot c_{season} \cdot v_{b,0} \quad (\text{A.2})$$

- c_{dir} = direction factor : Dutch National Annex states $c_{dir} = 1.0$
- c_{season} = season factor : Dutch National Annex states $c_{season} = 1.0$
- $v_{b,0}$ = fundamental wind velocity : (I:29.5 m/s, II: 27 m/s, III: 24.5 m/s)

$$c_r(z) = k_r \cdot \ln \left(\frac{z}{z_0} \right) \quad (\text{A.3})$$

- k_r = terrain factor
- z_0 = roughness length : coastal = 0.003, sub-urban = 0.3, urban = 1.0

$$k_r = 0.19 \cdot \left(\frac{z_0}{0.05} \right)^{0.07} \quad (\text{A.4})$$

Peak Wind Pressure

According to Eurocode NEN-EN 1991-1-4, the peak wind pressure function over the height of a high-rise structure, can be described based on the mean wind velocity using formula A.5.

$$q_p(z) = (1 + 7 \cdot I_v(z)) \cdot \frac{1}{2} \cdot \rho \cdot v_m^2 \quad (\text{A.5})$$

- I_v = turbulence intensity
- ρ = air density
- v_m = mean wind velocity (see equation A.1)

$$I_v = \frac{\sigma_v}{v_m(z)} = \frac{k_l}{c_o \cdot \ln \left(\frac{z}{z_0} \right)} \quad (\text{A.6})$$

- k_l = turbulence factor : Dutch National Annex states $k_l = 1.0$
 c_o = orography factor

Wind Pressure

The wind pressure applied on the building can be determined based on the peak wind pressure and the mean wind velocity. Eurocode states two methods for estimating this pressure and for high-rise buildings the most applicable method is the force coefficient method which quantifies the characteristic global wind loading of the structure as seen in equation A.7.

$$F_w = c_s c_d \cdot \sum_{surfaces} q_p(z) \cdot c_f \cdot A_{ref} \quad (A.7)$$

- $c_s c_d$ = structural factor
 $q_p(z)$ = peak wind pressure
 c_f = force coefficient
 A_{ref} = reference area

$$c_s c_d = \frac{1 + 2 \cdot k_p \cdot I_v(z) \cdot \sqrt{B^2 + R^2}}{1 + 7 \cdot I_v(z)} \quad (A.8)$$

- k_p = peak factor
 $I_v(z)$ = turbulence intensity (see equation A.6)
 B^2 = background factor
 R^2 = resonance response factor

$$k_p = \sqrt{2 \cdot \ln(v \cdot T)} + \frac{0.6}{\sqrt{2 \cdot \ln(v \cdot T)}} \geq 3 \quad (A.9)$$

- T = average period of the reference wind velocity
 v = estimation of the gust frequency

$$v = n_{1,x} \cdot \sqrt{\frac{R^2}{B^2 + R^2}} \quad (A.10)$$

- $n_{1,x}$ = natural frequency

$$B^2 = \frac{1}{1 + \frac{3}{2} \cdot \sqrt{\left(\frac{b}{L(z)}\right)^2 + \left(\frac{h}{L(z)}\right)^2 + \left(\frac{b}{L(z)} \cdot \frac{h}{L(z)}\right)^2}} \quad (A.11)$$

b = width of structure
 h = height of structure
 $L(z)$ = turbulence length scale

$$L(z) = L_t \cdot \left(\frac{z}{z_t} \right)^\alpha \quad (\text{A.12})$$

L_t = 300 m
 z_t = 200 m
 α = $0.67 + 0.05 \ln z_0$

$$R^2 = \frac{\pi^2}{2 \cdot \delta} \cdot S_L \cdot K_s \quad (\text{A.13})$$

δ = logarithmic decrement of damping
 S_L = non-dimensional spectral density function
 K_s = size reduction factor

$$\delta = \frac{c_f \cdot \rho \cdot b \cdot v_m(z)}{2 \cdot n_{1,x} \cdot m_e} \quad (\text{A.14})$$

c_f = force coefficient
 ρ = air density
 $v_m(z)$ = mean wind velocity
 $n_{1,x}$ = natural frequency
 m_e = equivalent mass

$$S_L = \frac{6.8 \cdot f_l}{(1 + 10.2 f_l)^2} \quad (\text{A.15})$$

$$f_l = \frac{n_{1,x} \cdot L(z)}{v_m(Z)} = 0 \quad (\text{A.16})$$

$$K_s = \frac{1}{1 + \sqrt{(G_y \cdot \phi_y)^2 + (G_z \cdot \phi_z)^2 + \left(\frac{2}{\pi} \cdot G_y \cdot \phi_y \cdot G_z \cdot \phi_z \right)^2}} \quad (\text{A.17})$$

The constants are based on the vibration mode of the structure, height and width $c_y = c_z = 11.5$, $G_y = 1/2$ and $G_z = 5/18$.

Finally, in order to determine the force coefficient needed to determine the logarithmic decrement of damping and the characteristic global wind loading equation A.18 and figure A.1 can be used.

$$c_f = c_{f,0} \cdot \psi_r \cdot \psi_\lambda \tag{A.18}$$

- $c_{f,0}$ = force coefficient for rectangular sections without free-end flow (see figure A.1)
- ψ_r = reduction factor for rounded corners = 1.0
- ψ_λ = end effect factor = 1.0

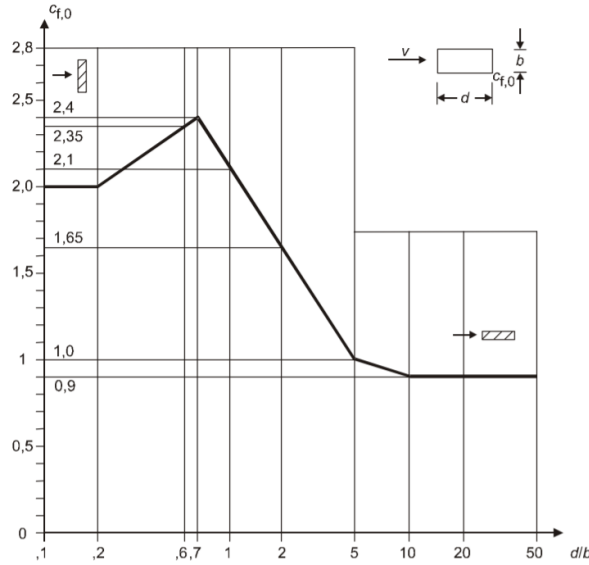


Figure A.1: Force coefficient for rectangular sections according to NEN-EN 1991-1-4

The wind pressure will vary along the height of the structure, corresponding to its width. Figure A.2 shows the methodology proposed by Eurocode in order to model the simplified pressure distribution along the height of a structure.

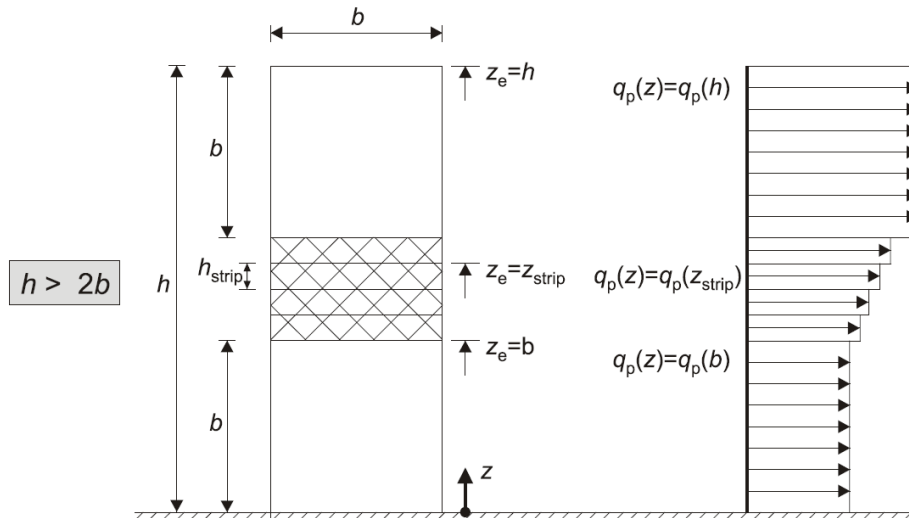


Figure A.2: Wind pressure distribution over height according to NEN-EN 1991-1-4

Appendix B Connection Design

Appendix B.1 Connection types

Based on the selected stability systems, there are various relevant connection types. As previously mentioned, the scope of this investigation focuses on studying the influence of rotational stiffness on the design of the structure only for column-beam connections. However, feasible configurations for the other connection types are presented in this section.

Frame connections

As previously mentioned, both moment resistant and pinned connections will be studied for the column-beam joints. The design configuration of the moment resistant connections is explained in section 4.1. The pinned connections will be designed using steel a T-shape steel plate that goes into the beam with dowels, and screws that connect them to the column. This configuration can be seen in figure B.1. The verification method for this type of connection is presented in section B.2.2.

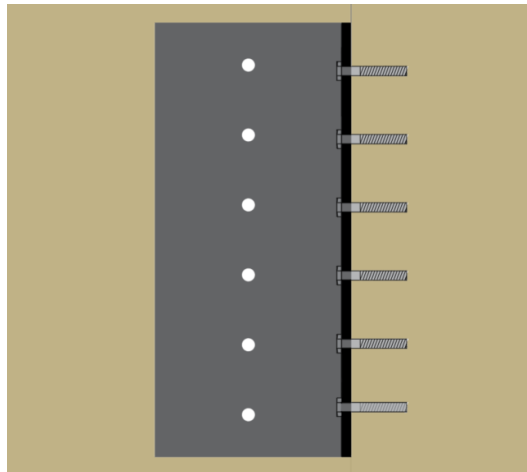


Figure B.1: *Pinned column-beam connections*

Core connections

The connection between the perpendicular CLT panels that form the stability core are designed using self-tapping screws (STS). As shown in figure B.2, two screws are used at each location, and they are both be placed at 45 degrees, providing a slip factor of $16,6 \text{ kN/mm}$. It is assumed that the screws will be placed every 300 mm along the height.

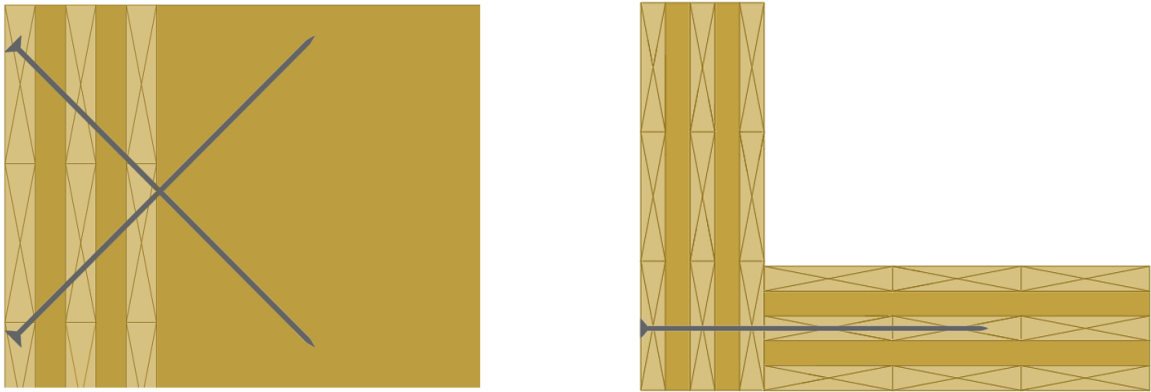


Figure B.2: *Perpendicular CLT panels connection configuration*

As previously mentioned, based on literature it is assumed that the displacements due to sliding and rocking is neglected for the design of the CLT core, which can only be achieved by incorporating fully rigid connections between the stacked panels, or by installing tension rods throughout the length of the panels. For the purpose of this investigation, it is assumed that the implementation of glued-in rods between the stacked CLT panels will provide sufficient rigidity to transfer the moment along the core and mitigate the displacements due to sliding and rocking. Figure B.3, shows a proposed configuration incorporating glued-in rods to transfer the moment and an additional wood profile at the end of each panel, in order to guarantee an even transfer of the stresses in the cross-section of the panels. Finally, it is assumed that the CLT panels will have a height equal to three storeys in order to reduce the number of connections, because the installation of glued-in rods requires high precision, which can be a challenge at a construction site.

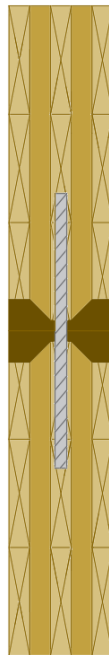


Figure B.3: *Stacked CLT panels connection configuration*

Diagrid connections

The connection between the diagonal members will have a similar configuration to the beam-column connections. The capacity of the connection is given by the implementation of slotted-in steel plates with dowels; however, the rotational stiffness is provided by the triangular configuration of the structural elements and not by the steel plates. Figure B.4 shows a proposed configuration for this type of connection, but as it can be seen, the configuration depends on the angle between the diagonal elements, which is one of the studied parameters.

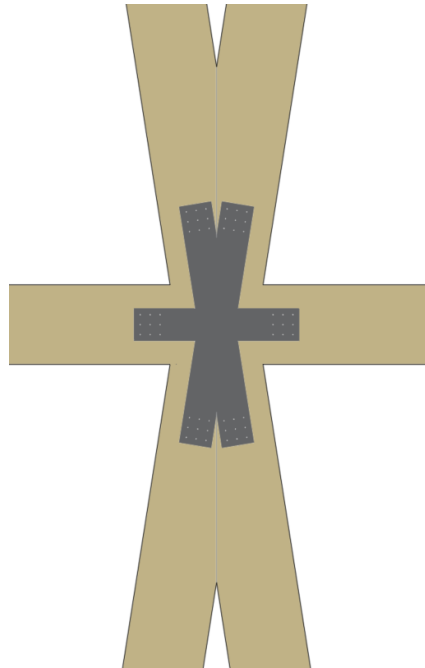


Figure B.4: *Diagrid connection configuration*

Appendix B.2 Column-beam connections

Appendix B.2.1 Semi-rigid connections

As previously mentioned, column-beam connections are designed using slotted-in steel plates and dowels. EC5 presents a method for evaluating the strength and stiffness of this type of connection; however, this method is limited to one steel plate, for which the research done by Pedersen (2002) will be used to determine the strength and stiffness of these connections. In order to use the research done by Pedersen it needs to be assumed that both the steel and the timber elements can reach a plastic deformation and that the maximum strength of the connection will be reached when the timber fails [27].

Connection Strength

The maximum strength resistance of the connection can be determined by evaluating all possible failure mechanisms that this connection could present as show in figure B.5. The definition of each presented failure mechanism can be seen in figure B.6. The design load found from the critical failure mechanism is the design load per fastener per shear plane. If two steel plates are incorporated into the design, the connection will have four shear planes. On the other hand, not all dowels will be fully effective, so formula B.2 can be used to determine the number of effective dowels. After calculating the number of effective dowels and determining the number of shear

planes, the design load taken by the dowels can be determined using formula B.3.

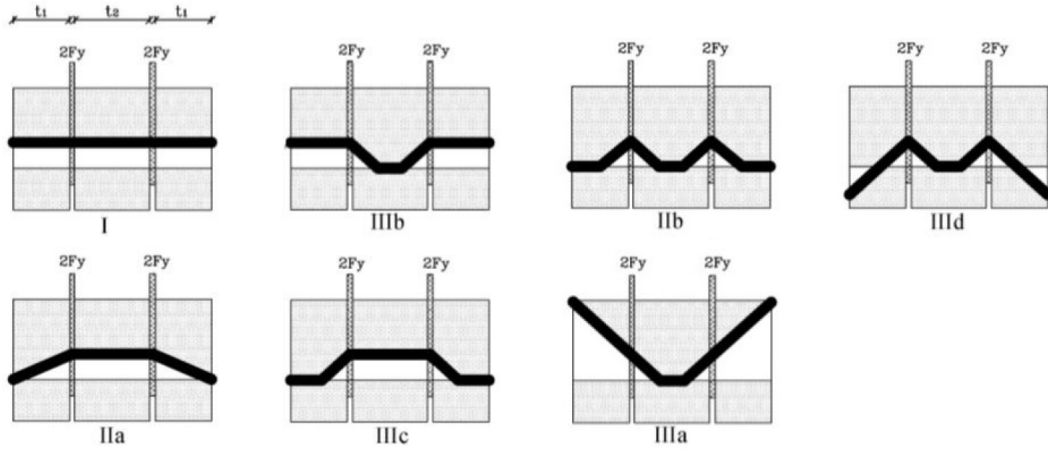


Figure B.5: *Slotted-in steel plated with dowels failure mechanisms [27]*

$$F_y = \min \begin{cases} \frac{1}{4}(2t_1 + t_2)d f_h & \text{Mode I} \\ \left(-\frac{1}{2}t_1 + \frac{t_2}{4} + \sqrt{\frac{1}{2}t_1^2 + \frac{M_y}{d f_h}}\right) d f_h & \text{Mode IIa} \\ \sqrt{4M_y d f_h} & \text{Mode IIb} \\ \left(\frac{1}{2}t_1 + \frac{1}{2}\sqrt{t_1^2 + \frac{2M_y}{d f_h}}\right) d f_h & \text{Mode IIIa} \\ \left(\sqrt{\frac{M_y}{d f_h}} + \frac{1}{2}t_1\right) d f_h & \text{Mode IIIb} \\ \left(\sqrt{\frac{M_y}{d f_h}} + \frac{1}{4}t_2\right) d f_h & \text{Mode IIIc} \\ \left(-\frac{1}{2}t_1 + \sqrt{\frac{1}{2}t_1^2 + \frac{M_y}{d f_h}} + \sqrt{\frac{M_y}{d f_h}}\right) d f_h & \text{Mode IIId} \end{cases}$$

Figure B.6: *Slotted-in steel plated with dowels failure mechanisms definition [27]*

$$f_{h,k} = 0,082(1 - 0,01 \cdot d)\rho_k \quad (\text{B.1})$$

$$n_{eff} = \min \left[n_{columns}; n_{columns}^{0.9} \cdot \left(\frac{a_1}{13d}\right)^{0.25} \right] \quad (\text{B.2})$$

$n_{columns}$ = dowels parallel to the grain
 a_1 = spacing between dowels

$$F_{max,dowels} = 4 \cdot n_{eff} \cdot F_{governing} \cdot n_{rows} \quad (\text{B.3})$$

The failure of the dowels is not the only possible failure mechanism, there can also be a failure of the timber member or the steel plate. The net area of the timber member can be checked using formulae B.4 and B.5 and the resistance of the steel plates can be checked using formula B.6.

Finally, the block and plug shear resistance can be checked needs to be checked using formula B.7 and figure B.7.

$$F_{max,c} = f_{c,0,k} \cdot A_{net,timber} \quad (B.4)$$

$$F_{max,t} = f_{t,0,k} \cdot A_{net,timber} \quad (B.5)$$

$$F_{max,plates} = \min \left(f_y \cdot t_{plate} \cdot b_{plate}; \frac{0.9 \cdot f_u A_{net}}{\gamma_{M,2}} \right) \quad (B.6)$$

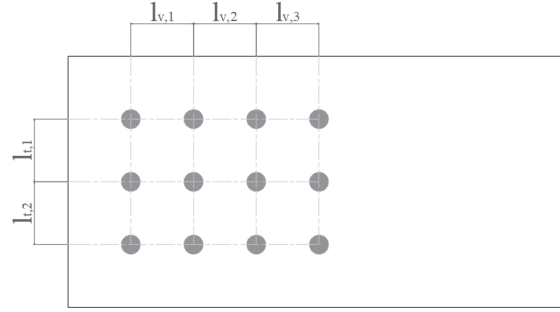


Figure B.7: Block and plug shear in slotted-in steel plates and dowel connections

$$F_{max,block,plug} = \max (1.5A_{net,t} \cdot f_{t,0,k}; 0.7A_{net,v} \cdot f_{v,k}) \quad (B.7)$$

$$\begin{aligned} A_{net,t} &= L_{net,t} \cdot t \\ A_{net,v} &= L_{net,v} \cdot t \\ L_{net,t} &= \sum l_{t,i} \\ L_{net,v} &= \sum l_{v,i} \end{aligned}$$

Connection Stiffness

The stiffness of slotted-in steel plates with dowel connections can be determined using formulae B.8 and B.9. The formulae provide the rotational stiffness of each individual dowel per shear plane, and for this specific connection design it needs to be multiplied by four, which equals the number of shear planes. Finally, in order to consider the interaction of timber and steel the density of timber can be doubled [27].

$$K_{ser} = \rho_m^{1.5} \cdot \frac{d}{23} \quad (B.8)$$

$$K_{rot,connection} = K_{ser,fastener} \cdot I_p \quad (B.9)$$

Appendix B.2.2 Pinned connections

Pinned column-beam connections following the configuration shown in figure B.1 need to be validated in terms of the capacity of the dowels, and the capacity of the bolt group presented in EC5.

Dowels capacity

The maximum capacity resistance of the dowels in the connection can be determined by evaluating all possible failure mechanisms that this connection could present as show in figure B.5. The definition of each presented failure mechanism can be seen in figure B.6. The design load found from the critical failure mechanism is the design load per fastener per shear plane. If one steel plate is incorporated into the design the connection has two shear planes.

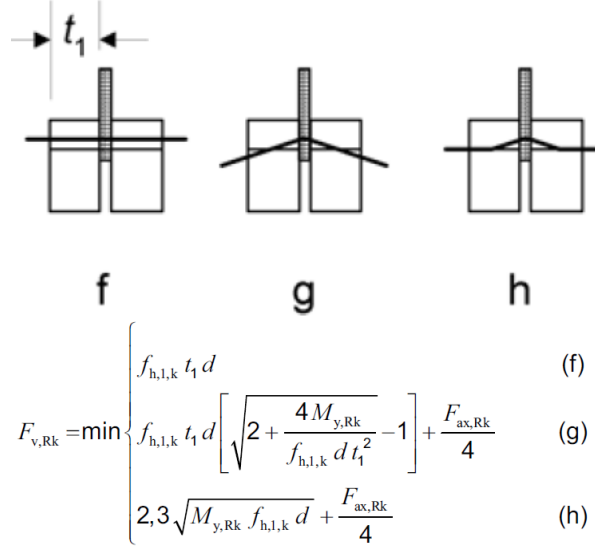


Figure B.8: *Pinned column-beam failure mechanisms*

- $f_{h,k}$ = characteristic embedment strength
- $F_{ax,Rk}$ = characteristic withdrawal capacity
- $M_{y,Rk}$ = fastener yield moment
- d = dowel diameter

$$f_{h,k} = 0.082(1 - 0.1d) \cdot \rho_k \quad \text{(B.10)}$$

$$M_{y,k} = 0.3 \cdot f_{u,k} \cdot d^{2.6} \quad \text{(B.11)}$$

Bolts capacity

The bolts in this connection carry both axial and shear loads, so their capacity needs to be checked for their combined action as seen in formula B.12. Moreover, the column needs to resist the load perpendicular to the grain direction caused by the bolts. In order to check for compliance, the design splitting capacity (formula B.16) must be larger than the tension force.

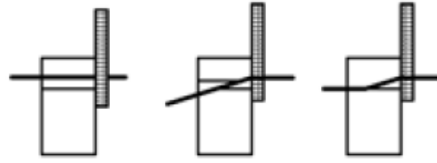
$$\left(\frac{F_{ax,Ed}}{F_{ax,Rd}} \right)^2 + \left(\frac{F_{v,Ed}}{F_{v,Rd}} \right)^2 \leq 1 \quad \text{(B.12)}$$

$$F_{ax,Rk} = n_{ef} (\pi d l_{eq})^{0.8} \cdot f_{ax,k} \quad \text{(B.13)}$$

n_{ef} = effective number of bolts
 l_{ef} = bolt penetration length
 $f_{ax,k}$ = characteristic withdrawal strength

$$n_{ef} = n^{0.9} \quad (\text{B.14})$$

$$f_{ax,k} = 3.6 \cdot 10^{-3} \cdot \rho_k^{1.5} \quad (\text{B.15})$$



c **d** **e**

$$F_{v,Rk} = \min \begin{cases} f_{h,k} t_1 d \left[\sqrt{2 + \frac{4M_{y,Rk}}{f_{h,k} d t_1^2}} - 1 \right] + \frac{F_{ax,Rk}}{4} & (\text{c}) \\ 2,3 \sqrt{M_{y,Rk} f_{h,k} d} + \frac{F_{ax,Rk}}{4} & (\text{d}) \\ f_{h,k} t_1 d & (\text{e}) \end{cases}$$

Figure B.9: Bolts column-beam connection failure mechanisms

$$F_{90,Rk} = 14b \sqrt{\frac{h_e}{1 - \frac{h_e}{h}}} \quad (\text{B.16})$$

b = timber member thickness
 h = timber member height
 h_e = distance loaded edge to opposite bolt

Appendix B.3 Connection design check

Column-beam connections

The connection design of column-beam connections with moment capacity is governed by the rotational stiffness they provide. For this investigation four different rotational stiffness were used to determine the influence of connection stiffness in the design of the different timber stability systems. This section provides an example of the design configurations that are required to achieve each rotational stiffness. The rotational capacity will be determined using the method presented in section B.2.

The different rotational stiffness will be determined using the design configuration presented in figure B.10. This connection includes two steel plates placed 40 cm apart from each other and 20 cm from the edge of the beam, which equals a beam width of 80 cm. The steel plates penetrated both the beam and the column, and used 3 cm diameter dowels.

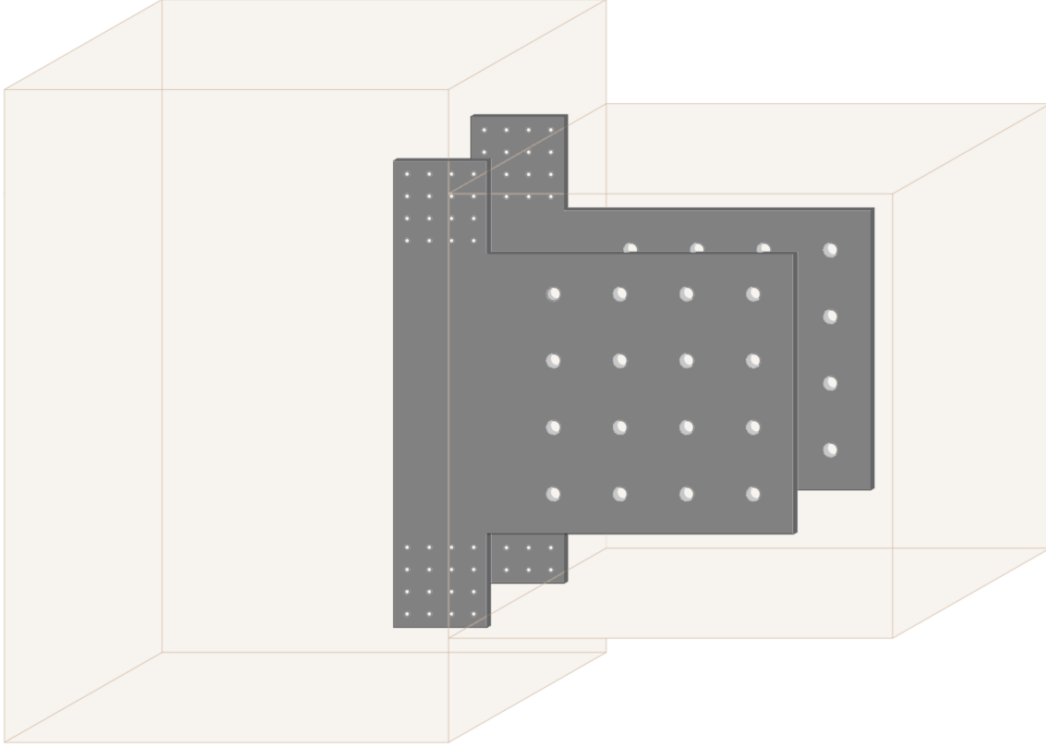


Figure B.10: *Column-beam connection configuration*

The slip modulus (K_{ser}) of each individual dowel per shear plane is determined based on the mean density of timber (ρ_m) and the dowel diameter (d). Moreover, when designing timber-steel connections the density of timber is doubled.

$$K_{ser} = \rho_m^{1.5} \cdot \frac{d}{23} \quad (\text{B.17})$$

$$K_{ser} = 4 \cdot 2 \cdot (490)^{1.5} \cdot \frac{30}{23} = 102948 N/mm \quad (\text{B.18})$$

The rotational stiffness of the configuration is determined based on the number of dowels and their distance to the center of rotation. For this calculation, the following dowel distributions are considered.

$$K_{r,ser} = K_{ser} \cdot \sum r^2 \quad (\text{B.19})$$

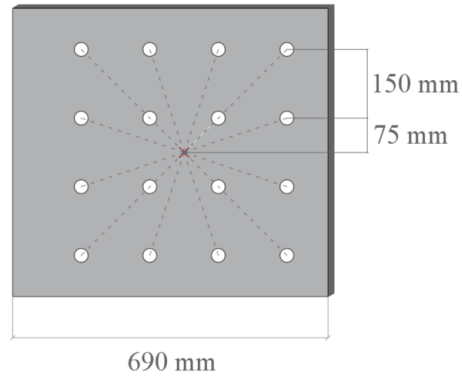


Figure B.11: *Column-beam connection 100 000 kNm/rad rotational stiffness*

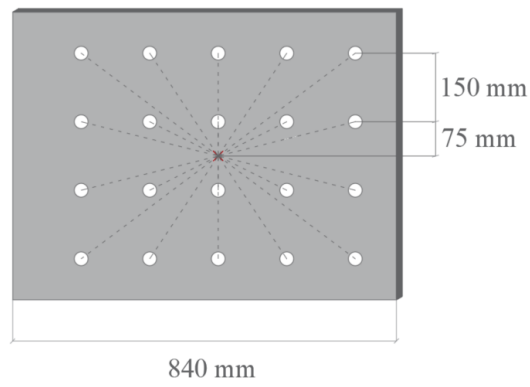


Figure B.12: *Column-beam connection 200 000 kNm/rad rotational stiffness*

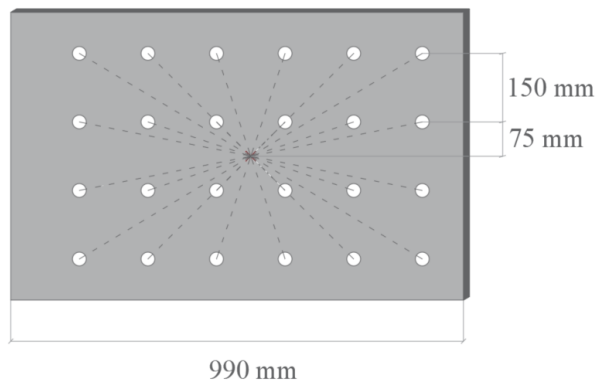


Figure B.13: *Column-beam connection 300 000 kNm/rad rotational stiffness*

The following rotational stiffnesses can be determined from the presented configurations:

	Figure B.11	Figure B.12	Figure B.13
$\sum r^2$ (mm^2/rad)	900 000	1462500	2250000
$k_{r,ser}$ (kNm/rad)	101 000	195 500	295 000

Figure B.14 shows the procedure used to determine $\sum r^2$ for the 100 000 kNm/rad configuration. The same procedure was used for all configurations.

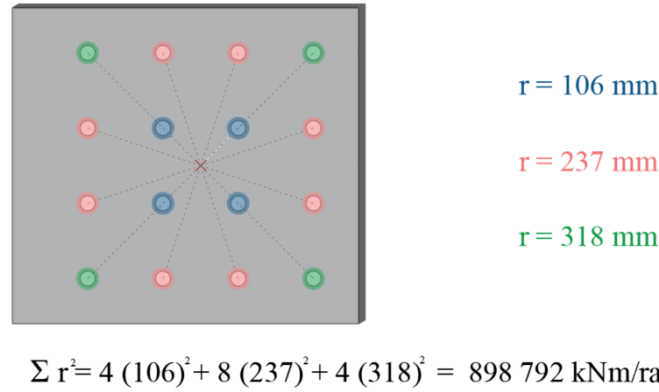


Figure B.14: Calculation of $\sum r^2$ for 100 000 kNm/rad configuration

From the results presented it is determined that the plate dimensions required to achieve 300 000 kNm/rad are 630 x 990 mm. In terms of element dimensions, this plate size can be implemented for the design configurations studied during this investigation due to the large elements used to provide lateral stability. However, the amount of material required for each connection exponentially increases the cost and environmental footprint of the structure. Moreover, the assembly of these connections require of significantly high precision, which also increases the labor costs. These observations suggest that the implementation of rotational stiffness in the connection by using the presented method is not feasible in practice.

Diagonal elements connections

The connections between the diagonal members in the glulam diagrid are assumed to be pinned, given that the global stiffness of this system is provided by the triangular configuration of the elements. The configuration of these connections must be designed to transfer the axial loads developed across the elements. The capacity of the connection is determined by the governing failure mechanism between dowel group check, timber element check and plate check. Figure B.15 shows a design verification for the critical joint in the design configuration of 130 meters and 4 storey diagonal angles. From the figure it can be seen that the design of this connection is governed by the capacity of the dowel group.

Structural system	Glulam diagrid	
Diagonal angle (storeys)	4	
Building height (m)	130	
Connection stiffness (kNm/rad)	400000	
Column cross-section (cm)	100-100	
Beams cross-section (cm)	60-100	
Diagonal cross-section (cm)	50-50	
Governing force (kN)	560 compression	

Dowel check		
diameter dowels (mm)	15	
steel tensile strength (N/mm ²)	490	
timber density (kg/m ³)	380	
number of dowels in column	3	
number of dowel rows	2	
dowel spacing (mm)	75	
t1 (mm)	125	
t2 (mm)	250	
number of plates	1	
M _{y,Rk}	167940,178	
f _{h,k} (MPa)	211,888	
F ₁	397290	397,29
F ₂	281874,865	281,874865
F ₃	46206,8231	46,2068231
F ₄	397960,629	397,960629
F ₅	221748,412	221,748412
F ₆	221748,412	221,748412
F ₇	106333,277	106,333277
Governing (kN)	46,2068231	
Total (kN)	184,827292	
n _{eff1}	3	
n _{eff2}	2,11673159	
n _{eff}	2,11673159	
F _{max,dowels} (kN)	782,459539	

Timber check		
element height (mm)	500	
element width (mm)	500	
f _{c,0,k} (MPa)	24	
f _{t,0,k} (MPa)	19,2	
		(kN)
F _{c,max}	6000000	6000
F _{t,max}	4800000	4800

Plate check		
steel tensile strength (N/mm ²)	490	
steel yield strength (N/mm ²)	355	
plate thickness (mm)	10	
plate width (mm)	330	
partial factor	1,25	
		(kN)
F _{plate1}	1171500	1171,5
F _{plate2}	1164240	1164,24

Figure B.15: Example diagrid connection design verification

Appendix C Member Check

Appendix C.1 Verification of glulam elements

Axial Stress

The selection of design parameters like stability system design and connection stiffness will have an influence on the load distribution throughout the structure, which will as a result influence the axial stresses experienced by the structural elements. Based on the structural design of the structure, the axial stresses will manifest as either compression or tension stresses and this will have an effect on the design strength of the element. The design check for axial strength should be done for both elements experiencing compression and tension stresses using formulae C.2 and C.1 respectively.

$$\sigma_{t,0,d} \leq f_{t,0,d} \quad (\text{C.1})$$

$$\sigma_{c,0,d} \leq f_{t,0,d} \quad (\text{C.2})$$

Shear Stress

The design validation for the shear stress experienced by all glulam structural elements should be done using formula C.3

$$\tau_d \leq f_{v,d} \quad (\text{C.3})$$

Bending Stress

The structural design of a building influences the magnitude of the bending stresses experienced by the structural elements as well as the occurrence of bending stresses in one or two of the principal axes. When biaxial bending stresses are experienced, the design validation needs to incorporate a factor k_m which takes into account the inhomogeneity of the cross-section and the stress re-distribution [4], as seen in formulae C.4 and C.5 which consider the effect of this factor on both the y- and z- axis.

$$\frac{\sigma_{m,y,d}}{f_{m,y,d}} + k_m \frac{\sigma_{m,z,d}}{f_{m,z,d}} \leq 1 \quad (\text{C.4})$$

$$\frac{\sigma_{m,z,d}}{f_{m,z,d}} + k_m \frac{\sigma_{m,y,d}}{f_{m,y,d}} \leq 1 \quad (\text{C.5})$$

Combined Axial and Bending Stress

Structural elements experiencing both bending and axial stresses need to be checked for their combined action in order to verify that the integrity of the element. Elements experiencing combined bending and tension stresses need to be validated using the following formulae.

$$\frac{\sigma_{t,0,d}}{f_{t,0,d}} + k_m \frac{\sigma_{m,y,d}}{f_{m,y,d}} + \frac{\sigma_{m,z,d}}{f_{m,z,d}} \leq 1 \quad (\text{C.6})$$

$$\frac{\sigma_{t,0,d}}{f_{t,0,d}} + \frac{\sigma_{m,y,d}}{f_{m,y,d}} + k_m \frac{\sigma_{m,z,d}}{f_{m,z,d}} \leq 1 \quad (\text{C.7})$$

Elements experiencing combined bending and compression stresses need to be validated using the following formulae.

$$\left(\frac{\sigma_{c,0,d}}{f_{c,0,d}} \right)^2 + k_m \frac{\sigma_{m,y,d}}{f_{m,y,d}} + \frac{\sigma_{m,z,d}}{f_{m,z,d}} \leq 1 \quad (\text{C.8})$$

$$\left(\frac{\sigma_{c,0,d}}{f_{c,0,d}} \right)^2 + \frac{\sigma_{m,y,d}}{f_{m,y,d}} + k_m \frac{\sigma_{m,z,d}}{f_{m,z,d}} \leq 1 \quad (\text{C.9})$$

Member Stability

Elements loaded by bending stress or combined bending and compression stresses, need to be verified for lateral torsional stability, which can govern the design of unrestrained elements exposed to both lateral deformations and twisting [35]. Formula C.10 should be used for the verification of members loaded by bending and and formula C.13 should be used for the verification of members loaded by bending and axial loads.

$$\sigma_{m,d} \leq k_{crit} \cdot f_{m,d} \quad (\text{C.10})$$

$$k_{crit} = \begin{cases} 1 & \lambda_{rel,m} \leq 0.75 \\ 1.56 - 0.75\lambda_{rel,m} & 0.75 \leq \lambda_{rel,m} \leq 1.4 \\ 1/\lambda_{rel,m}^2 & 1.4 \leq \lambda_{rel,m} \end{cases}$$

$$\lambda_{rel,m} = \sqrt{\frac{f_{m,k}}{\sigma_{m,crit}}} \quad (\text{C.11})$$

$$\sigma_{m,crit} = \frac{M_{y,crit}}{W_y} \quad (\text{C.12})$$

$M_{y,crit}$ = critical bending moment
 W_y = section modulus about y-axis

$$\left(\frac{\sigma_{m,d}}{k_{crit} \cdot f_{m,d}} \right)^2 + \frac{\sigma_{c,d}}{k_{c,z} \cdot f_{c,0,d}} \leq 1 \quad (\text{C.13})$$

$$k_{c,z} = \frac{1}{k_z + \sqrt{k_z^2 - \lambda_{rel,z}^2}} \quad (\text{C.14})$$

$$k_z = 0.5(1 + \beta_c(\lambda_{rel,z} - 0.3) + \lambda_{rel,z}^2) \quad (\text{C.15})$$

$$\lambda_{rel,z} = \frac{\lambda_z}{\pi} \sqrt{\frac{f_{c,0,k}}{E_{0.05}}} \quad (C.16)$$

- β_c = factor for elements within straightness limits = 0.1 for glulam
- λ_y = slenderness ratio corresponding to bending about the z-axis
- $E_{0.05}$ = fifth percentile value of modulus of elasticity parallel to the grain

All elements loaded in bending and compression should satisfy the condition presented in formula C.13, but they should also satisfy a criteria where $\lambda_{rel,z} \leq 0.3$. Elements which do not satisfy this criteria need to be further examined in order to verify that their deflections remain under an acceptable range.

Appendix C.2 Verification of CLT elements

Axial Stress

The design validation for the axial stress developed by CLT structural elements loaded in plane should be done using formula C.17

$$\sigma_{c,0,d} \leq f_{c,0,d} \quad (C.17)$$

$$\frac{N_{0,d}}{A_{0,net}} \leq f_{c,0,d} \quad (C.18)$$

Bending Stress

The verification for bending stress can be done using formulae C.19 and C.20, together with figure 4.10, which shows the net area of the cross-section for in-plane loading where d_0 is the thickness of the highlighted lamellae.

$$\sigma_{m,z,d} \leq f_{m,d} \quad (C.19)$$

$$\frac{M_{z,d}}{W_{z,0,net}} \leq f_{m,d} \quad (C.20)$$

$$W_{z,0,net} = \frac{\sum d_0 \cdot h^2}{b} \quad (C.21)$$

Combined Axial and Bending Stress

The verification for combined axial and bending stresses is done together with the verification for buckling of the panel. This verification is done with the procedure provided by proHolz [30], which is taken from the Eurocode column buckling theory and it can be seen in formula C.22.

$$\frac{\sigma_{c,0,d}}{k_{c,y} \cdot f_{c,0,d}} \pm \frac{\sigma_{m,d}}{f_{m,d}} \leq 1 \quad (C.22)$$

$$k_{c,y} = \frac{1}{k_y + \sqrt{k_y^2 - \lambda_{rel,y}^2}} \quad (\text{C.23})$$

$$k_y = 0.5 \left(1 + 0.1 (\lambda_{rel,y} - 0.3) + \lambda_{rel,y}^2 \right) \quad (\text{C.24})$$

$$\lambda_{rel,y} = \frac{\lambda_y}{\pi} \sqrt{\frac{f_{c,0,k}}{E_{0.05}}} \quad (\text{C.25})$$

$$\lambda_y = \frac{l}{i_{y,0,net}} \quad (\text{C.26})$$

$$i_{y,0,net} = \sqrt{\frac{I_{y,0,net}}{A_{0,net}}} \quad (\text{C.27})$$

Appendix D CLT Design Assumptions

1. Displacements due to sliding and rocking can be neglected

The displacement of CLT can be divided into four categories which are bending, shear, sliding and rocking as it can be seen in figure D.1. The magnitude of the bending and shear displacements will be based on the stiffness of the CLT panels, while the magnitude of the sliding and rocking displacements will be based on the stiffness of the connection between the panels. For the purpose of this investigation the displacements due to sliding and rocking will be neglected by the assumption of fully rigid connections between the panels or the implementation of tensioning in the CLT panels [42].

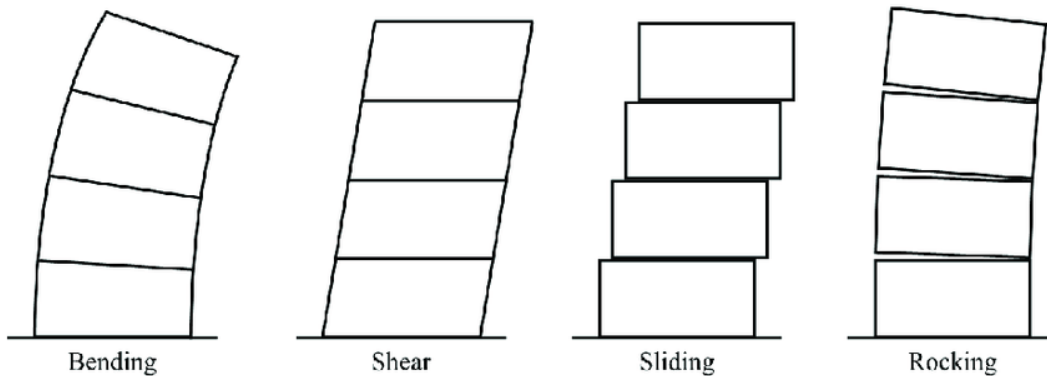


Figure D.1: *CLT displacement modes* [5]

2. No cooperation between C-shaped cores

Stability cores are commonly formed by the interaction of four shear walls, two acting in the same plane and the other two in the opposite plane, as seen on the left side of figure D.2. However, in reality these walls commonly have openings in each storey such that users can access elevators and emergency stairs. These openings will cause a disruption on the load transfer mechanism of the connected shear walls. In concrete cores, the magnitude of the disruption is determined by the remaining beam size, opening width, opening position, building height and rotational stiffness of the foundations [8]. However, the magnitude of the disruption between the shear walls for CLT cores has not been widely addressed on existing literature, so for the purpose of this investigation a conservative assumption will be made, that there is no cooperation between the walls.

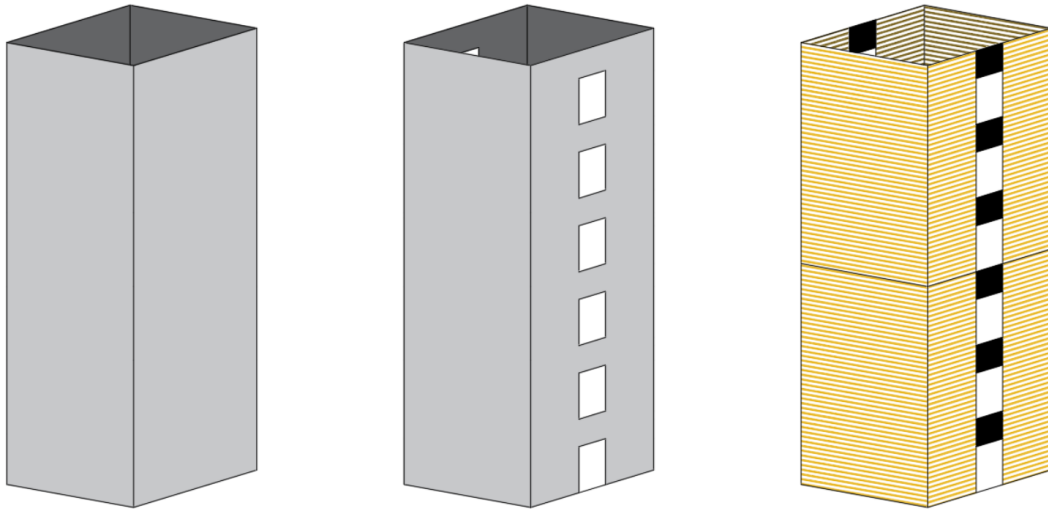


Figure D.2: *C-Shaped core*

3. Bernoulli's hypothesis is applied

In order to apply Bernoulli's hypothesis for beam theory the following assumption needs to be made "plane cross-sections remain planar and normal to the beam axis in a beam subjected to bending" [33]. However, this assumption is not applicable when there are shear forces in the cross-section. For core structures, a shear flow in the connections between the walls is developed, creating shear deformations in the panels making the stress distribution over the length of the element not uniform [21]. The development of this shear lag effect will reduce the effectiveness of the panels, so in order to be able to use Bernoulli's beam theory this reduction needs to be taken into account, as shown in figure D.3.

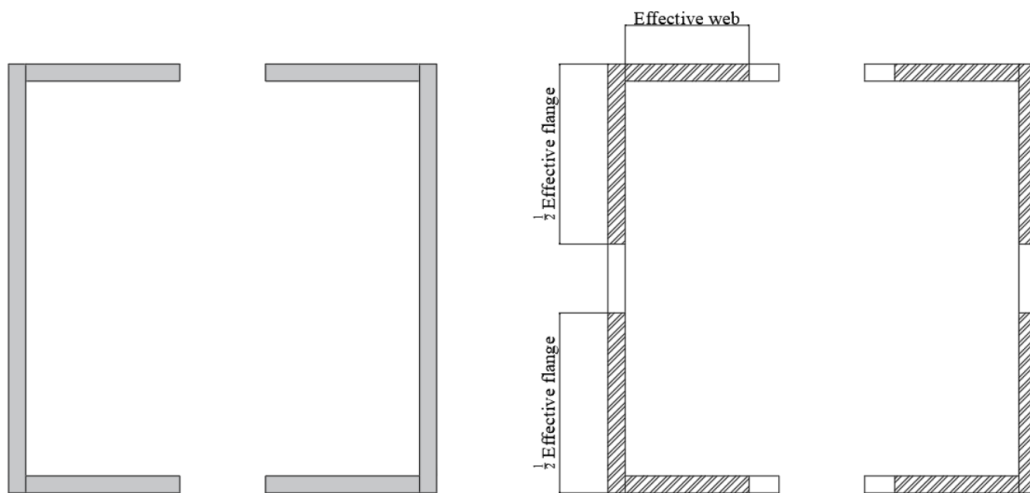


Figure D.3: *Shear-lag effective length*

4. Effective width will be used to counteract shear lag effect

In the British Standard BS 5400: Part 5 equations are presented to take into account the shear lag effect in concrete cores. Given that there are no regulations that study this effect in CLT cores, these equations will be used.

$$b_{eff} = \alpha \cdot b(1 + \beta \cdot ALR) \quad (D.1)$$

b_{eff} = effective width
 b = length of the wall
 ALR = axial load ratio
 α, β = load type coefficients

Due to the loading direction of stability cores, the corresponding mode of bending is Minor (WiT) and assuming ULS design the load coefficients become, $\alpha=0,88$ and $\beta=0$.

5. Cross-sectional stiffness is determined using Steiner's theory

In order to determine the cross-sectional stiffness of mechanically jointed elements, the interaction at the connection needs to be considered. Steiner's parts theory determines this stiffness by considering a γ -factor which takes into account the cooperation of the elements based on the rigidity of the connection as seen in figure D.4 and equation D.2, $\gamma=0$ is used when there are no effective fasteners between the elements and $\gamma=1$ is used when the fasteners provide a fully rigid connection. The γ -method can be used to determine this factor for semi-rigid fasteners using formula D.3; however, this formula only applies for simply supported beams with sinusoidal loads [4]. The difference between the action of uniform and sinusoidal loads is negligible and in order to apply it to cantilever beams, the length needs to be taken as twice the height of the building [4].

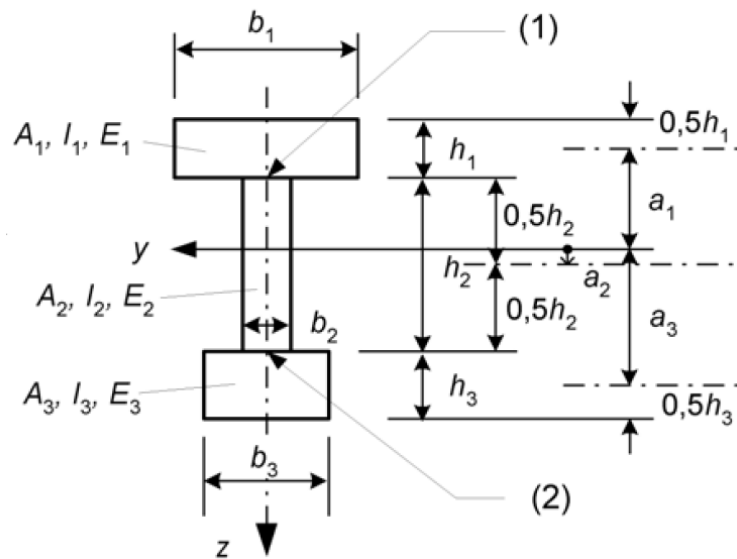


Figure D.4: Mechanically jointed beams according to NEN-EN 1995-1-1

$$(EI)_{eff} = \sum_{n=1}^3 (E_i I_i + \gamma_i E_i A_i a_i^2) \quad (D.2)$$

$$\gamma_i = \frac{1}{1 + \frac{\pi^2 E_i A_i s_i}{K_i l^2}} \quad (D.3)$$

- s_i = fastener spacing in joint between individual components
- K_i = slip factor of fastener

6. Self-tapping screws will connect the core walls together

The fastener type used between the core elements will determine the cross-sectional stiffness of the construction. Ideally this fasteners should provide full rigidity to the connections, such that $\gamma=1$; however, the experimental data for fully rigid connections is currently very limited. For the purpose of this investigation a conservative approach will be made that self-tapping screws will connect the wall elements. In order to determine K_i (slip factor of the fasteners), experimental data will be used. It will be assumed that a pair of 600 mm screws placed at an angle of 45° every 450 mm along the connection length between the elements, as seen in figure . Based on this assumption it is determined that the slip coefficient for axial loads is as shown in equation D.4 [10].

$$K_i = 16,6 \frac{kN}{mm} \tag{D.4}$$

Appendix E Results Verification

Appendix E.1 Karamba Model

The structural analysis for this investigation was done using Karamba 3D, which is a Grasshopper plugin. Karamba 3D is intended to be used as a fast tool for structural optimization during the preliminary design stage of a project; however, for the final design it is recommended to use an advanced professional structural analysis package [20]. The data collected during this investigation is intended to be used during a preliminary design, for which the utilization of Karamba for the structural analysis is assumed to be sufficient; however, in order to verify the results collected, the structure was modelled in the structural package MatrixFrame 5.5 and compared to the results obtained using the parametric script. The results verification was done for both the glulam frame and glulam diagrid models. Figure E.1 shows the loaded model for the glulam frame in both Karamba 3D and MatrixFrame and table E.1 describes the design alternative that was evaluated. Table E.2 shows the comparison of the results obtained from the two different packages. Figure E.2 shows the loaded model for the glulam diagrid in both Karamba 3D and MatrixFrame and table ?? describes the design alternative that was evaluated. Table E.4 shows the comparison of the results obtained from the two different packages.

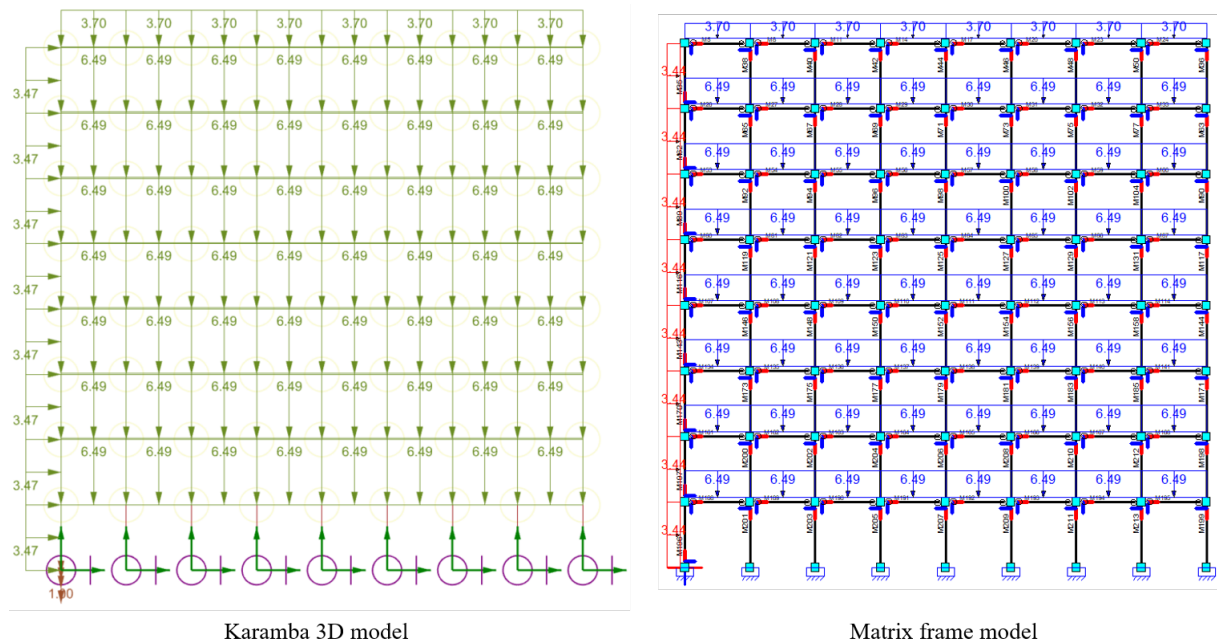


Figure E.1: MatrixFrame glulam frame structural analysis verification

Stability system	Glulam frame
Building height	30 m
Building width	30 m
Structural storey height	4 m
Effective span	3.75 m
Connection stiffness	300 000 kNm/rad
Columns cross-section	60-60 cm
Beams cross-sections	60-130 cm

Table E.1: Matrix frame validation design alternative

Design Constraint	Karamba 3D	MatrixFrame	Difference
Global deflection (m)	0.0062	0.0060	2.5%
Beam max. moment (kNm)	29.6	29	2%
Beam max. axial (kN)	-11.7	-11.87	1.5%
Column max. moment (kNm)	28.98	29.2	1%
Column max. axial (kN)	395	387	2%

Table E.2: Matrix frame validation

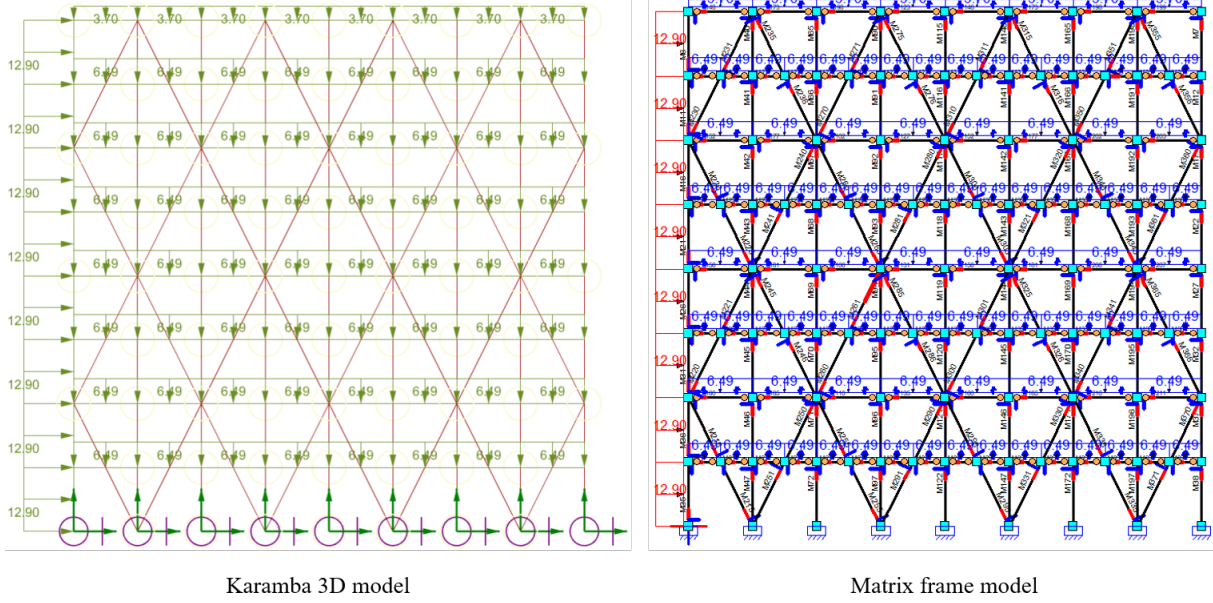


Figure E.2: MatrixFrame glulam diagrid structural analysis verification

Stability system	Glulam diagrid
Building height	30 m
Building width	30 m
Structural storey height	4 m
Effective span	3.75 m
Diagonal angle	2 storey
Columns cross-section	20-20 cm
Beams cross-sections	20-40 cm
Diagonal cross-sections	20-20 cm

Table E.3: Matrix frame validation design alternative

Design Constraint	Karamba 3D	MatrixFrame	Difference
Global deflection (m)	0.0062	0.0063	1.6%
Beam max. moment (kNm)	14.92	14.43	2.9%
Beam max. axial (kN)	-51.36	-49.82	3%
Column max. moment (kNm)	0.25	0.25	1.1%
Column max. axial (kN)	0.33	0.33	1.1%
Diagonal max. axial (kN)	-70.6	-72.72	3%

Table E.4: Matrix frame validation

The slight deviations from the two different packages can be easily visualized in figure E.3, which compares the moment distribution for one frame implementing the connection stiffness and element cross-sections mentioned in table E.1. In the Karamba 3D model the rotational stiffness is applied to the joints, which affects both the connection with the beams and the connection with the columns, while in the MatrixFrame model the rotational stiffness is applied at both the beam and column ends. From the figure it can be seen that Karamba 3D, does not consider the moment distribution across the length of the elements, but it rather computes the moment at three locations, which causes the slight deviations between the two software. Given that the moment capacity is not governing for the sizing of the structural elements in this investigation, this deviations are acceptable for the preliminary design phase.

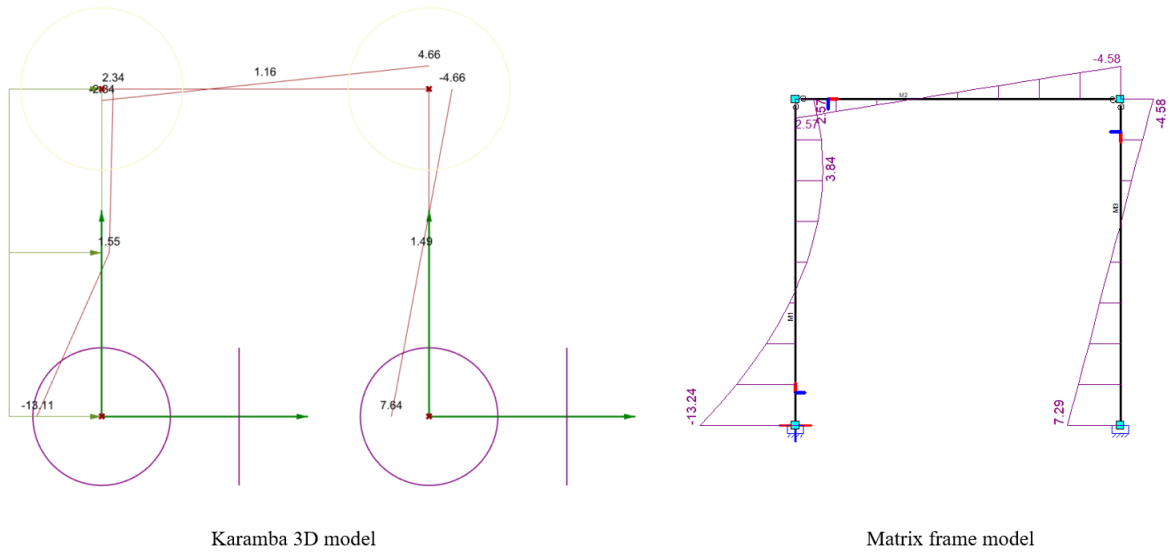


Figure E.3: *MatrixFrame glulam frame one-bay moment distribution*

Figure E.4 shows the deflected shapes of the design configurations presented in tables E.1 and E.3 gathered from the Karamba 3D models. Tables E.2 and E.4 show that these configurations yield to the same global deflection; however, from the figure presented it can be seen that the amount of material required for the different systems is significantly different, showing the efficiency of the glulam diaphragm configuration. Moreover, it is important to mention the difference between the systems in terms of rotational stiffness in the connections. The glulam frame uses 300 000 kNm/rad connections, while the glulam diaphragm uses pinned connections, which means that the efficiency of the glulam diaphragm is not only reflected on the amount of timber required, but also on the amount of steel implemented at the connections. The maximum deflection of both systems is compared with the allowable maximum deflection presented in formula E.1, to check for compliance.

$$\delta_{max} = \frac{h}{500} = \frac{30m}{500} = 0.06 \quad (E.1)$$

$$UC_{\delta,frame} = \frac{0.0062}{0.06} = 0.103 \quad (E.2)$$

$$UC_{\delta,diagrid} = \frac{0.0062}{0.06} = 0.103 \quad (E.3)$$

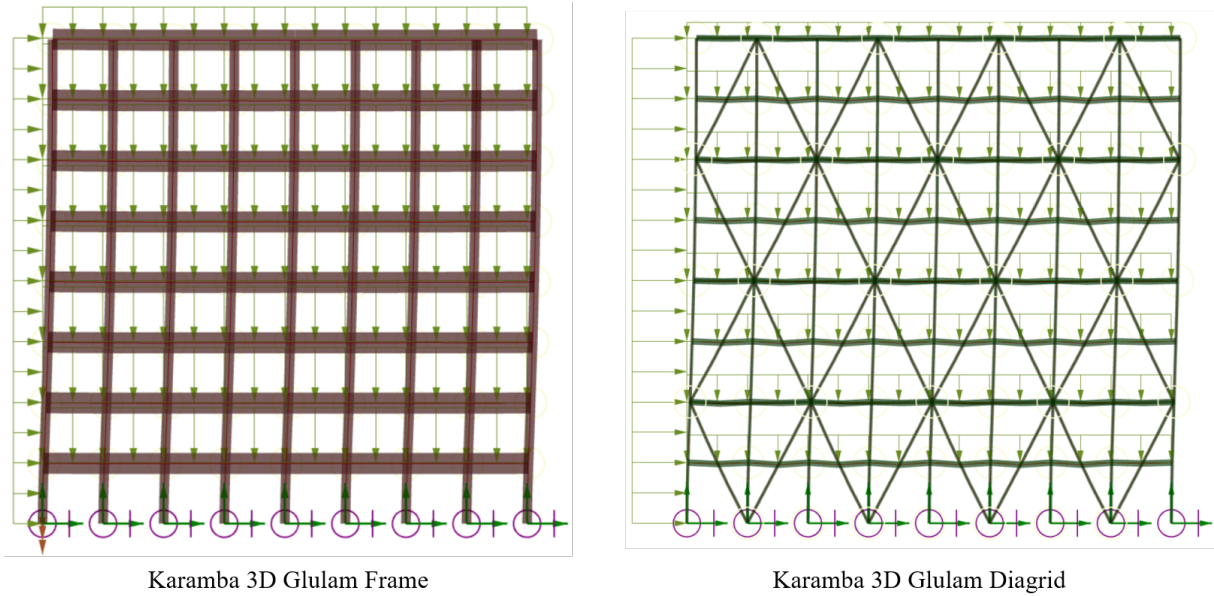


Figure E.4: *Deflected shape Karamba 3D glulam frame and diagrid*

Appendix E.2 Dynamic Behaviour

The dynamic behavior of high-rise structures is commonly quantified by the magnitude of the acceleration at which the structure oscillates after being excited by a horizontal load such as wind. In order to estimate the magnitude of the acceleration there are different methodologies based on the natural frequency of the structure which can be used, as explained in chapter 3. As previously mentioned, Eurocode does not provide a methodology for estimating the natural frequency of timber structures, for which this was done using the investigation presented by Oosterhout (1996). In order to validate the calculated natural frequency, a component from Karamba 3D which studies the assembled model was used. Figure E.5 shows the output from the Python script which was developed using Oosterhout's investigation and the output from the Karamba 3D component. This verification was done using the design alternative presented in table E.1 and it was concluded that the difference between the two methodologies was less than 3% which is acceptable for a preliminary design study. The procedure for calculating the natural frequency using Oosterhout's method can be seen below for both when the structure is assumed to act in pure shear ($f(\alpha h) = 0.176$) and in pure bending ($f(\alpha h) = 0.198$). From the output it can be seen that the behaviour of the frame correspond with the pure shear assumption.

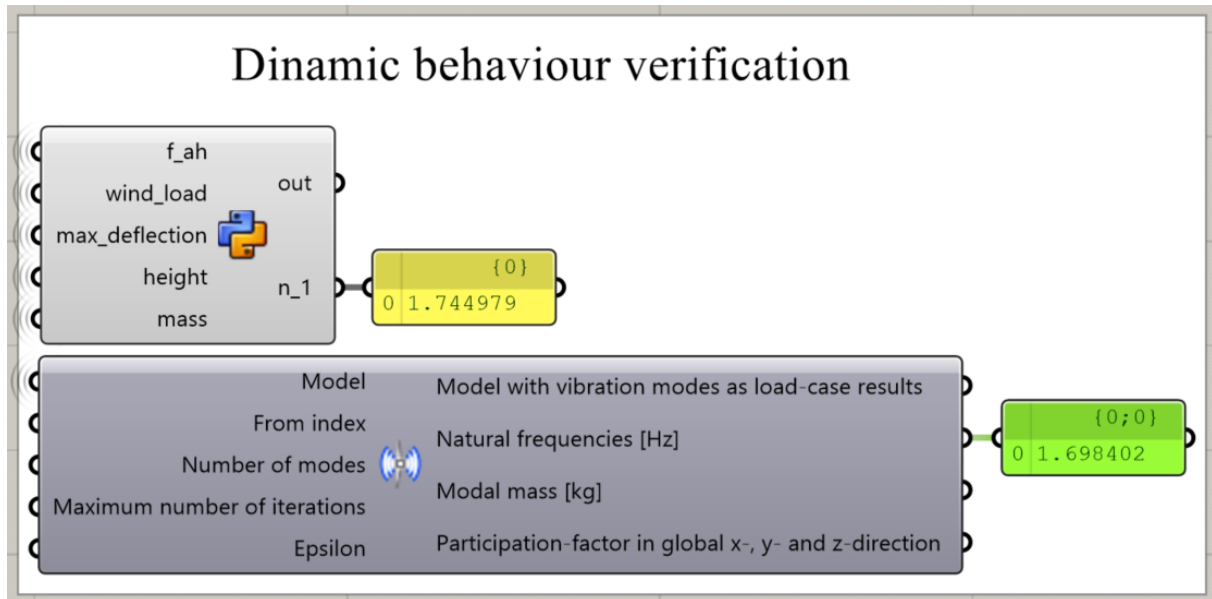


Figure E.5: *Dynamic behaviour verification*

$$n_{1,x} = f(\alpha h) \cdot \sqrt{\frac{q_w \cdot h}{\mu \cdot \delta_{max}}} \quad (\text{E.4})$$

$$n_{1,x, \text{shear}} = 0.176 \cdot \sqrt{\frac{3468 \cdot 30}{171493 \cdot 0.0062}} = 1.74 \quad (\text{E.5})$$

$$n_{1,x, \text{bending}} = 0.198 \cdot \sqrt{\frac{3468 \cdot 30}{171493 \cdot 0.0062}} = 1.95 \quad (\text{E.6})$$

Appendix F EA Data

Glulam Frame

Building height [m]	Input		Amount of material [tons/m]	Net floor area [%]	Output			
	Effective span [m]	Rotational stiffness [kNm/rad]			Failure mechanism	Column cross- section	Beam cross- section	Moment resistance [kNm]
30	6	400000	90,94336	96	along-wind acceleration	110-110	80-130	118,4
30	6	300000	107,736	93,049587	along-wind acceleration	145-145	80-130	107,1
30	6	200000	139,722667	87,429752	along-wind acceleration	195-195	80-130	101
30	4	400000	118,920347	97,75	along-wind acceleration	55-55	80-130	75,6
40	4	400000	130,4816	94,529247	along-wind acceleration	85-85	80-130	91,2
50	4	400000	156,534864	90,874747	along-wind acceleration	110-110	80-130	113,6
60	4	400000	186,894933	84,196465	along-wind acceleration	145-145	80-130	146,4
70	4	400000	204,762503	81,953673	along-wind acceleration	155-155	80-130	173,6
80	4	400000	225,817075	77,021809	along-wind acceleration	175-175	80-130	209,6
90	4	400000	238,181191	75,695868	along-wind acceleration	180-180	80-130	241,2
100	4	400000	247,95748	72,932415	along-wind acceleration	180-180	80-130	281,2
40	6	400000	141,785	85,874013	along-wind acceleration	180-180	80-130	168
110	4	400000	252,463084	72,932415	along-wind acceleration	180-180	80-130	316
120	4	400000	255,7316	71,494904	along-wind acceleration	180-180	80-130	360,4
130	4	400000	259,665932	71,494904	along-wind acceleration	180-181	80-130	398,4
30	4	300000	121,354667	97,322314	along-wind acceleration	60-60	80-130	64,5
40	4	300000	137,8991	93,179017	along-wind acceleration	95-95	80-130	80,7
50	4	300000	176,916864	87,281726	along-wind acceleration	130-130	80-130	104,1
60	4	300000	205,463267	80,776492	along-wind acceleration	160-160	80-130	138,6
70	4	300000	225,086789	78,31056	along-wind acceleration	170-170	80-130	165,3
80	4	300000	240,3816	74,332736	along-wind acceleration	185-185	80-130	201,3
90	4	300000	253,47008	72,932415	along-wind acceleration	180-180	80-130	231,6
100	4	300000	263,71	70,020202	along-wind acceleration	180-180	80-130	270,6
110	4	300000	268,508538	70,020202	along-wind acceleration	180-180	80-130	303,9
30	4	200000	126,858347	96,355372	along-wind acceleration	70-70	80-130	53,4
40	4	200000	164,914975	88,235767	along-wind acceleration	125-125	80-130	71
50	4	200000	207,036864	81,953673	along-wind acceleration	155-155	80-130	97,2
60	4	200000	232,998267	75,695868	along-wind acceleration	180-180	80-130	132
70	4	200000	247,252503	74,332736	along-wind acceleration	185-185	80-130	158,2
80	4	200000	263,71	70,020202	along-wind acceleration	180-180	80-130	193
90	4	200000	269,57008	70,020202	along-wind acceleration	180-180	80-130	222,4
100	4	200000	271,8816	68,50831	along-wind acceleration	180-180	80-130	260,6
30	4	100000	162,103707	90,163223	along-wind acceleration	115-115	80-130	43
40	4	100000	218,8341	78,31056	along-wind acceleration	170-170	80-130	66,1
50	4	100000	249,994864	74,332736	along-wind acceleration	185-185	80-130	92,2
60	4	100000	271,8816	68,50831	along-wind acceleration	180-180	80-130	126,2
70	4	100000	279,652503	68,50831	along-wind acceleration	180-180	80-130	151,4

CLT Core

Building height [m]	Input		Output					
	Core width	Rotational stiffness [kNm/rad]	Amount of material [tons/m]	Net floor area [%]	Failure mechanism	Column cross- section	Beam cross- section	Moment resistance [kNm]
30	0,1	0	94,576667	93,149388	along-wind acceleration	80-80	80-120	0
40	0,1	0	120,5	84,790204	along-wind acceleration	120-120	80-130	0
50	0,1	0	161,59	73,087347	along-wind acceleration	160-160	80-130	0
60	0,2	0	149,926667	73,524444	along-wind acceleration	180-180	80-130	0
50	0,2	0	121,296	83,764444	along-wind acceleration	140-140	80-130	0
40	0,2	0	94,4525	91,444444	along-wind acceleration	100-100	80-130	0
30	0,2	0	73,4	96,564444	along-wind acceleration	60-60	80-120	0
30	0,3	0	54,436667	98,20753	along-wind acceleration	40-40	20-100	0
40	0,3	0	77,21	95,033976	along-wind acceleration	80-80	80-120	0
50	0,3	0	105,848	89,74472	along-wind acceleration	120-120	80-130	0
60	0,3	0	144,563333	77,843893	along-wind acceleration	180-180	80-120	0
70	0,3	0	168,685714	72,8191	along-wind acceleration	200-200	80-130	0
30	0,3	100000	61,546667	98,20753	along-wind acceleration	40-40	40-140	56,3
40	0,3	100000	68,0525	96,885216	along-wind acceleration	60-60	60-120	89,4
50	0,3	100000	88,722	92,653811	along-wind acceleration	100-100	80-130	114,4
60	0,3	100000	115,826667	86,306703	along-wind acceleration	140-140	80-130	140,7
70	0,3	100000	149,785714	77,843893	along-wind acceleration	180-180	80-130	169,6
80	0,3	100000	166,35	72,8191	along-wind acceleration	200-200	80-130	215,1
70	0,2	100000	152,257143	73,524444	along-wind acceleration	180-180	80-130	189,8
60	0,2	100000	133,086667	78,964444	along-wind acceleration	160-160	80-130	155,4
50	0,2	100000	97,384	91,444444	along-wind acceleration	100-100	80-130	128,1
40	0,2	100000	76,2225	94,324444	along-wind acceleration	80-80	60-120	115,9
30	0,2	100000	62,076667	98,164444	along-wind acceleration	40-40	40-120	101,2
30	0,1	100000	77,95	96,075102	along-wind acceleration	60-60	60-120	97,6
40	0,1	100000	93,6025	93,149388	along-wind acceleration	80-80	80-130	101
50	0,1	100000	123,694	84,790204	along-wind acceleration	120-120	80-130	122,1
30	0,1	200000	74,9	96,075102	along-wind acceleration	60-60	60-120	193
40	0,1	200000	89,7925	93,149388	along-wind acceleration	80-80	80-120	186,4
50	0,1	200000	108,806	89,387755	along-wind acceleration	100-100	80-130	204,6
60	0,1	200000	134,171667	79,356735	along-wind acceleration	140-140	80-120	294
30	0,2	200000	62,076667	98,164444	along-wind acceleration	40-40	40-120	185,4
40	0,2	200000	71,8275	96,564444	along-wind acceleration	60-60	80-130	204,4
50	0,2	200000	88,416	94,324444	along-wind acceleration	80-80	80-130	239,6
60	0,2	200000	118,226667	83,764444	along-wind acceleration	140-140	80-130	278,2
70	0,2	200000	135,34	78,964444	along-wind acceleration	160-160	80-130	335,6
80	0,3	200000	166,35	72,8191	along-wind acceleration	200-200	80-130	362,6
70	0,3	200000	132,871429	82,339761	along-wind acceleration	160-160	80-130	298
60	0,3	200000	102,948333	89,74472	along-wind acceleration	120-120	80-130	251
50	0,3	200000	82,838	95,033976	along-wind acceleration	80-80	80-120	209
40	0,3	200000	68,0525	96,885216	along-wind acceleration	60-60	60-120	155,2
30	0,3	200000	56,806667	98,20753	along-wind acceleration	40-40	40-80	132,4

Figure F.1: Core EA data

Glulam Diagrid

Input				Output			
Building height [m]	Diagonal angle	Amount of material [tons/m]	Net floor area [%]	Failure mechanism	Column cross-section	Beam cross-section	Diagonal cross-section
30	2	27,700854	99,683594	along-wind acceleration	20-20	20-40	20-20
30	4	28,17205	99,683594	along-wind acceleration	20-20	20-40	40-40
30	6	28,544603	99,683594	along-wind acceleration	20-20	20-40	50-50
40	6	36,838157	99,683594	along-wind acceleration	20-20	20-120	50-50
40	4	26,82691	99,683594	along-wind acceleration	20-20	20-40	50-50
40	2	26,149984	99,683594	along-wind acceleration	20-20	20-40	30-30
50	2	27,237609	99,683594	along-wind acceleration	20-20	20-40	30-30
50	4	27,563428	99,683594	along-wind acceleration	20-20	20-40	50-50
50	6	64,121767	98,734375	along-wind acceleration	40-40	40-140	50-50
60	6	87,17206	97,152344	along-wind acceleration	60-60	60-140	50-50
60	4	43,854178	98,734375	along-wind acceleration	40-40	20-140	50-50
60	2	26,416665	99,683594	along-wind acceleration	20-20	20-40	40-40
70	2	27,19502	99,683594	along-wind acceleration	20-20	20-40	40-40
70	4	58,262665	98,734375	along-wind acceleration	40-40	40-120	50-50
70	6	97,09136	97,152344	along-wind acceleration	60-60	60-130	50-50
80	6	115,551367	94,9375	along-wind acceleration	80-80	80-130	50-50
80	4	79,497983	97,152344	along-wind acceleration	60-60	60-120	50-50
80	2	26,887524	99,683594	along-wind acceleration	20-20	20-40	50-50
90	2	27,382618	99,683594	along-wind acceleration	20-20	20-40	50-50
90	4	88,923	97,152344	along-wind acceleration	60-60	60-130	50-50
90	6	128,393596	94,9375	along-wind acceleration	80-80	80-130	50-50
100	6	140,177548	92,089844	along-wind acceleration	100-100	80-130	50-50
100	4	105,832827	94,9375	along-wind acceleration	80-80	60-130	50-50
100	2	26,897964	99,683594	along-wind acceleration	20-20	20-40	50-50
110	2	32,469532	99,683594	diagonals normal and bending	20-20	20-80	50-50
110	4	117,870405	94,9375	along-wind acceleration	80-80	80-130	50-50
110	6	160,479949	88,609375	along-wind acceleration	120-120	80-130	50-50
120	6	177,802448	84,496094	along-wind acceleration	140-140	80-130	40-40
120	4	125,7606	94,9375	along-wind acceleration	80-80	80-130	50-50
120	2	41,643994	98,734375	along-wind acceleration	40-40	40-60	50-50
130	2	47,415762	98,734375	along-wind acceleration	40-40	20-130	50-50
130	4	142,328613	92,089844	along-wind acceleration	100-100	80-130	50-50
130	6	180,818187	84,496094	along-wind acceleration	140-140	80-130	50-50
140	6	178,096593	84,496094	along-wind acceleration	140-140	80-130	50-50
150	6	180,633089	84,496094	along-wind acceleration	140-140	80-130	50-50
160	6	202,081357	79,75	along-wind acceleration	160-160	80-130	50-50
170	6	204,317361	79,75	along-wind acceleration	160-160	80-130	50-50
180	6	201,949962	79,75	along-wind acceleration	160-160	80-130	50-50
190	6	204,213588	79,75	along-wind acceleration	160-160	80-130	50-50
200	6	202,083508	79,75	interstorey drift	160-160	80-130	50-50
140	4	140,179886	92,089844	along-wind acceleration	100-100	80-130	50-50
150	4	159,627988	88,609375	along-wind acceleration	120-120	80-130	50-50
160	4	157,641757	88,609375	along-wind acceleration	120-120	80-130	50-50
170	4	159,48744	88,609375	along-wind acceleration	120-120	80-130	50-50

Appendix G Parametric Model

As previously mentioned, individual parametric models were assembled in Grasshopper for each of the studied stability systems. The geometry created based on the selected preliminary design parameters was inputted into the structural analysis plugin Karamba 3D and together with the system loads the structural model was assembled. Figure G.1 shows the assembled structural model for each stability system.

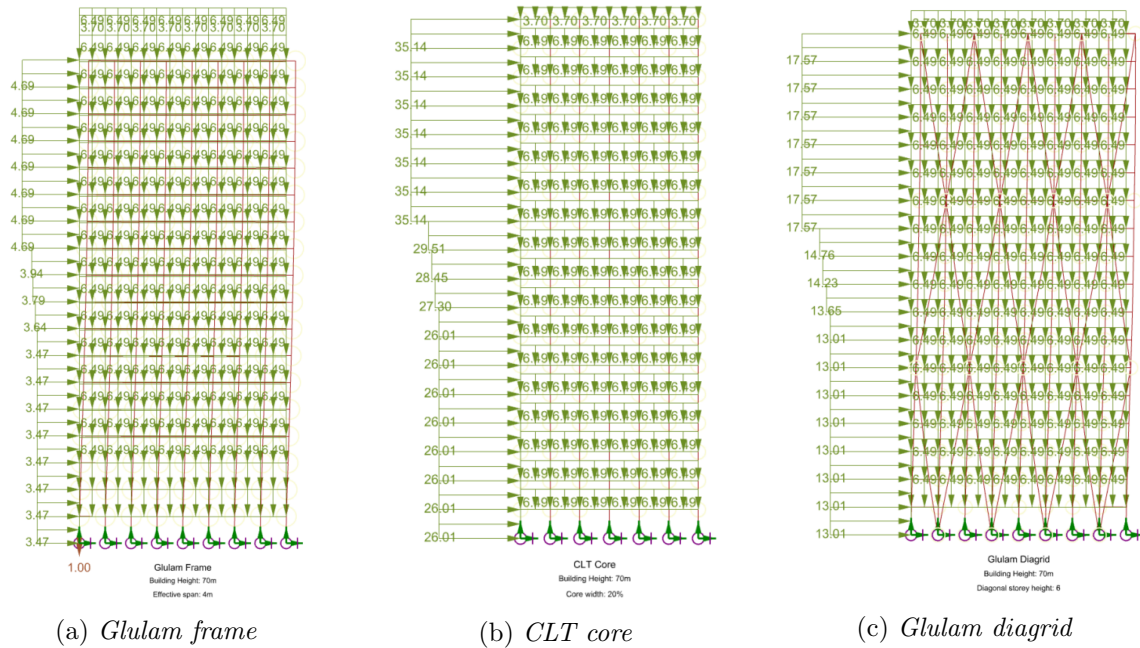


Figure G.1: Assembled Karamba model

The script developed for each stability system consisted of five main sections: general geometry, model assemble, design constraints, results and post-processing. Figures G.2, G.3 and G.4 show the script for the glulam frame, where the mentioned sections can be distinguished, together with all relevant sub-sections.

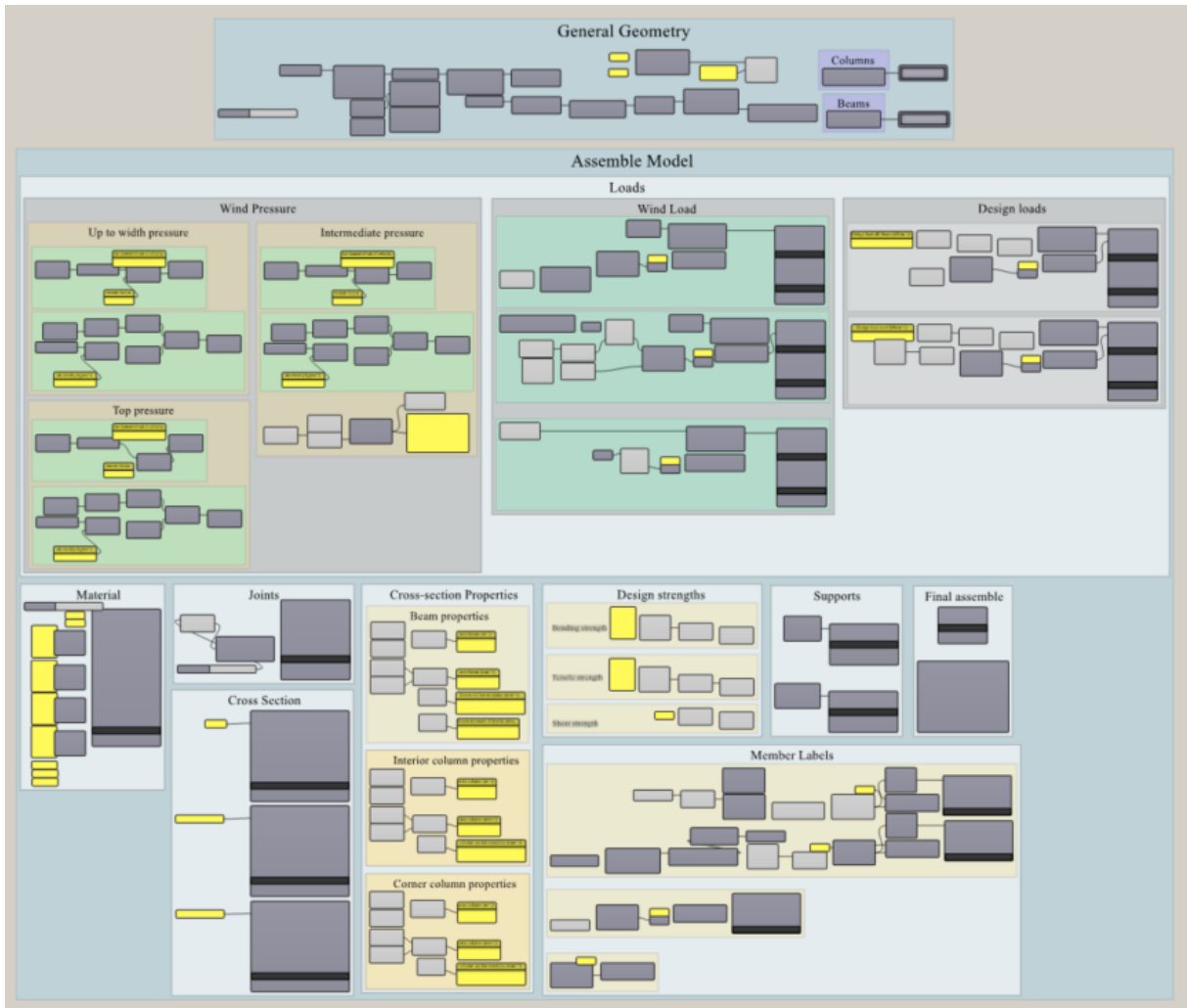


Figure G.2: Parametric model: general geometry and model assemble

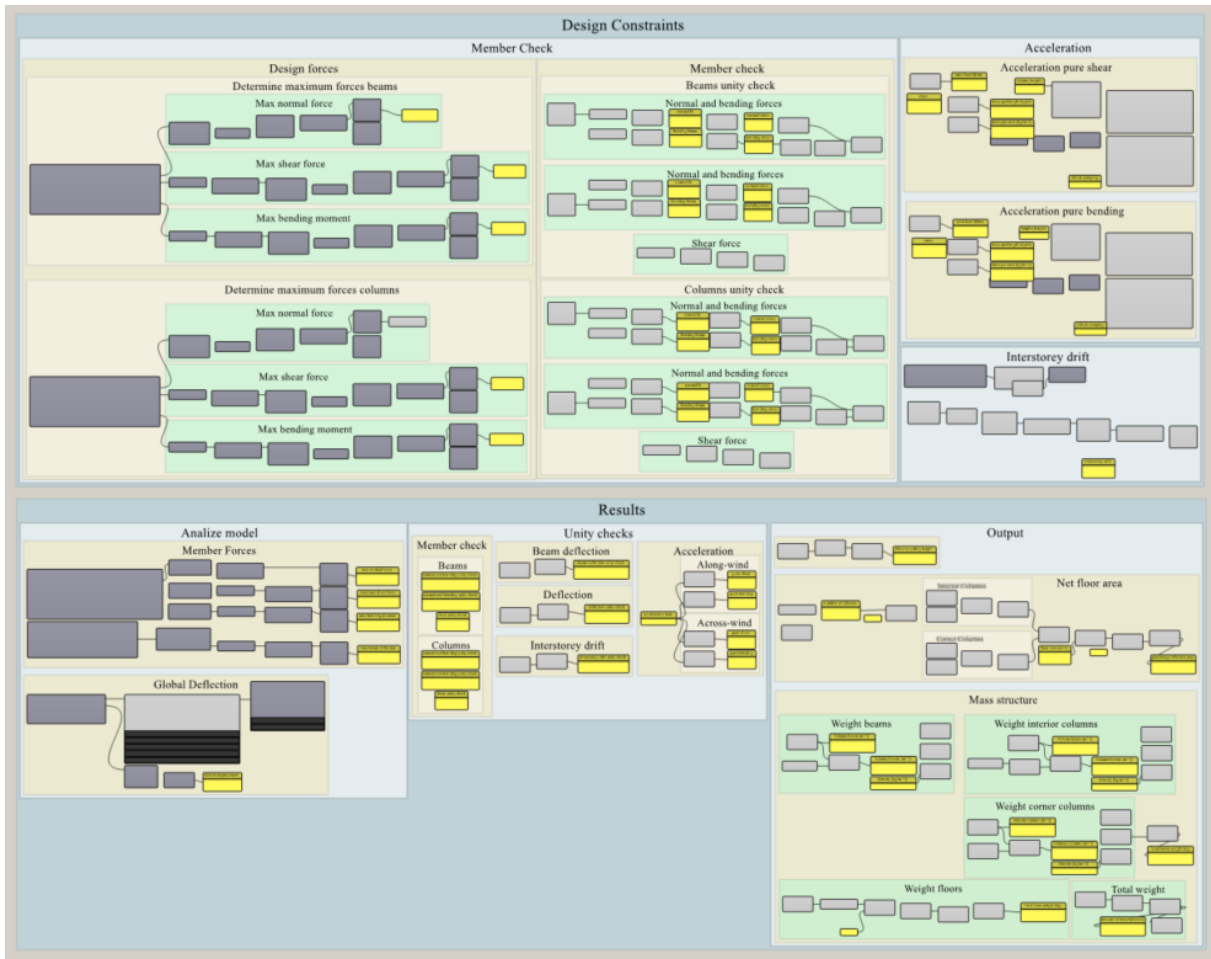


Figure G.3: *Parametric model: design constraints and results*

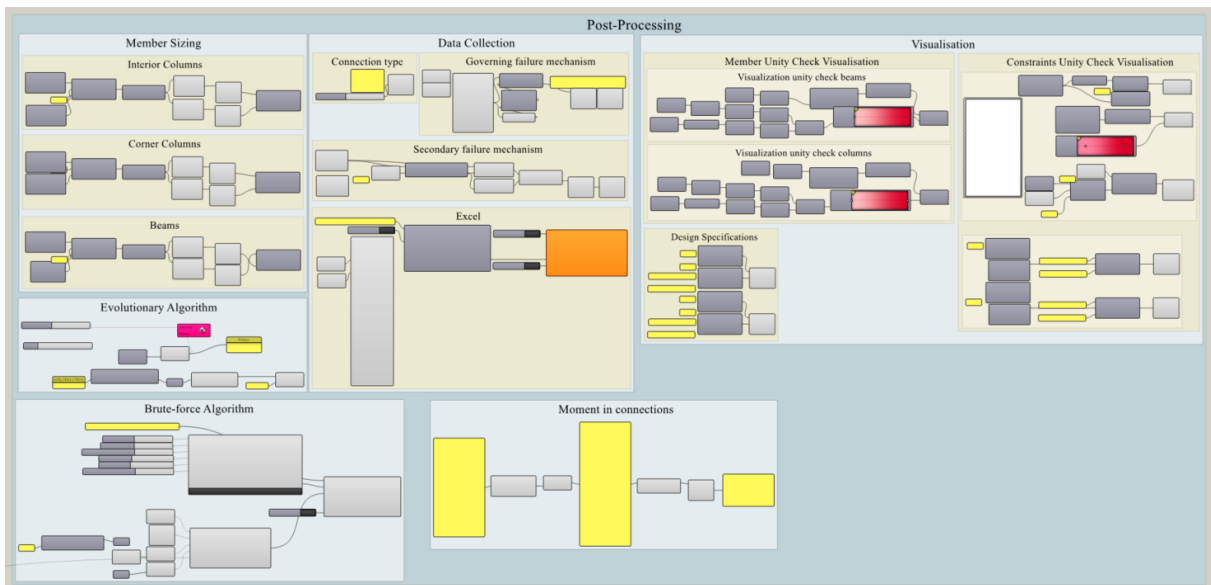


Figure G.4: *Parametric model: post processing*